RHODIUM PHOSPHINE CATALYSED HYDROFORMYLATION

by

KONRAD MARABE MOKHESENG

DISSERTATION

Submitted in the fulfilment of the requirements for the degree:

MASTER OF SCIENCE

in the

DEPARTMENT OF CHEMISTRY

FACULTY OF SCIENCE

at the

UNIVERSITY OF THE FREE STATE

Supervisor: PROF. A. ROODT
Co-supervisor: Dr. N. E. GRIMMER

December 2005

ACKNOWLEDGEMENTS

First and foremost, I want to thank the good Lord our God for making everything possible. It was through God's will and His everlasting love and mercy that this work was accomplished, may His name forever be glorified and may His will be done forever and ever.

My sincere gratitude goes to my supervisor, Professor Andreas Roodt, for his valuable guidance that came with great enthusiasm and expertise. It was through a magnificent leadership of Dr Mike Green that this work was made a reality and I want to thank him from the bottom of my heart. I am truly grateful for the priceless support and mentorship from my co-supervisor, Dr. Neil Grimmer.

Everything was also made possible by a much appreciated assistance of: Dr. Reinout Meijboom, Dr. Fanie Otto, Dr. Linette Bennie and Stephan Wagenaar.

I thank the University of the Free State and SASOL for their financial assistance and resources, not forgetting to also mention the University of Johannesburg in this regard.

My deepest thankfulness is extended to my colleagues, with special mentioning of the Hydroformylation group for their valuable support through thick and thin.

ABBREVIATIONS

acac	Acetylacetonato
TPP	Triphenylphosphine, PPh_3
Xp	4,5-Bis(diphenylphosphino)-9,9-dimethylxanthene, xantphos
DPEphos	(Oxydi-2,1-phenylene)bis(diphenylphosphine)
$P(O\text{-}t\text{But})_3$	Tris(*tert*-butyl)phosphite
Rh-TPP	$[RhH(CO)_2(PPh_3)_2]$
Rh-Xp	$[RhH(CO)_2(xantphos)]$
Rh-TPP-Xp	$[RhH(CO)(PPh_3)(xantphos)]$
ee	equatorial-equatorial, indicating the arrangement of the two phosphorus ligands atoms in a trigonal bipyramidal structure
ea	equatorial-axial, see *ee*
ppm	parts per million
DHN	Decahydronaphthalene
MVK	Methyl vinly Ketone, 3-Buten-2-one
NMR	Nuclear Magnetic Resonance spectroscopy
IR	Infra Red
HP	High Pressure
RV	Rupture Valve
Rxn	Reaction
GC	Gas Chromatography
k_{obs}	Observed pseudo first-order rate constant
k_{calc}	Calculated pseudo first-order rate constant
k_{Xp}	$[RhH(CO)_2(xantphos)_2]$ rate constant
k_P	$[RhH(CO)_2(PPh_3)_2]$ rate constant
K_e	Equilibrium constant

Abstract

The aim of this study was to investigate hydroformylation reactions using phosphine modified rhodium catalyst systems. Comparisons between the traditional monodentate PPh_3 ligand and the bidentate xantphos ligand were performed. Xantphos was chosen due to its capability of producing high normal:isomer (n:iso) ratios and linearities resulting from its configuration (wide bite angle). Another benefit of using xantphos as a ligand of choice is the inhibitor resistance it confers to the rhodium catalyst.

Unfortunately xantphos, a bidentate ligand, results in the formation of low activity hydroformylation catalysts. It was therefore decided that PPh_3 and xantphos be used together with the aim of harnessing the benefits of both ligands, i.e. high rates from PPh_3 as well as high selectivities and inhibitor resistance from xantphos. Both NMR and IR spectroscopic studies were performed for the characterisation of these catalytic species. Due to advancements in spectroscopic technology, HP-NMR and HP-IR experiments could be carried out under actual hydroformylation conditions which allowed the study of the actual catalytic species involved during hydroformylation reactions.

High pressure autoclave experiments were conducted to investigate the kinetics and selectivity of the three different catalyst systems, *i.e.* $[RhH(CO)_2(PPh_3)_2]$, $[RhH(CO)_2(xantphos)]$ and the mixed species $[RhH(CO)_2(PPh_3)(xantphos)]$. Unless otherwise stated, typical conditions employed were 90 ℃ and 20 bar syngas (H_2:CO = 1:1 $[Rh(acac)(CO)_2]$ was also employed as the catalyst precursor together with the ligand(s) of choice .

It was found that in a mixed system, where both PPh_3 and xantphos were employed in one reactor, the higher the PPh_3 concentration the lower the selectivity towards the linear product and the higher the reaction rate. Conversely, higher xantphos concentrations led to higher selectivities but lower rates.

Equally importantly is the stability of the catalyst especially when there are components in the feed that might have a negative impact on the catalyst. For instance, the presence of acids in the feed might lead to heavy products formed at the expense of the intended product. Other components inhibit the catalyst making it inaccessible to hydroformylation either temporarily or permanently. The inhibitory effect of methyl vinyl ketone (MVK) on the selected catalyst system was investigated whilst varying the amount of both PPh_3 and xantphos with the aim of shifting the equilibrium either to the right or left hand side following the scheme below:

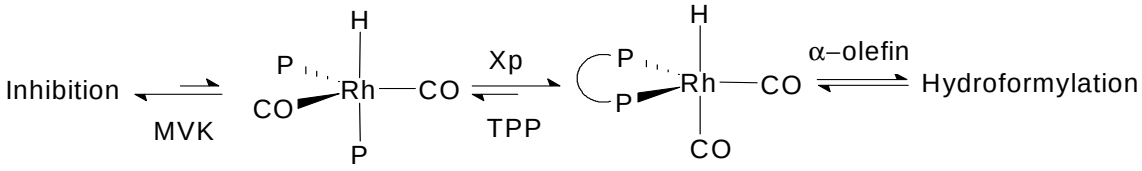

The more xantphos species formed, the less the inhibition time thus the equilibrium is shifted to the right hand side. The more the PPh_3 concentration the longer the inhibition time, resulting from the population of the $[RhH(CO)_2(PPh_3)_2]$ species which is sensitive to MVK inhibition.

Key words: Homogeneous catalysis, Hydroformylation, Rhodium, Cobalt, Triphenylphosphine, Bidentate ligands, Xantphos, Kinetics and selectivity, Inhibition, Methyl vinyl ketone, HP-NMR, HP-IR.

Opsomming

Die doel van die studie was om hidroformilerings-reaksies te ondersoek wat gebruik maak van fosfien gemodifiseerde rodium katalis sisteme. Vergelykings tussen die algemene monodentate PPh_3 ligand en die bidentate xantphos ligand is getref. Xantphos is gekies aangesien dit in staat is om hoë normaal:isomeer verhoudings en hoë lineariteit te lewer as gevolg van sy konfigurasie (wye ko-ordinasie hoek). Nog 'n voordeel om xantphos as eerste keuse ligand te gebruik is die inhiberings weerstand wat dit aan die rodium katalis verleen.

Ongelukkig lei xantphos, 'n bidentate ligand, tot die vorming van hidroformilerings-kataliste met 'n lae aktiwiteit. Daar is dus besluit om PPh_3 en xantphos te kombineer met die doel om die voordele van beide ligand sisteme te probeer vasvang, i.e. die hoë tempos van PPh_3 sowel as die hoë selektiwiteite en inhiberings weerstandigheid van xantphos. Beide KMR en IR spektroskopiese studies is gedoen vir die karakterisering van hierdie katalitiese spesies. As gevolg van vooruitgang in spektroskopie tegnologie, kon hoëdruk-KMR (HD-KMR) en hoëdruk-IR (HD-IR) eksperimente onder werklike hidroformilerings kondisies uitgevoer word wat in staat gestel het om

die werklike katalitiese spesies wat betrokke is tydens hidroformilering te ondersoek .

Hoëdruk outoklaaf eksperimente is uitgevoer om die kinetika en selektiwiteite van die drie verskillende katalis sisteme, i.e. $[RhH(CO)_2(PPh_3)_2]$, $[RhH(CO)_2(xantphos)]$ en die gemengde spesie $[RhH(CO)_2(PPh_3)(xantphos)]$, te ondersoek. Tensy ander gestel was die tipiese kondisies gebruik 90 ℃ en 20 bar singas (H_2:CO = 1:1) $[Rh(acac)(CO)_2]$ was altyd gebruik as die katalis uitgangstof tesame met die ligand(e) van voorkeur.

Dit is gevind dat in ‘n gemengde sisteem, waar beide PPh_3 en xantphos in een reaktor gebruik is, hoe hoër die PPh_3 konsentrasie hoe laer die selektiwiteit ten gunste van die lineêre produk en hoe hoër die reaksie tempo. Omgekeerd, hoër xantphos konsentrasies lei tot hoër selektiwiteite maar stadiger reaksie tempos.

Ewe belangrik is die stabiliteit van die katalis veral wanneer daar komponente in die voer is wat ’n negatiewe impak op die katalis kan hê. Byvoorbeeld, die teenwoordigheid van sure in die voer kan aanleiding gee tot die vorming van hoë koolstof getal produkte ten koste van die verlangde produk. Ander verbindings inhibeer die katalis wat dit ontoeganklik maak vir hidroformilering, tydelik of permanent. Die inhiberings effek van metiel viniel ketoon (MVK) op die gekose katalis sisteem is ondersoek terwyl beide die hoeveelhede PPh_3 en

xantphos gevarieer is met die doel om die ewewig na regs of links te skuif volgens die onderstaande skema:

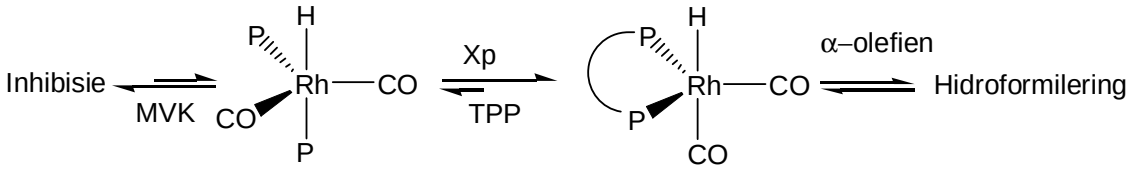

Hoe meer van die xantphos spesie gevorm is, hoe minder die inhiberings tyd en die ewewig is dus na regs verskuif. Hoe meer die PPh_3 konsentrasie hoe langer die inhiberings tyd as gevolg van die vermeerdering van die $[RhH(CO)_2(PPh_3)_2]$ spesie wat meer sensitief is vir MVK inhibering.

Sleutelwoorde: Homogene katalise, Hidroformilering, Rodium, Kobalt, Trifenielfosfien, Bidentate ligande, Xantphos, Kinetika en selektiwiteit, Inhibeerder, Metiel viniel ketoon, Hoëdruk-KMR, Hoëdruk-IR.

Apendix

Table 1. Crystal data and structure refinement for 5fkm1.

Identification code	5fkm1	
Empirical formula	C20 H20 Cl0.50 O0 P1.50 Rh0.50	
Formula weight	375.99	
Temperature	293(2) K	
Wavelength	0.71069 Å	
Crystal system	Orthorhombic	
Space group	Pbca	
Unit cell dimensions	a = 20.320(5) Å	□= 90.000(5)°.
	b = 7.911(5) Å	□= 90.000(5)°.
	c = 23.045(5) Å	□ = 90.000(5)°.
Volume	3705(3) $Å^3$	
Z	8	
Density (calculated)	1.348 Mg/m^3	
Absorption coefficient	0.689 mm^{-1}	
F(000)	1548	
Crystal size	? x ? x ? mm^3	
Theta range for data collection	5.15 to 28.28°.	
Index ranges	-23<=h<=26, -10<=k<=9, -18<=l<=30	
Reflections collected	15590	
Independent reflections	4524 [R(int) = 0.0803]	
Completeness to theta = 28.28°	98.3 %	
Refinement method	Full-matrix least-squares on F^2	
Data / restraints / parameters	4524 / 0 / 220	
Goodness-of-fit on F^2	0.989	
Final R indices [I>2sigma(I)]	R1 = 0.0432, wR2 = 0.0789	

R indices (all data)	R1 = 0.0998, wR2 = 0.0967
Largest diff. peak and hole	0.460 and -0.483 e.Å^{-3}

Table 2. Atomic coordinates (x 10^4) and equivalent isotropic displacement parameters ($Å^2$x 10^3) for 5fkm1. U(eq) is defined as one third of the trace of the orthogonalized U^{ij} tensor.

	x	y	z	U(eq)
Rh	5000	0	5000	11(1)
P(1)	4365(1)	1483(1)	5659(1)	10(1)
Cl	4005(1)	-458(3)	4481(1)	16(1)
O(1)	6211(4)	590(14)	5636(4)	16(1)
C(1)	5722(5)	363(15)	5392(5)	16(1)
C(11)	3842(2)	135(4)	6111(1)	12(1)
C(12)	3565(2)	749(4)	6620(1)	15(1)
C(13)	3182(2)	-304(4)	6963(1)	16(1)
C(14)	3068(2)	-1967(4)	6799(2)	17(1)
C(15)	3342(2)	-2574(4)	6291(2)	18(1)
C(16)	3726(2)	-1537(4)	5947(2)	16(1)
C(21)	3820(2)	2955(4)	5292(1)	11(1)
C(22)	4095(2)	3945(4)	4849(1)	15(1)
C(23)	3719(2)	5127(4)	4556(1)	19(1)
C(24)	3058(2)	5310(4)	4690(2)	20(1)
C(25)	2777(2)	4302(4)	5114(2)	19(1)
C(26)	3154(2)	3141(4)	5419(1)	15(1)
C(31)	4777(2)	2807(4)	6200(1)	12(1)
C(32)	4695(2)	4552(4)	6222(2)	15(1)
C(33)	5009(2)	5503(4)	6641(2)	21(1)
C(34)	5411(2)	4734(4)	7045(2)	21(1)
C(35)	5499(2)	3001(5)	7029(2)	21(1)
C(36)	5181(2)	2033(4)	6610(1)	16(1)
C(2)	3229(3)	2853(6)	8443(2)	44(1)
Cl(1)	3600(1)	3778(1)	7827(1)	35(1)
Cl(2)	2402(1)	2342(1)	8329(1)	39(1)

Table 3. Bond lengths [Å] and angles [°] for 5fkm1.

Rh-C(1)	1.747(9)
Rh-C(1)#1	1.747(9)
Rh-P(1)	2.3129(10)
Rh-P(1)#1	2.3129(10)
Rh-Cl#1	2.376(2)
Rh-Cl	2.376(2)
P(1)-C(21)	1.817(4)
P(1)-C(11)	1.830(3)
P(1)-C(31)	1.831(3)
Cl-C(1)#1	0.631(8)
O(1)-Cl#1	0.527(6)
O(1)-C(1)	1.156(10)
C(1)-Cl#1	0.631(8)
C(11)-C(12)	1.389(4)
C(11)-C(16)	1.397(4)
C(12)-C(13)	1.387(5)
C(13)-C(14)	1.389(5)
C(14)-C(15)	1.381(5)
C(15)-C(16)	1.382(5)
C(21)-C(26)	1.391(5)
C(21)-C(22)	1.404(5)
C(22)-C(23)	1.383(5)
C(23)-C(24)	1.385(5)
C(24)-C(25)	1.384(5)
C(25)-C(26)	1.387(5)
C(31)-C(32)	1.391(5)
C(31)-C(36)	1.393(5)
C(32)-C(33)	1.381(5)
C(33)-C(34)	1.380(5)
C(34)-C(35)	1.383(5)
C(35)-C(36)	1.392(5)
C(2)-Cl(2)	1.748(5)
C(2)-Cl(1)	1.766(5)

C(1)-Rh-C(1)#1	180.0(4)
C(1)-Rh-P(1)	92.6(4)
C(1)#1-Rh-P(1)	87.4(4)
C(1)-Rh-P(1)#1	87.4(4)
C(1)#1-Rh-P(1)#1	92.6(4)
P(1)-Rh-P(1)#1	180.00(3)
C(1)-Rh-Cl#1	1.2(4)
C(1)#1-Rh-Cl#1	178.8(4)
P(1)-Rh-Cl#1	93.85(6)
P(1)#1-Rh-Cl#1	86.15(6)
C(1)-Rh-Cl	178.8(4)
C(1)#1-Rh-Cl	1.2(4)
P(1)-Rh-Cl	86.15(6)
P(1)#1-Rh-Cl	93.85(6)
Cl#1-Rh-Cl	180.00(6)
C(21)-P(1)-C(11)	106.55(16)
C(21)-P(1)-C(31)	103.25(16)
C(11)-P(1)-C(31)	102.16(15)
C(21)-P(1)-Rh	111.07(11)
C(11)-P(1)-Rh	113.72(11)
C(31)-P(1)-Rh	118.85(12)
C(1)#1-Cl-Rh	3.4(10)
Cl#1-O(1)-C(1)	3.3(7)
Cl#1-C(1)-O(1)	2.8(6)
Cl#1-C(1)-Rh	175.4(14)
O(1)-C(1)-Rh	178.0(14)
C(12)-C(11)-C(16)	119.4(3)
C(12)-C(11)-P(1)	120.8(3)
C(16)-C(11)-P(1)	119.7(2)
C(13)-C(12)-C(11)	119.9(3)
C(12)-C(13)-C(14)	120.5(3)
C(15)-C(14)-C(13)	119.6(3)
C(14)-C(15)-C(16)	120.4(3)
C(15)-C(16)-C(11)	120.1(3)
C(26)-C(21)-C(22)	118.8(3)
C(26)-C(21)-P(1)	124.2(3)

C(22)-C(21)-P(1)	117.0(3)
C(23)-C(22)-C(21)	120.7(4)
C(22)-C(23)-C(24)	119.9(3)
C(25)-C(24)-C(23)	119.8(3)
C(24)-C(25)-C(26)	120.6(4)
C(25)-C(26)-C(21)	120.1(3)
C(32)-C(31)-C(36)	118.9(3)
C(32)-C(31)-P(1)	122.5(3)
C(36)-C(31)-P(1)	118.6(3)
C(33)-C(32)-C(31)	120.7(3)
C(34)-C(33)-C(32)	120.4(3)
C(33)-C(34)-C(35)	119.7(3)
C(34)-C(35)-C(36)	120.3(3)
C(35)-C(36)-C(31)	120.1(3)
Cl(2)-C(2)-Cl(1)	112.7(2)

Symmetry transformations used to generate equivalent atoms: #1 -x+1,-y,-z+1

Table 4. Anisotropic displacement parameters ($Å^2 x\ 10^3$) for 5fkm1. The anisotropic
displacement factor exponent takes the form: $-2\pi^2[\ h^2 a^{*2} U^{11} + ... + 2\ h\ k\ a^*\ b^*\ U^{12}\ ]$

	U^{11}	U^{22}	U^{33}	U^{23}	U^{13}	U^{12}
Rh	10(1)	14(1)	8(1)	-2(1)	0(1)	0(1)
P(1)	10(1)	13(1)	8(1)	-1(1)	1(1)	1(1)
Cl	11(2)	22(1)	14(2)	-5(1)	-4(1)	0(2)
O(1)	11(2)	22(1)	14(2)	-5(1)	-4(1)	0(2)
C(1)	11(2)	22(1)	14(2)	-5(1)	-4(1)	0(2)
C(11)	9(2)	16(2)	10(2)	0(1)	2(1)	1(2)
C(12)	14(2)	14(2)	15(2)	-1(1)	0(2)	1(2)
C(13)	14(2)	25(2)	9(2)	3(1)	1(1)	2(2)
C(14)	11(2)	22(2)	17(2)	8(1)	1(2)	-3(2)
C(15)	20(2)	16(2)	19(2)	1(1)	-1(2)	-3(2)
C(16)	15(2)	16(2)	16(2)	-1(1)	2(2)	2(2)
C(21)	12(2)	11(2)	10(2)	-4(1)	0(1)	-3(2)
C(22)	14(2)	17(2)	14(2)	1(1)	2(1)	1(2)
C(23)	25(2)	17(2)	14(2)	3(1)	0(2)	1(2)
C(24)	21(2)	22(2)	18(2)	1(1)	-5(2)	7(2)
C(25)	14(2)	22(2)	21(2)	-1(1)	-1(2)	6(2)
C(26)	17(2)	16(2)	12(2)	-1(1)	-1(2)	-4(2)
C(31)	9(2)	19(2)	8(2)	1(1)	3(1)	-1(2)
C(32)	14(2)	19(2)	13(2)	-2(1)	-1(2)	1(2)
C(33)	25(2)	13(2)	26(2)	-6(1)	-3(2)	-2(2)
C(34)	23(2)	27(2)	14(2)	-7(1)	-1(2)	-5(2)
C(35)	20(2)	28(2)	15(2)	2(1)	-6(2)	2(2)
C(36)	16(2)	19(2)	15(2)	2(1)	2(2)	-2(2)
C(2)	46(3)	63(3)	23(2)	0(2)	-7(2)	-8(3)
Cl(1)	44(1)	31(1)	31(1)	-7(1)	2(1)	-1(1)
Cl(2)	47(1)	46(1)	24(1)	-4(1)	-4(1)	-11(1)

Table 5. Hydrogen coordinates (x 10^4) and isotropic displacement parameters ($Å^2$x 10^3) for 5fkm1.

	x	y	z	U(eq)
H(12)	3636	1864	6731	18
H(13)	3000	107	7306	19
H(14)	2809	-2667	7028	20
H(15)	3267	-3689	6180	22
H(06)	3907	-1954	5605	19
H(22)	4536	3806	4751	18
H(23)	3909	5797	4270	23
H(24)	2804	6107	4496	24
H(25)	2330	4404	5195	23
H(26)	2962	2486	5708	18
H(32)	4425	5083	5951	18
H(33)	4949	6668	6652	26
H(34)	5622	5378	7327	25
H(35)	5772	2480	7299	25
H(21)	5239	867	6603	20
H(2A)	3468	1836	8546	53
H(2B)	3261	3633	8766	53

CHAPTER 1 ..... **1**
1 Introduction and Aim of the Study **1**
1.1 Introduction **1**
1.2 Aim of the study **2**
References **4**

CHAPTER 1

Introduction and Aim of the Study

1.1 Introduction

Despite being one of the oldest industrially commercialised processes, having been discovered in 1938,[1] the hydroformylation reaction is still actively studied today by a large number of scientists. In addition to this, more than 8 million tons/year of aldehydes and alcohols (oxo chemicals) are produced world-wide through a hydroformylation reaction.[2] Oxo chemicals find applications in a wide range of processes including detergents, adhesives, plastisizers and solvents. While rhodium processes produce primarily aldehydes, many industrial processes extend the production to alcohols from a subsequent hydrogenation of the corresponding aldehyde. Amongst many a ruthenium-based catalyst has been successfully used in selectively hydrogenating aldehydes to corresponding alcohols.[3] Detergent range alcohols lie in the C_{12}-C_{16} carbon number range, providing the primary feedstock for detergent intermediates for detergents manufactured in developed economies. The global market for detergent alcohols was 1.47 million tons in 2000 where over the medium term, a demand growth (volume based) of 3.0 % percent per year has been estimated.[4]

Oxo chemicals are mainly produced by either using a rhodium or a cobalt catalyst. Although rhodium offers high rates and selectivities, the downfall of the catalyst relative to other catalysts such as Co is its sensitivity towards poisons/inhibitors in the feed. The presence of components like dienes and/or unsaturated aldehydes leads to incubation periods where these chemicals should be reacted away before the catalyst can

hydroformylate the intended substrate. On the other hand, chemicals like sulphur will permanently deactivated the catalyst. The negative impact acids have on hydroformylation is the formation of “heavies” and the need to use expensive plant material due to corrosion issues. It is for these reasons that the olefinic feed has to be purified before commencing with the actual hydroformylation so as to remove unwanted components. Maintaining feed purification is a very expensive exercise; moreover, valuable feed is lost during the feed preparation. Due to cost implications involved in the washing of feedstock, investigations on inhibitor resistant catalysts were found to be a very valuable exercise. Obtaining a catalyst system that is tolerant to certain quantities of some inhibitors would allow the relaxation of the feed specifications resulting in major cost savings. Equally important, this inhibitor resistant catalyst should offer same or better rates and selectivities as those obtained with the traditional Rh-PPh_3 catalyst. These reasons therefore warrant research on this subject.

1.2 Aim of the study

It has recently been established that bidentate ligands such as 4,5-bis(diphenylphosphino)-9,9-dimethylxanthene (xantphos, Xp) have the potential to satisfy the above requirements.[5]. The xantphos ligand system results in remarkable selectivities, but unfortunately the reaction rates are low. It was therefore decided to investigate a mixed system where xantphos is employed with PPh_3 in an attempt to increase the rates whilst still retaining the benefits of xantphos ligand system, i.e. inhibitor resistance and high selectivities.

In this study, the following aspects will be addressed:

- A literature review on hydroformylation will be presented where more focus will be directed towards rhodium catalysis.

- The synthesis of xantphos and related ligands (DPEphos) will be highlighted. Rhodium catalyst precursors such as $[RhH(CO)(PPh_3)_3]$ and $[RhCl(PPh_3)_3]$ will be synthesised. The synthesis section will discuss crystallography and attempts will be made to grow crystals of the mixed catalyst and those of $[Rh(acac)(PPh_3)_2]$.
- Major techniques of characterisation include NMR and IR spectroscopy. In this study, both techniques will be employed to obtain complementary results. The value of performing *in situ* characterisation with both techniques will also be demonstrated
- Extensive autoclave studies will be conducted where rates and selectivities of the mixed system were investigated with the aim of deriving the rate equation as well as obtaining equilibrium constants. The inhibitor resistance of triphenylphosphine, xantphos, as well as mixed ligand catalyst systems will be extensively investigated by means of autoclave as well as spectroscopic studies. For comparison purposes, different bidentate ligands will be employed to study the effect of the bite angle on rates and selectivities.

References

1. Roelen, O.; U. S. Patent 2,317,006 **1943.**

2. Srivastava, V. K.; Sharma, S. K.; Shukla, R. S.; Subrahmanyam, N.; Jasra, R. V. *Ind. Eng. Chem. Res*. **2005**, *44*, 1764.

3. Ohkuma, T.; Ooka, H.; Ikariya, T.; Noyori, R. *J. Am. Chem. Soc.* **1995**, *117*, 10417.

4. Storck, W. J.; C&EN Northeast news bureau *Chemical and Engineering News* **20 January 2003**, *81(3)*, 21.

5. Van Leeuwen, P. W. N. M., private communication.

CHAPTER 2.....5
2 Rhodium Catalysed Hydroformylation Reactions.....5
2.1 An Introduction to hydroformylation: Rh and Co.....5
Rhodium.....8
2.2 Ligand effects.....12
2.3 Hydroformylation reactions.....16
2.4 Separation processes.....18
2.4.1 Distillation.....21
2.4.2 Extraction.....23
2.4.3 Precipitation.....24
2.4.4 Supported catalysis.....24
2.4.5 Biphasic separation.....25
2.5 Poisons/Inhibitors.....26
References.....30

CHAPTER 2

Rhodium Catalysed Hydroformylation Reactions

2.1 An Introduction to hydroformylation: Rh and Co

The economical feasibility of many chemical reactions is dependent on catalysis, be it for commodity or fine chemicals production. A catalyst is a substance that increases the rate at which a chemical reaction approaches equilibrium without itself being consumed or forming part of the product(s).[1] If a reaction is not thermodynamically viable a catalyst will not render it otherwise, thus a catalyst only lowers the barrier of the reaction's activation energy. Catalysts are normally first in the form of a precursor that should be activated following specific procedures before it can perform a specific task. Homogeneous catalysis is a reaction where the catalyst and the reactants are in the same phase as opposed to heterogeneous catalysis where the catalyst is normally in a solid state and the reactants in the liquid or gaseous state. In the case of homogeneous catalysis, the reactants and the catalyst are normally in the liquid phase. Though there are numerous heterogeneously catalysed processes, homogeneous catalysis has recently gained a lot of world-wide interest in industry. There has been an enormous growth in homogeneous catalysis with both academia and industry contributing significantly. A few selected comparisons between homogeneous and heterogeneous catalysis are shown in the table below.

Table 2.1. Homogeneous vs. Heterogeneous catalysis[2]

Homogeneous catalysis	Heterogeneous catalysis
Mechanisms are better understood.	Mechanisms usually less well understood.
Mild conditions are applicable.	Require harsh conditions.
High activity and selectivity.	Variable activity and selectivity.
Low thermal stability.	High thermal stability.
No diffusion limitations.	Limited by diffusion.
More flexible in variability of steric and electronic properties of a ligand and more predictable.	Less flexible and less predictable.
Expensive catalyst separation and recycling.	Usually no separation and recycling complications.

Hydroformylation was discovered by Otto Roelen in 1938 and was then known as “oxo synthesis” before the correct expression, hydroformylation, was later introduced.[2] Otto Roelen was heterogeneously trained and he discovered the “oxo synthesis” through serendipity following an attempt to increase the chain length of Fischer-Tropsch derived hydrocarbons. Hydroformylation is one of the most prominent homogeneously catalysed applications in industry. Hydroformylation reactions involve the reaction of an alkene with syngas (a mixture of H_2 and CO in a specified ratio) to yield an aldehyde or alcohol of one carbon number longer than the alkene as shown in Scheme 1.1. For simplicity sake, propene was used as a model feed in the scheme. Longer chain as well as internal and/or branched alkenes may be used. The scheme below summarises the major products formed, although a number of side products may also form in a typical hydroformylation reaction.

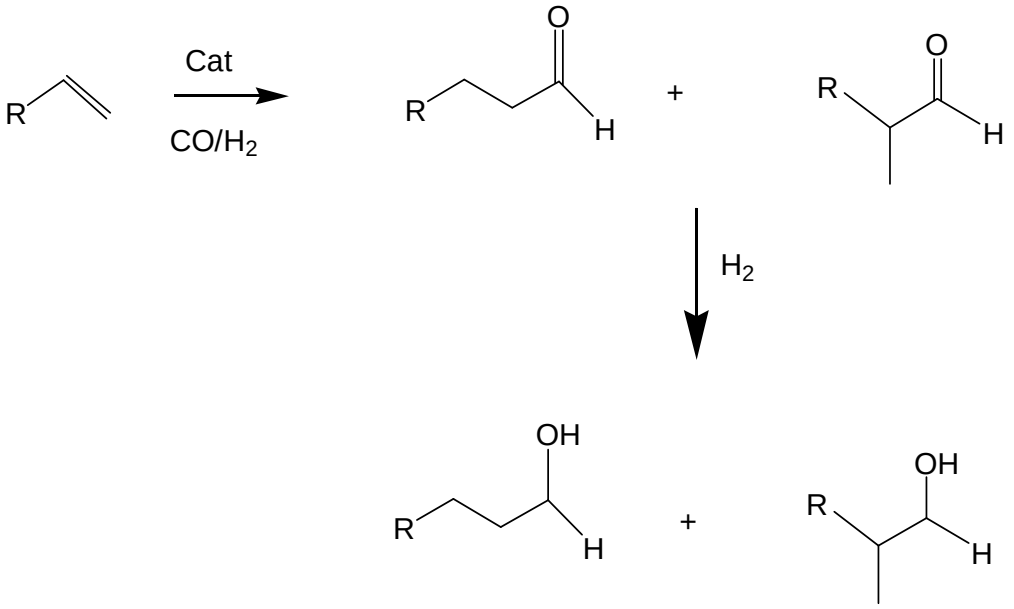

Scheme 2.1. Hydroformylation reaction

A number of metals have been studied with cobalt and rhodium being by far the most dominant ones. Within these two metals one may find the "modified" and the "unmodified" catalysis. The "modified" catalysis is where a ligand is used to bond to the metal centre in order to alter the properties of the catalyst. Amongst many potential ligands, traditional ones used are compounds containing phosphine, phosphite, nitrogen and sulphur. In the "unmodified" regime, no ligand is used, thus a metal precursor is used as is and preformed with syngas. The H_2:CO ratio in syngas may vary depending on the requirements of the process. The stoichiometry required by the rhodium process is a H_2:CO ratio of 1:1, whereas this is 2:1 with the modified cobalt process. The reason for this is that rhodium produces aldehyde, whereas modified cobalt will further hydrogenate the aldehyde to the corresponding alcohol. The advantage of this hydrogenation is that it occurs in the hydroformylation reactor. This represents a major cost saving as it eliminates a costly hydrogenation

section. However, a polishing hydrogenation section may be required to ensure complete conversion of the aldehyde to the corresponding alcohol, though it is normally much cheaper to operate because it is only a polishing step rather than a bulk hydrogenation, as is the case in rhodium processes.

The first generation of hydroformylation catalysts employed was cobalt without ligand, better known as unmodified cobalt hydroformylation. This was then followed by unmodified rhodium systems. The fist commercial application of unmodified rhodium hydroformylation was introduced by Mitsubishi in 1970.[3] Selected comparisons between cobalt and rhodium hydroformylation are tabulated below.

Table 2.2. Comparison between Cobalt and Rhodium hydroformylation[2]

Cobalt	**Rhodium**
Relatively cheap.	A very expensive metal.
Robust against many impurities normally found in the feed.	Rhodium is very sensitive towards feed impurities.
Best applicable to higher alkenes.	Used for lower alkenes (lower than C_{10} carbon chain).
Normally high concentrations needed relative to the feed.	Normally low concentrations.
Relatively harsh conditions are required, i.e. high temperatures and pressures.	Temperatures as mild as 70 °C and pressures as low as 15 bar have been used.
Rates are normally slow.	Relatively high rates can be obtained.

Although rhodium has been used extensively in hydroformylation and other homogeneously catalysed processes, it is a very expensive metal and thus very low loses can be tolerated. On the other hand tolerance of cobalt loses are high due to the fact that it is a cheap metal, however, recovery of the metal is still essential for environmental reasons.

Due to harsh conditions required in unmodified catalysis, the next generation of hydroformylation catalysts was developed, namely modified cobalt and rhodium where milder conditions relative to unmodified systems were applied. Although a wide range of ligands may be used for modified hydroformylation reactions, phosphine and phosphite ligands have been studied extensively. Incorporation of the ligand opened a wide scope in catalysis as it allowed for manipulation of selectivity and activity. Subtle changes in ligand properties can bring about very significant changes in activity and selectivity.

Modified rhodium hydroformylation involves the activation of a rhodium precursor with syngas and a ligand of choice to form the active hydride species. High pressure spectroscopic studies have helped tremendously in the understanding of the different catalytic species during the hydroformylation reaction. Amongst many known rhodium precursors, the widely used ones are $[RhH(CO)(PPh_3)_3]$ and $[Rh(CO)_2(acac)]$ (acac = acetylacetonato).

A simplified rhodium hydroformylation mechanism, as reported by Heck, is given below.[4] The hydride is a trigonal bipyramidal complex (**1**) which loses a ligand (CO/L) to form an unsaturated square planar species (**2**) which in turn opens a site that allows an alkene to bond to the metal centre (**3**) (Scheme 1.2). It has been shown through high-pressure spectroscopy that there is always an equilibrium between equatorial-equatorial (*ee*) and equatorial-axial (*ea*) orientation of the phosphine

ligands with (**1**). As can be seen from the scheme below, the preferred mechanism is the dissociative mechanism where there is a loss of a ligand before the incorporation of the alkene to form (**3**). The alkyl species (**4**) is formed through a migratory insertion of the hydride. After the incorporation of a CO to form a trigonal bipyramidal alkyl species (**5**), CO migratory insertion occurs to form the acyl species (**6**). While only the formation of the *n*-product is shown for simplicity sake, there is also a possibility of a branched product formation. Liberation of an aldehyde and introduction of a hydride reforms the square planar (**2**) and thus emphasising the characteristics of a catalyst, i.e. a catalyst should not be consumed or be permanently involved in a reaction.

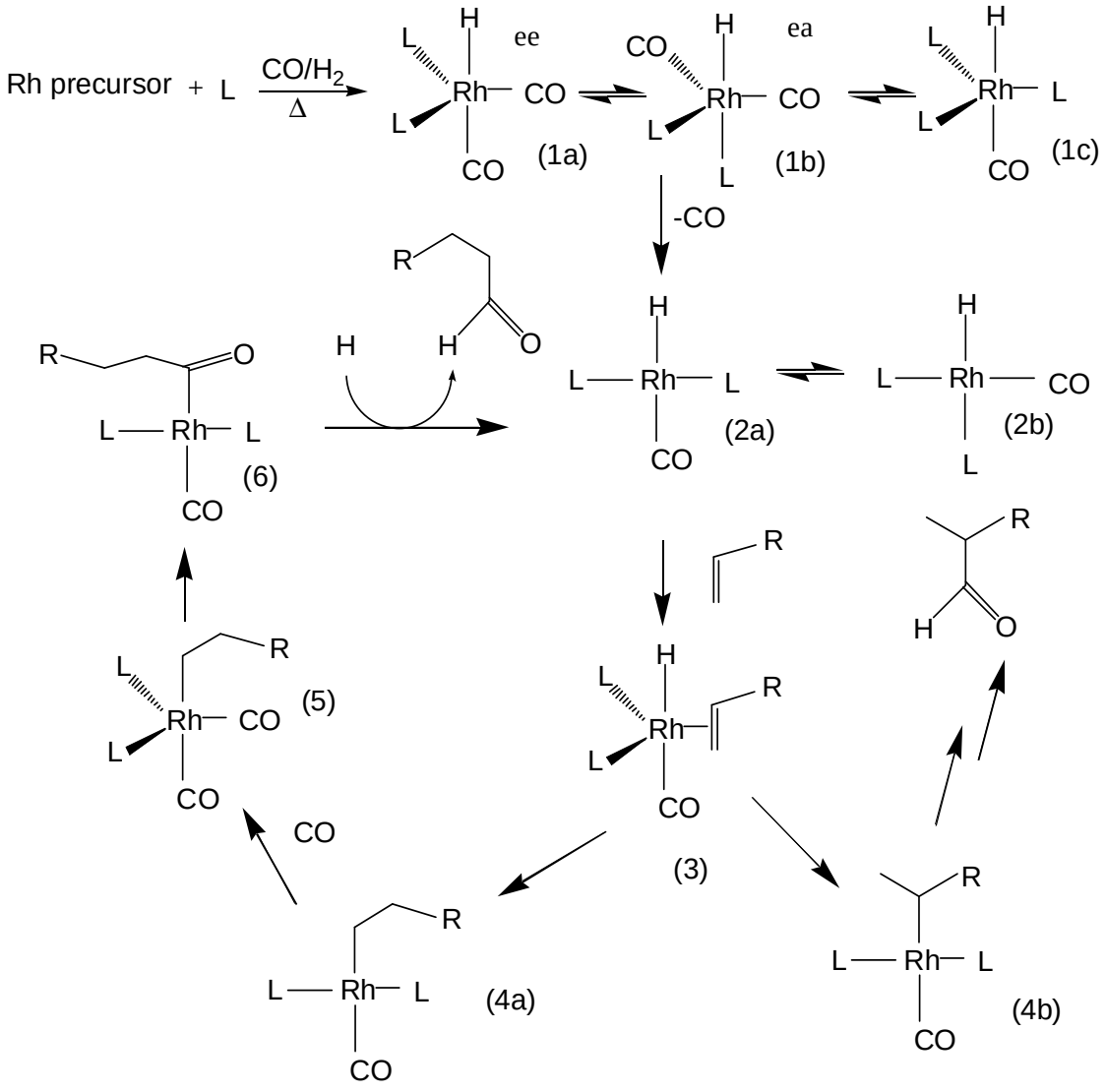

Scheme 2.2. Simplified rhodium hydroformylation mechanism.[4]

One of the undesirable side reactions is hydrogenation. This hydrogenation side reaction depends greatly on the syngas ratio, i.e. CO vs. H_2 partial pressures. Higher H_2 pressures will favour hydrogenation while higher CO pressures will favour the association of CO (**5**) to yield the desired product. In support of this, cobalt processes produce more alkane from the side reaction than rhodium because of a higher H_2 partial pressure used.[3] Another undesired side reaction is the formation of

heavies which is discussed later in more detail (Section 2.4). Isomerisation of the reactant also occurs to give internal alkenes that are difficult to hydroformylate, with rhodium resulting in residual alkene being present in the product, leading to lower conversions. The reason why one should minimise or totally eliminate (if possible) side reactions is two fold. Reactant loses from these side reactions resulting in decreased production output can be very costly and separation of these side products results in more costs, moreover, may cause complications.

2.2 Ligand effects

Since the linear aldehyde is usually the most desired isomer, extensive studies have been carried out to investigate the effect of ligands on linearity of the product and subsequently to drive the reactions towards the linear product. Studies of ligands also included the effect of the ligand on activity and catalyst stability. Amongst many ligands that can be applied in hydroformylation reactions, phosphine and phosphite ligands were studied in depth. Arylphosphines were found to be the best ligands for rhodium due to their superior performance in comparison to their alkylphosphine counterparts.[5] Phosphite ligands give faster hydroformylation rates than phosphine ligands due to increased π-back bonding from the metal resulting from the presence of electron withdrawing substituents on the ligand.[6] The strength of metal to ligand bond depends greatly on π-back bonding and this has a direct effect on the rate of hydroformylation. Because phosphite ligands are π-acceptors, the metal to ligand bond is stronger and this results in a facile CO dissociation and a subsequent stronger alkene association. In comparison to their phosphine counterparts, phosphite ligands are easier to prepare and stable towards oxidation, but are very sensitive towards hydrolysis.

Ligand effects on reactions were originally rationalised in terms of electronic effects and steric effects were only later realised to be just as important, the latter being highlighted by the work of Tolman.[7] The Tolman cone angle was defined for monodentate phosphorous ligands as the apex angle of a cylindrical cone, centred at 2.28 Å from the centre of the P atom, which is large enough to enclose the van der Waals radii of the outermost atoms of the ligand.

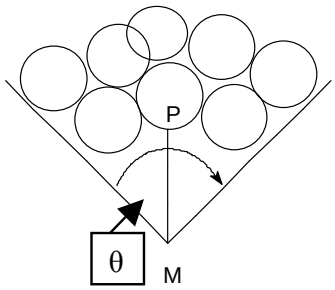

Figure 2.1. Cone angle

The cone angle measurement is a method employed to measure the steric bulk of monodentate phosphine and phosphite ligands. It was found that an increase in the steric bulkiness of monodentate phosphine ligands leads to higher regioselectivity in hydroformylation reactions. Although bulky phosphites may display high reaction rates, they do not always give high n:iso ratios as is the case with P(O-*t*But)$_3$ where n:iso ratios as low as 1:1 may be obtained.

During the studies of understanding the ligand effect on Rh hydroformylation systems, the natural bite angle, $\beta n_{,}$ was defined by Casey and Whiteker as the preferred chelation angle determined only by ligand backbone constraints and not metal valence angles.[8]

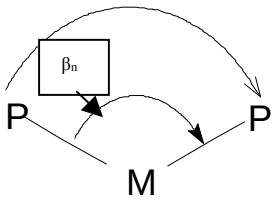

Figure 2.2. Bite angle

Van Leeuwen and co-workers recently illustrated the importance of the bite angle for bidentate ligand systems on the catalytic behaviour. It was revealed that bidentate ligands with wider bite angles yield considerably higher n:iso aldehyde ratios than the ligands with narrower bite angles.[9] This observation was attributed mainly to steric effects. It has been shown that ligands with wider bite angles will preferentially co-ordinate in an equatorial-equatorial (*ee*) fashion leading to the linear product due to steric constrains while the narrower bite angle ligands will populate the equatorial-axial (*ea*) isomer leading to the branched product. The *ee* co-ordination of bidentate ligands is also superior to that of monodentate ligands except under special conditions where very high ligand concentrations are used.

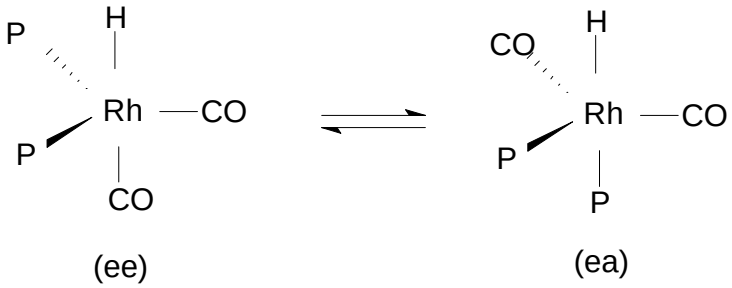

Scheme 2.3. Co-ordination structures. ee vs. ea

Depending on the backbone in bidentate ligands, chelation may stabilise specific geometries. Chelating ligands preferring bite angles of 90° would

for instance stabilise square planar geometries. Wider bite angles would then induce distortions of certain geometries and since this will have a huge impact on activity and selectivity of reactions, alternative reaction pathways can become accessible. Xantphos ligand displayed enhanced preference for *ee* chelation and this lead to more studies being conducted on xantphos derivatives. Due to their well-defined bite angle, these ligands do not only stabilize the *ee* co-ordination mode in trigonal bipyramidal Rh complexes, but also stabilise a tetrahedral over a square planar geometry. It should, however, be noted that not all bidentate ligands with well defined bite angles behave in this way.

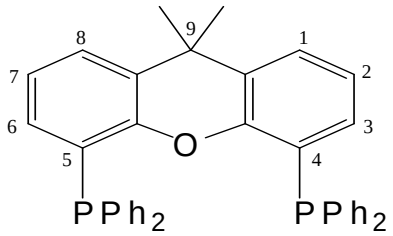

Figure 2.3 4,5-Bis(diphenylphosphino)-9,9-dimethylxanthene commonly known as xantphos (Xp)

A series of xantphos ligands with a range of natural bite angle size was studied on a quest to investigate the effect of bite angle on activity and selectivity in the hydroformylation reaction. Substitution of the standard diphenylphosphine moieties was found to have a direct influence on the ligand bite angle size. Direct correlations between the bite angle size and selectivity towards linear aldehyde were displayed[10] with wider natural bite angles giving more of the linear aldehyde. The basicity of the phosphine also plays a big role where the lower basicity leads to higher activities.

2.3 Hydroformylation reactions

In order to obtain a better understanding on the xantphos system, the literature on xantphos derivatives was studied with special reference to their behaviour in hydroformylation reactions. It was revealed that the most direct way of attaining a range of different bite angles i.e. ligands with various bulkiness, is by changing substituents (X) on position 9 (Fig 2.4.).

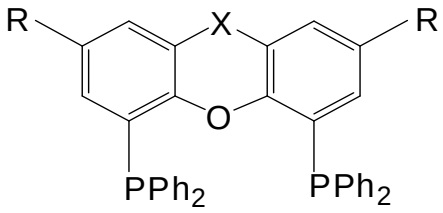

Figure 2.4. Xantphos derivatives skeleton to enable functionalisation.

This literature survey compared the behaviour of different ligands in hydroformylation reactions carried out at 80° C and 20 bar with a 1.0 mM rhodium phosphine solution prepared from $[Rh(CO)_2(acac)]$. Phosphine molar equivalences of 5 relative to rhodium were used. High selectivies towards linear aldehyde were obtained with xantphos ligands and selectivities generally increased with an increase in bite angle. Introduction of phosphacycles resulted in considerably higher activities. Ligands were designed in a way that electronic differences were minimal so that only steric effects were studied and the following selected ligands were investigated (see Table 2.3.).

Table 2.3. Xantphos derivatives and their natural bite angles[10]

Ligand	X[b]	R[b]	βn[a] (deg)	l:b ratio[c]	% linearity[d]
Phosxantphos (1)	PPh	H	107.9	0.68	40.4
Sixantphos (2)	$Si(CH_3)_2$	H	108.7	1.13	53.0
Thixantphos (3)	S	CH_3	109.4	1.22	54.9
Xantphos (4)	$C(CH_3)_2$	H	111.7	1.45	59.1
Isopropxantphos (5)	$C{=}C(CH_3)_2$	H	113.2	1.45	59.1
Nixantphos (6)	NH	H	114.2	2.04	67.0
Benzoxantphos (7)	Fused benzene ring	H	120.6	1.78	64.1

a) Natural bite angle expressed in degrees.
b) Use Figure 2.3 as a guideline.
c) Calculated as the total linear aldehyde over the total branched aldehyde ratio.
d) Calculated as the percentage of the total linear aldehyde over the total aldehyde formed.

Synthesis of these bisphosphine xanthene type ligands will be discussed later in this chapter. To summarise, the synthesis involves dilithiation of the desired xantphos backbone using butyllithium/TMEDA (tertamethylethylenediamine) and a subsequent reaction with two equivalents of chlorodiphenylphosphine to yield the desired ligand.

The observed P···P distance of 4.080 Å for the free ligand **(4)** was reported where molecular modelling studies indicated that a decrease to 3.84 Å was necessary for chelation with a P–Rh–P angle of 111.7°. This decrease is attained by a decrease of the angle between the two phenyl planes in the backbone of the ligand from ca. 166° to 158°. Crystal structures of these ligands were also studied with Rh complexes to investigate the effect of the natural bite angle on chelation behaviour. $[Rh(H)(CO)(PPh_3)_3]$ was reacted with a bisphosphine to obtain $[Rh(H)(CO)(PPh_3)$(bisphosphine)] through a displacement of two PPh_3 by the bisphosphine. Crystal structures of ligands **(6)** and **(7)** were studied in

more detail. These complexes reveal a distorted trigonal bipyramidal geometry with all phosphines occupying equatorial sites.

2.4 Separation processes

Activity and selectivity are of great importance when developing a process and are normally cost drivers. If the activity of the catalytic reaction is too low, it has a negative impact on the size of the production. In order for a slow catalytic reaction to meet economic demands when building a commercial plant, large reactors are required and this has a negative impact on the cost of the process. One way of improving the reaction rate is by increasing the metal concentration, which also has a negative impact on the cost of the process, especially with rhodium being a very expensive metal. More metal usage may also lead to more loses through the formation of metal-clusters and other related unwanted reactions the metal will be subjected to. Poor selectivities are no better than low activities because reactant loses to undesired side products formed are just as costly in their own way. If, for instance, a process of 100 kilo tons per annum (kt/a) has a 90 % selectivity and 10 % loss of reactant that translates into a 10 kt/a loss. This kind of loss puts serious constraints on the cost of the product versus cost of the reactant in order for a process to make a reasonable profit. A large amount of undesired products formed occupy a lot of reactor volume rendering it a lot less useful. As a result, an even bigger reactor will be required to provide more volume in order for a process to produce a specific amount of product in a given time. Other undesired side reactions include heavies formation. This is the reaction where the reactants and/or the product react to give a much heavier (higher boiling) products. In the case of hydroformylation, possible reactions that are likely to give rise to heavy products, and should be minimised or eliminated where possible, are aldol condensations, acetal formation and esterification.[11]

➢ Aldol condensation: 'Aldol' is an abbreviation of **ald**ehyde and alcoh**ol**. When the enolate of an aldehyde or a ketone reacts at the α-carbon with the carbonyl of another molecule under basic or acidic conditions to obtain a *β*-hydroxy aldehyde or ketone, this reaction is called an Aldol reaction. In some cases, the adducts obtained from the Aldol addition can easily be converted (*in situ*) to α,β-unsaturated carbonyl compounds, either thermally or under acidic or basic catalysis. The formation of the conjugated system is the driving force for this spontaneous dehydration.

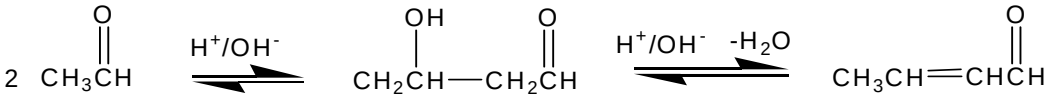

Scheme 2.4. A simplified Aldol condensation scheme

➢ Acetal formation: Acetals are geminal-diether derivatives of aldehydes or ketones. They are formed by an acid catalysed reaction of two equivalents of an alcohol and a subsequent dehydation reaction with alcohols or diols.

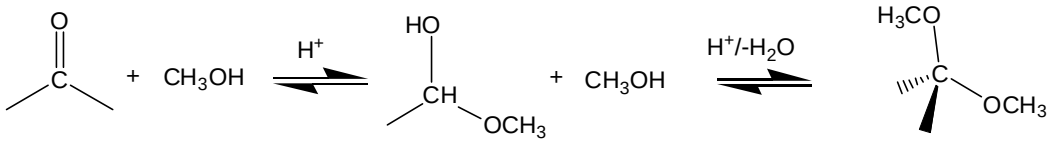

Scheme 2.5. A simplified Acetal formation scheme

➢ Esterification: Yet another acid catalysed reaction of heavies formation. Esterification entails an acid catalysed reaction of carboxylic acids and alcohols to form esters

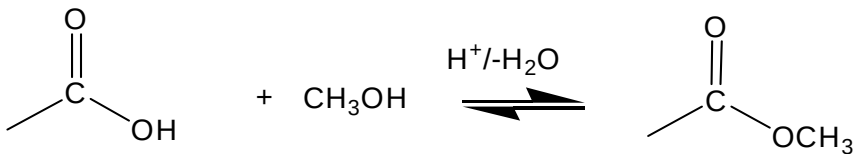

Scheme 2.6. A simplified Esterification reaction

In some instances, the boiling point the heavies formed will overlap with the ligand, making recovery by distillation complicated, if not impossible. In continuous processes, more heavies formed result in more frequent purge to minimise, as well as to regulate, the amount of unwanted material in the reactor. This subsequently leads to more catalyst loses that are highly undesirable especially when working with expensive rhodium and bidentate phosphine/phosphite ligands. The fact that these reactions are acid or base catalysed necessitates proper feed preparation to remove these unfavourable components. In the feed preparation process, other unwanted material that will negatively affect the selectivity and/or activity of the desired hydroformylation reaction also needs to be removed. Another negative impact impurities may have on the reaction is the inhibition and/or poisoning effect on the catalyst and this topic is discussed below (Section 2.5).

Major shortcomings of homogeneous catalysis are the problems associated with separation. The reason for this is that the catalyst is in the same phase as that of the reactants and in most cases the product(s) as well. A catalyst needs to be recovered while the product is collected, together with any other material removed from the reactor, to allow for more reactants to be introduced into the reactor. It is very important to not only recover the catalyst, but also to be able to recycle and regenerate it as this has a major impact on the process economics, especially with

expensive catalysts like rhodium systems. Apart from economics, environmental issues also play a vital role in industry and thus recovery of all materials is of paramount concern. Disposing of unwanted material into the environment can lead to heavy penalties that have to be paid. More unwanted products formed result in more costly separations. This is yet another reason why it is very important for the process to be as highly selective as possible. A few selected separation techniques are listed below.

2.4.1 Distillation

The most traditional separation technique used is distillation, where the components to be separated are done so according to their boiling points. A process can have binary distillation where there are only two components to separate or a multi-component distillation that involves the separation of a mixture of chemicals and can be a lot more complex than the former. A lot of processes require multi-component distillation as there are normally more than two chemicals to separate due to factors like side reactions, unreacted material, the solvent and the catalyst. Studies have been conducted to make the multi-component distillation economical by minimizing the energy demands and this has led to thermally coupled distillation sequences.[12,13] Distillation may occur in a batch or a continuous mode.

Amongst many, the major problems that limit distillation processes are close-boilers (chemicals boiling at temperatures very close to each other) and azeotropes (systems where the vapour and the liquid reach the same composition at some point in the distillation, at which point no further separation can occur). Other problems that may require using special

system configurations include heat sensitive materials. While close boilers are economic problems that can be overcome by distillation equipment manipulations, azeotropic systems are fundamental thermodynamic problems. Different ways to get around these problems include using other techniques such as membranes/dendrimers, crystallization, adsorption, adduction, extraction, and precipitation; a few of which will be briefly discussed below. Other ways involve using complex distillation configurations, changing system conditions or adding extra chemicals to the process as in extractive distillation. Extractive distillation is defined as distillation in the presence of a miscible, high boiling, relatively nonvolatile component, the solvent, that forms no azeotropes with the other components in the mixture. In the extractive column, the component having the greater volatility, not necessarily the component having the lowest boiling point, is taken overhead as a relatively pure distillate. The other components leave with the solvent via the column bottoms where the solvent is subsequently separated from the remaining components in a second distillation column and then recycled back to the first column. The choice of solvent should be such that it interacts differently with the components of the original mixture, thereby altering their relative volatilities to enable separation. One disadvantage of extractive distillation is the large volumes of solvent used. To overcome this shortcoming, salt-containing extractive distillation may be applied to improve solvent efficiency and reduce the solvent consumption.[14] Another applied distillation technique is reactive distillation. Reactive distillation uses a reaction in the distillation equipment to aid the separation. One example of reactive distillation is in the production of methyl acetate through the reaction between acetic acid and methanol.[15] This reaction has equilibrium constrains that require complex separation processes due to the two methyl acetate-methanol and methyl acetate-water azeotropes.

2.4.2 Extraction

Liquid-liquid extraction is a mass transfer operation in which a liquid solution (the feed) is contacted with an immiscible or nearly immiscible liquid (solvent) that exhibits preferential affinity or selectivity towards one or more of the components in the feed.[16,17] As a result, two streams are generated in the process: the extract, which is the solvent rich solution containing the desired extracted solute, and the raffinate, the residual feed solution containing little solute. It is through this process a homogeneous catalyst may be separated from the product and other chemicals. For the extraction to be effective, a careful evaluation of solvent selection is vital. Solvents differ in their extraction capabilities depending on their own and the solute's chemical structure. Also, the solvent should be easily recoverable for recycle. Other factors affecting solvent selection are boiling point, density, interfacial tension, viscosity, corrosiveness, flammability, toxicity, stability, compatibility with product, availability and cost. Together with solvent selection, operating conditions, mode of operation, extractor type and design criteria are crucial in ensuring effective extraction. One disadvantage of extraction is the formation of emulsions which may be due to over agitation and in such cases, settling needs to be carried out over an extended period. Emulsions can also form due to the inherent nature of the chemical compounds involved or due to contaminants that substantially lower the interfacial tension. Sometimes coagulants are added to prevent or minimize emulsification. While the most traditional method of extraction is aqueous extraction (liquid-liquid extraction), there are many other innovative methods known such as solid-phase extraction, flourous-phase extraction and solid-supported liquid-liquid extraction.[18] These are the extraction techniques that may be used to overcome emulsion shortcomings.

2.4.3 Precipitation

This technique involves separating a substance from a solution in a solid form.[19,20] In the homogeneous catalyst context, this process translates to precipitating out the catalyst in a salt form and subsequently decanting the liquid that will mostly consist of the product and other reaction materials. The two streams can then be worked up to recover the product and the catalyst for recycling. Although this technique may work very effectively, it is normally very complicated and not convenient for homogeneous processes, as it is not strictly homogeneous. Salt formation translates to solids and solids are normally difficult to handle, especially in large quantities.

2.4.4 Supported catalysis

Another innovative method applied to overcome separation shortcomings in homogeneous catalysis is the use of support surfaces thereby immobilising the catalyst. Although the surface may be a solid, the reaction may still be deemed homogeneous as the catalyst itself and reagents are all in the same phase, normally the liquid phase. This technique entails supporting the catalyst on a solid support during catalysis and subsequently performing a simple filtration and washing purification upon completion of the reaction. For example, despite it's enormous advantages, the Wilkinson's catalyst suffers from separation of the catalyst from the product which is the intrinsic disadvantage of all homogeneous catalysts. Studies have been undertaken to address this issue where the catalyst was immobilised and selective hydrogenation of a variety of alkenes and terminal alkynes performed.[21] In order to attain high rates and selectivities using supported catalysis, silica was used as a support where xantphos ligands were applied.[22] Dendrimers, to support

catalysts, have also been used as a technique of addressing separation issues in homogeneous catalysis .[23, 24]

2.4.5 Biphasic separation

Biphasic catalysis is another effective technique used for catalyst separation and recycling. The idea behind a biphasic reaction mode is to have the catalyst in one phase and the products in the other thereby allowing for a simple separation through decanting. The product phase should retain as much product and other material as possible to minimise or eliminate contamination of the catalyst phase. Contaminated catalyst phase would require not only tedious but also expensive work up to render catalyst recycling feasible. In some unfortunate instances, contamination of the catalyst phase may lead to poisoning and/or inhibition of the catalyst making regeneration difficult or even impossible. Catalyst inhibition and poisoning are discussed below under Section 2.5. The catalyst phase solvent should be carefully chosen such that negligible amounts, if none at all, of the catalyst leach out into the product phase to limit catalyst loses. Catalyst loses as low as parts per million (ppm) levels may be costly in continuos systems, especially when working with precious metals like rhodium. Retaining or even improving on the integrity of the catalyst is one crucial property a catalyst phase solvent should also possess. Activity and selectivity are major markers of a good catalyst and should therefore not be compromised. In the process of resolving separation issues, catalyst activity and selectivity still remain vital properties that warrant attention. Equally important is the stability of the catalyst that should never be left unnoticed especially in continuous systems.

Aqueous catalysis has been used but is unfortunately limited to lower alkenes due to the low water solubility of higher alkenes and it is for this reason that ionic liquids may be used for higher alkenes.[25] Ionic liquids,

molten salts consisting of ion pairs, have gained a lot of interest in biphasic catalysis. These novel solvents have been successfully applied to overcome separation issues in homogeneous catalysis through biphasic catalysis. By changing the nature of the cations and anions of the ionic liquid, one can optimise the reaction rate, regioselectivity as well as the retention of the catalyst and hydroformylation reactions have been carried out with these solvents.[26,27] Even xantphos-ligands have been studied and they have shown high overall activity and regioselectivity in the biphasic hydroformylation of octene.[28] Also, methods to recycle homogeneous catalysts from monophasic reaction mixtures using ionic liquids have been studied.[29] The use of ionic liquids allowed for a successful catalyst recycling while retaining selectivity and activity, without the need of additional regeneration of the active catalyst. One other important advantage of ionic liquids is the stability they confer to the catalyst against thermal stress normally experienced during distillation.

2.5 Poisons/Inhibitors

Along with kinetics and separation, catalyst stability is the most important aspect in homogeneous catalysis. Catalyst stability studies include deactivation and regeneration as these are of paramount importance in continuous processes. There are substances normally found in the feedstock that will poison/inhibit the catalyst thereby preventing it from following the desired mechanism. A catalyst can either be temporarily trapped and later released to perform the desired reaction or it can be permanently trapped where it cannot perform the desired task. A temporarily trapped catalyst is normally referred to as being inhibited or at certain times it can be referred to be undergoing an incubation or induction period. This is the period during which an active catalyst is preformed from the precursor as can be seen from Scheme 2.7. Substances that temporarily tie the catalyst up and are reacted away under the reaction

conditions resulting in the release of the catalyst to perform the desired reaction are said to be inhibitors. There are numerous potential inhibitors including dienes, alkynes and unsaturated ketones/aldehydes. In the case of hydroformylation with the rhodium system, these are inhibitors that will preferably bind to the metal centre prohibiting alkene co-ordination, but are later reacted away to release the catalyst to perform hydroformylation. The most feasible way of reacting these inhibitors away under hydroformylation conditions is through hydrogenation and/or, hydroformylation. Studies have been conducted on the effect of these inhibitors on the rhodium catalyst with more emphasis on methyl vinyl ketone (MVK) due to its more pronounced inhibition effect relative to conjugated alkenes and alkynes.[30] $[Rh(CO)_2(acac)]$ was used as the catalyst precursor with PPh_3 as the ligand of choice. In order to obtain as much useful information from the inhibition process as possible, High Pressure Infra Red (HP-IR) was used in conjunction with High Pressure Nuclear Magnetic Resonance (HP-NMR) spectroscopy.

The catalysts precursor was allowed to react with PPh_3 under a syngas atmosphere for the pre-forming to take place (**1** of Scheme 2.7). Studies revealed that there would always be an equilibrium between different hydride isomers **1a** (*ee*) and **1b** (*ea*) where a high excess of PPh_3 may result in the population of the tri-substituted species (**1c**). After the pre-forming process, MVK was added to investigate its effect on the catalyst. As the reaction of (1) with MVK was fast and gave a mixture of compounds, a model catalyst $[RhH(CO)(PPh_3)_3]$ was used and the solution cooled to get a detailed understanding of the inhibition mechanism. The mechanism is believed to be through a nucleophilic attack by the oxygen on the rhodium centre with a subsequent hydride migratory insertion to form an enolate (**2** in Scheme 2.7). Although only two enolate isomers are shown, two more isomers may be present where the two methyl groups are either *cis* or *trans* relative to the double bond.

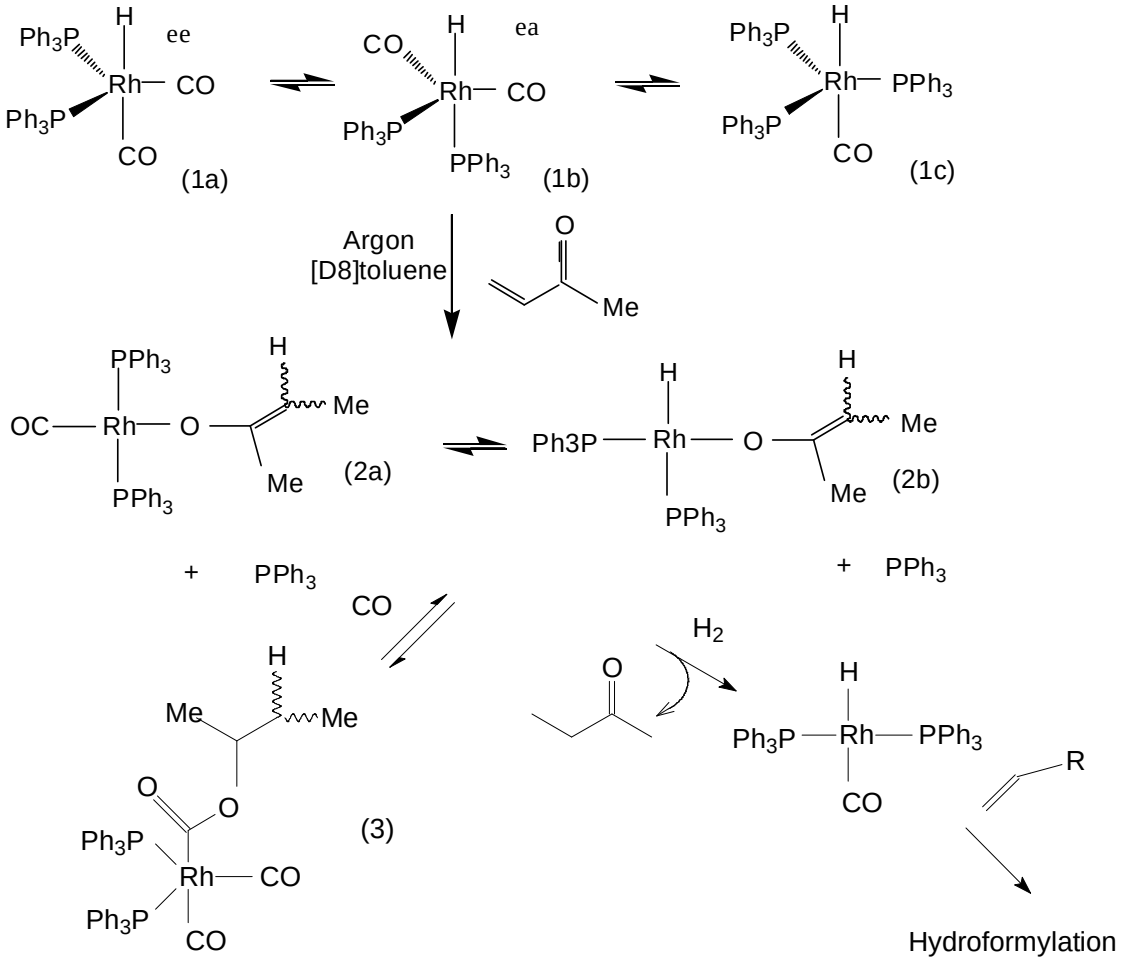

Scheme 2.7. A proposed inhibition scheme of the rhodium hydride by methyl vinyl ketone (MVK).[30]

NMR and HP-IR spectroscopy were used to characterise the enolate and other catalytic species formed under hydroformylation conditions. Reacting the formed enolate with CO resulted in the association of the CO to form the five co-ordinated enolate species and a subsequent migratory insertion step to form the acyl species which is most likely the resting state of the inhibited species. This species was unambiguously characterised by detailed NMR techniques including correlation and simulation studies. A reaction with hydrogen results in hydrogenation of the inhibitor thereby liberating the catalyst to hydroformylation. In the case of dienes, the

catalyst may be inhibited as a π-allyl species as illustrated below. The catalyst can be liberated either by the hydrogenation or hydroformylation of the alkene.

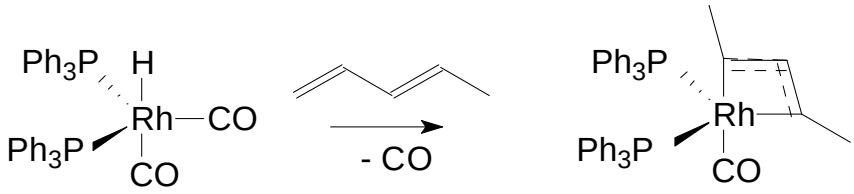

Scheme 2.8. Catalyst inhibition by a conjugated alkene.

Two additional ways in which the catalyst may be deactivated: The one is through the presence of other metals that will scavenge the ligand thereby making it unavailable for the active catalyst pre-forming or stabilisation. A deficiency of ligand(s) to the metal centre may lead to unmodified catalysis that normally only reacts under much harsher conditions than those of modified catalysis. The second route is in the presence of substances such as NO_x compounds that may form strong bonds with the metal centre thereby blocking a vacant space for the association of the ligand and/or the feed. These are severe circumstances as they normally lead to catalyst poisoning, meaning that the catalyst is permanently removed from the system.

References

1. Van Leeuwen, P.W.N. M. *Homogeneous Catalysis: Understanding the Art* University of Amsterdam, Amsterdam, The Netherlands **2004**.
2. Cornils, B.; Herrmann,W. A.; *Applied Homogeneous Catalysis with Organometallic Compounds*, New York, **1996**, Volume 2.
3. Van Leeuwen, P.W. N. M.; *Introduction to Hydroformylation*.
4. Heck, R. F.; Breslow, D. S. *J. Am. Chem. Soc.* **1961**, *83*, 4023.
5. Young, J.; Obson, J. A.; Jardine, F. A.; Wilkinson, G. *J. Chem. Soc. Chem. Comm.* **1965**, 131.
6. Van der Veen, L. A.; Boele, M. D. K.; Bregman, F. R.; Kamer, P. C. J.; Van Leeuven, P. W. N. M.; Goubitz, K.; Fraanje, J.; Schenk, H.; Bo, C. *J. Am. Chem. Soc.* **1998**, *120*, 11616.
7. a) Tolman, C. A. *Chem. Rev*. **1977**, *77*, 313.
b) Tolman, C. A. *J. Am. Chem. Soc.* **1970**, *92*, 2953.
8. Casey, C. P.; Whiteker, G. T. *Isr. J. Chem.* **1990**, *30*, 299.
9. Van Leeuven, P. W. N. M.; Kamer, P. C. J.; Reek, J. N. H. *Pure Appl. Chem.* **1999**, *71*, 1443.
10. Van der Veen, L. A.; Keeven, P. H.; Schoemaker, G. C.; Reek, J. N. H.; Kamer, P. C. J.; Van Leeuwen, P. W. N. M.; Lutz, M.; Spek, A. L. *Organometallics* **2000**, *19*, 872.
11. McMurry, J.; Organic Chemistry: Fourth Edition.
12. Olga, A.F.; Cardenas, J. C.; Hernandez, S.; Rico-Ramirez, V. *Ind. Eng. Chem. Res.* **2003**, *42*, 5940.
13. Agrawal, R.; Fidkowski, Z. T. *Ind. Eng. Chem. Res.* **1998**, *37*, 3444.
14. Fu, J. *Ind. Eng. Chem. Res.* **2004**, *43*, 1274.
15. Citro, F.; Lee, J. W. *Ind. Eng. Chem. Res.* **2004**, *43*, 375.
16. Robbins; *Chem. Eng. Prog.* **1980**, *76(10)*, 58.
17. Cusack, R.W.; Glatz, D. *A Fresh Look at Liquid-Liquid Extraction, Chemical Engineering* **1991**.

18. Breitenbucher, J. G.; Arienti, K. L.; McClure, K.J. *J. Comb. Chem.* **2001**, *3*, 528.

19. Bergbreiter, D. E.; Hughes, R.; Besinaiz, J.; Li, C.; Osburn, P. L. *J. Am. Chem. Soc.* **2003**, *125*, 8244.

20. Dickerson, T. J.; Reed, N. N.; Janda, K. D. *Chem. Rev.* **2002**, *102*, 3325.

21. Arstad, E.; Barret, A. G. M.; Tedeschi, L. *Tetrahedron Lett.* **2003**, *44*, 2703.

22. Van Leeuwen, P. W. N. M.; Sandee, A. J.; Reek, J. N. H.; Kamer, P. C. J. *J. Mol. Cat. A: Chem.* **2002**, *182*, 107.

23. Bourque, S. C.; Maltais, F.; Xiao, W.-J.; Tardiff, O.; Alper, H.; Arya, P.; Manzer, L. E. *J. Am. Chem. Soc.* **1999**, *121*, 3035.

24. Bourque, S. C.; Alper, H.; Manzer, L. E.; Arya, P. *J. Am. Chem. Soc.* **2000**, *122*, 956.

25.http://scholar.lib.vt.edu/theses/available/etd-5217143049751491/unrestricted/etd.pdf

26. Favre, F.; Olivier-Bourbigou, H.; Commereuc, D.; Saussine, L. *Chem. Commun.* **2001**, 1360.

27. Stenzel, O.; Raubenheimer, H. G.; Esterhuysen, C. *J. Chem. Soc. Dalton Trans.* **2002**, 1132.

28. Wasserscheid, P.; Waffenschmidt, H.; Machnitzki, P.; Kottsieper, W. K.; Stelzer, O. *Chem. Commun.* **2001**, 451.

29. Keim, W.; Vogt, D.; Waffenschmidt, H.; Wasserscheid, P. *J. Catal.* **1999**, *186*, 481.

30. Walczuk, E. B.; Kamer, P. C. J.; Van Leeuwen, P. W. N. M.; *Angew. Chem. Int. Ed.* **2003**, *42*, 4665.

CHAPTER 3 32
3 Synthesis and Characterisation of Rhodium Complexes and Free Ligands 32
3.1 Synthesis 32
3.1.1 Synthesis of 4,5-Bis(diphenylphosphino)-9,9-dimethylxanthene. 33
3.1.2 Synthesis of (Oxydi-2,1-phenylene)bis(diphenylphosphine)[1] 34
3.1.3 Synthesis of $[RhH(CO)(PPh_3)_3]$ 34
3.1.4 Synthesis of $[RhCl(PPh_3)_3]$[2] 35
3.1.5 [Rh(acac)(PP)] complexes 36
3.1.6 $[RhH(CO)(PPh_3)PP]$ complexes 37
3.2 Crystallographic characterisation of studied rhodium complexes 40
3.2.1 Introduction 40
3.2.2 Results and Discussion: X-ray structure of *trans*-$[RhCl(CO)(PPh_3)_2]$ 40
References 48

CHAPTER 3

Synthesis and Characterisation of Rhodium Complexes and Free Ligands

3.1 Synthesis

Transition metals may be employed to accomplish a number of extremely useful and versatile homogeneous reactions such as CO insertion, hydrogenation and coupling reactions. Most of these reactions would however not be possible without the use of ligands. Importantly, the properties of the end product is more often than not dictated by the nature of the ligand and the environment it creates around the metal. The most commonly employed ligands in homogeneous catalyses reactions contain phosphorus atoms, for example phosphines and phosphites.

This chapter describes the synthesis of many of the phosphine and organometallic complexes employed in the studies described elsewhere in this thesis. Since these compounds are sensitive (e.g. phosphine compounds are susceptible to oxidation), experiments were carried out under dry and inert atmosphere using inert air techniques and *Schlenk* glassware. Solvents were purified by passing through an Al_2O_3 column followed by a subsequent distillation. Solvents were also degassed and stored under an inert atmosphere before use. Glassware was oven-dried to ensure complete dryness and placed under vacuum before use to ensure an inert atmosphere.

The following chemicals were obtained from Aldrich: Butyllithium 1.3 M in 98/2 cyclohexane/hexane mixture, 9,9-dimethylxanthene at 96 % purity, tetramethylethylenediamine (TMEDA) at 99 % purity, diphenyl ether at 99 % purity, chlorodiphenylphosphine at 98 % purity and $RhCl_3{\cdot}3H_2O$. $MgSO_4$ (98 % pure), KOH (98 % pure) and formaldehyde (40 % w/v aqueous solution)

were obtained from Merck while PPh_3 was obtained from BASF with a purity of 99.9 %.

3.1.1 Synthesis of 4,5-Bis(diphenylphosphino)-9,9-dimethylxanthene.[1]

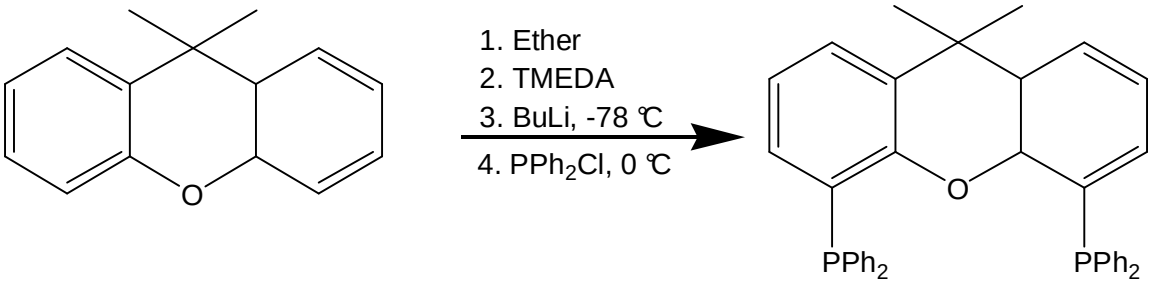

Scheme 3.1. Synthesis of xantphos from 9,9-dimethylxanthene.

Synthesis of 4,5-bis(diphenylphosphino)-9,9-dimethylxanthene (xantphos, Xp) was performed under dry and inert conditions using a Schlenk set-up. Butyllithium (1.3 M in 98/2 cyclohexane/hexane, 17.5 mmol, 11 mL) was added drop-wise to a solution of 9,9-dimethylxanthene (5 mmol; 1051.35 mg) and TMEDA (17.5 mmol; 2.64 mL) in dry ether (50 mL) at –78 ℃. After all the butyllithium was added, the reaction mixture was allowed to gradually heat to room temperature and stirred for 18 hours. A solution of chlorodiphenylphosphine (17.5 mmol; 3.14 mL) in hexane (20 mL) was then added to the reaction mixture at 0 ℃ and the reactio n stirred for another 18 hours after allowing it to heat to room temperature. At the set time (18 hours), the solvent was removed *in vacuo* and the resulting solid dissolved in dichloromethane (DCM). After washing this solution with water, it was dried with $MgSO_4$ and the solvent evaporated. The product was then washed with hexane and dried for later use. Xantphos was obtained in 75 % yield (2.17 g) with a melting point of 219 ℃. Pure product was obt ained by crystallization from propanol. All NMR and IR results collected for this compound and all other compounds synthesised were the same as those obtained in respective literatures referenced.

3.1.2 Synthesis of (Oxydi-2,1-phenylene)bis(diphenylphosphine)[1]

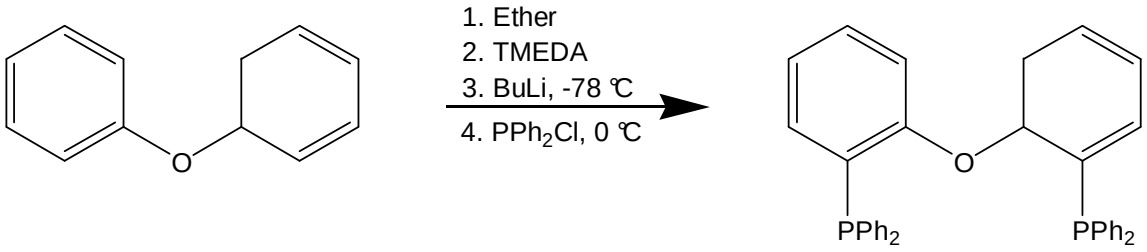

Scheme 3.2. Synthesis of xantphos derivative, DPEphos, from diphenyl ether.

A similar procedure as that of xantphos was followed in the synthesis of (oxydi-2,1-phenylene)bis(diphenylphosphine) (DPEphos) with similar quantities. In this instance, however, 9,9-dimethylxanthene was replaced with diphenyl ether. DPEphos was obtained in 62 % yield (1.67 g) with a melting point of 242 ℃. NMR and IR results collected for this were the same as those obtained in the literature as per reference.

3.1.3 Synthesis of $[RhH(CO)(PPh_3)_3]$[2]

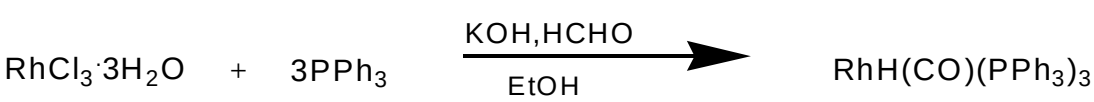

Scheme 3.3. Synthesis of $[RhH(CO)(PPh_3)_3]$ from $RhCl_3$.

To a stirred solution of PPh_3 (10 mmol; 2.62 g) in refluxing ethanol (100 mL) was added a solution of $RhCl_3 \cdot 3H_2O$ (1 mmol; 0.21 g) also in ethanol (20 mL). Aqueous formaldehyde (10 mL; 40 % w/v solution) and a solution of KOH (15 mmol; 0.8 g) in hot ethanol were added successively after a delay of 15 seconds. The reaction mixture was refluxed for 20 minutes and allowed to cool to room temperature. Green-yellowish crystalline precipitate was formed and the product was then filtered, washed with ethanol, water,

ethanol and hexane and dried *in vacuo*. The bright yellow crystalline product was collected in 90 % yield (0.83 g) with a melting point of 118 ℃. NMR and IR results collected for this were the same as those obtained in the literature as per reference

3.1.4 Synthesis of $[RhCl(PPh_3)_3]^2$

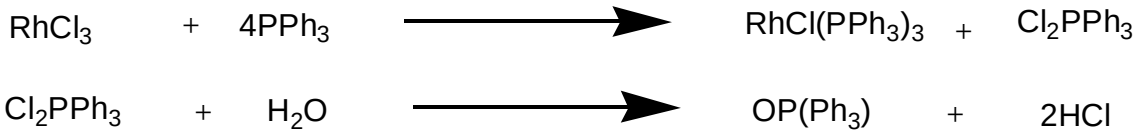

Scheme 3.4. Synthesis of the Wilkinson catalyst, $RhCl(PPh_3)_3$, from $RhCl_3{\cdot}3H_2O$.

$RhCl_3{\cdot}3H_2O$ (1 mmol; 0.21 g) was dissolved in ethanol (70 mL) in a round bottomed flask equipped with a reflux condenser, magnetic stirrer, a gas inlet tube and a gas exit bubbler. After all the contents were dissolved, a hot ethanol solution (370 mL) of PPh_3 (5.0 mol; 1.31 g) was added and the flask purged with nitrogen. The solution was then refluxed for 3 hours with a subsequent precipitation of reddish product that was filtered while still hot. Washing the product with portions of anhydrous ether yielded 84 % (0.78 g) of a deep red crystalline product with a melting point of 152 ℃.

Excess PPh_3 was employed to compensate for a loss through oxidation. Using small quantities of ethanol (≤ 200 mL) and refluxing for a shorter period of time (5 minutes) would yield an orange isomeric species that would convert to the deep red product with further refluxing. It is therefore important to ensure that enough solvent is employed and that the refluxing is given enough time. NMR and IR results collected for this were the same as those obtained in the literature as per reference

All chemicals prepared were compared with the pure compounds obtained from Aldrich by NMR and IR spectroscopy to confirm the quality, which was found to be satisfactory.

3.1.5 [Rh(acac)(PP)] complexes

Attempts were made to obtain [Rh(acac)(bisphosphine)] complexes from [Rh(acac)$(CO)_2$] and selected bidentate phosphines, xantphos and DPEphos. The solubility of the bidentate phosphines was very poor in an alkane solvent (hexane) and another solvent therefore had to be chosen. The preparation of [Rh(acac)(xantphos)] is desribed below. Similar procedures were followed for the preparation of [Rh(acac)(DPEphos)].

Two separate solutions of [Rh(acac)$(CO)_2$] (20 mg; 0.078 mmol) and xantphos (1.1 molar equivalent) were prepared in a minimum amount of toluene in separate glass tubes. After the solids had dissolved, a solution of the bisphosphine was slowly added to the Rh solution. During this addition, CO was replaced by the bisphosphine as witnessed by the evolution of gas bubbles from the reaction solution. The solutions were then allowed to concentrate in the fume hood for crystallization by passing argon over the solution.

After 24 hours, both [Rh(acac)(CO)(xantphos)] and [Rh(acac)(CO)(DPEphos)] solutions were closed and allowed to stand in the fume hood for 3 days to crystallize but with no success. The [Rh(acac)(CO)(xantphos)] solution was then placed in the fridge to try and effect crystallization. The [Rh(acac)(CO)(DPEphos)] solution was divided into two fractions. The first fraction, a concentrated toluene solution, was put in the fridge. The second fraction was covered with CH_2Cl_2 and allowed to stand in the fume hood. After standing for a week, no crystals were observed to have formed in any of the containers and alternative procedures were followed.

Following the literature procedures for the bulky phosphites,[3] solutions of [Rh(acac)$(CO)_2$] (20 mg) and bidentate phosphines (both DPEphos and xantphos) were stirred overnight at 40 ℃ to ensure that both CO ligands

were replaced by the bidentate phosphines before the reaction mixture was worked-up following the procedure below:

- [Rh(acac)(xantphos)]: The solution was divided into two fractions. The first fraction was concentrated and covered with a methanol layer. The second fraction was evaporated completely and the precipitate dissolved in CH_2Cl_2 before covering it with a methanol layer. Both fractions were allowed to settle for crystallization in the fume hood while passing a constant flow of Ar over the solutions.
- [Rh(acac)(DPEphos)]: This solution had a precipitate even after vigorous stirring. The solvent was decanted into a separate Schlenk tube, concentrated and covered with a methanol layer. The precipitate was dissolved in CH_2Cl_2 and covered with a methanol layer.

Several attempts to obtain crystals from $[Rh(acac)(PPh_3)_2]$ were made following the same procedure as above. After concentrating the reaction mixture, methanol was added to aid the crystallization process. All of the above solutions failed to produce crystals suitable for crystallographic analyses.

3.1.6 $[RhH(CO)(PPh_3)PP]$ complexes

Complexes of the form $[RhH(CO)(PPh_3)PP]$ were also investigated. Solutions of $[RhH(CO)(PPh_3)PP]$ were prepared by mixing $[RhH(CO)(PPh_3)_3]$ and bidentate ligands (xantphos and DPEphos) in a minimum amount of toluene with a M:L ratio of 1:1.1. After stirring for 5 hours at room temperature, the solvent was removed under vacuum and the contents washed with methanol to remove excess PPh_3. The product was then dissolved in the minimum amount of CH_2Cl_2, covered with an ethanol layer and allowed to crystallize in a fridge with success. A few solutions were prepared similarly, some of which were used for analysis.

In order to confirm the product formed, one batch of crystals was used for analyses. Most of the solvent mixture from which the crystals were grown was decanted with the aim of minimizing the impurities present in the solution. After vacuum drying the crystals, the contents were dissolved in $CDCl_3$ for NMR analyses. ^{31}P (^{1}H decoupled) NMR spectrum of $[RhH(CO)(PPh_3)(xantphos)]$ is shown below.

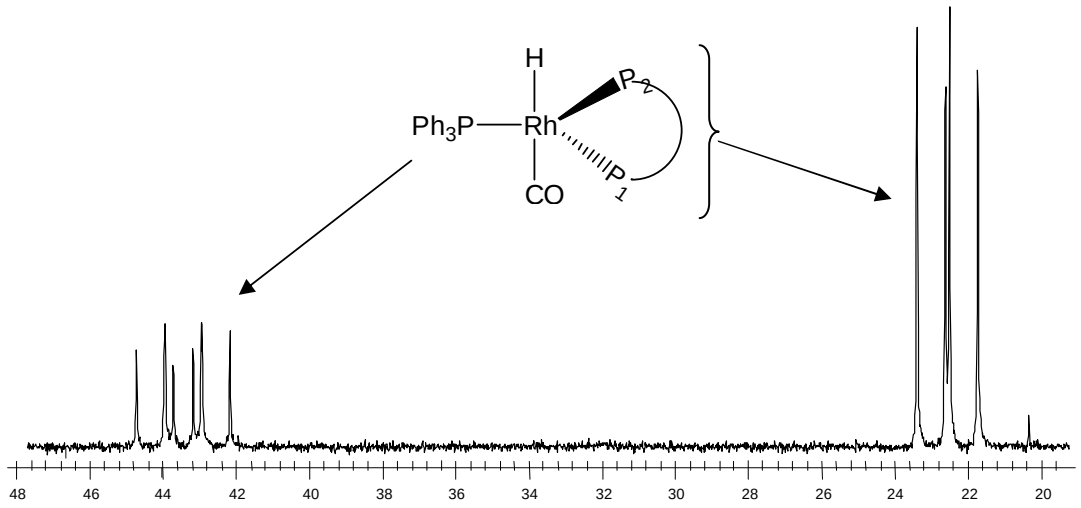

Figure 3.1. ^{31}P NMR spectrum of $[RhH(CO)(PPh_3)(xantphos)]$ recorded in $CDCl_3$ with a M:L ratio of 1:1.1 at room temperature.

The spectrum obtained was compared to the $[RhH(CO)(PPh_3)(xantphos)]$ spectra recorded earlier and that of the literature.[1] The good correlation between the compared spectra confirmed that the product formed was indeed the $[RhH(CO)(PPh_3)(xantphos)]$ species. To further verify the complex formed, an IR spectrum of the collected crystals was recorded as shown below in Figure 3.2, together with a spectrum of the starting material, $[RhH(CO)(PPh_3)_3]$.

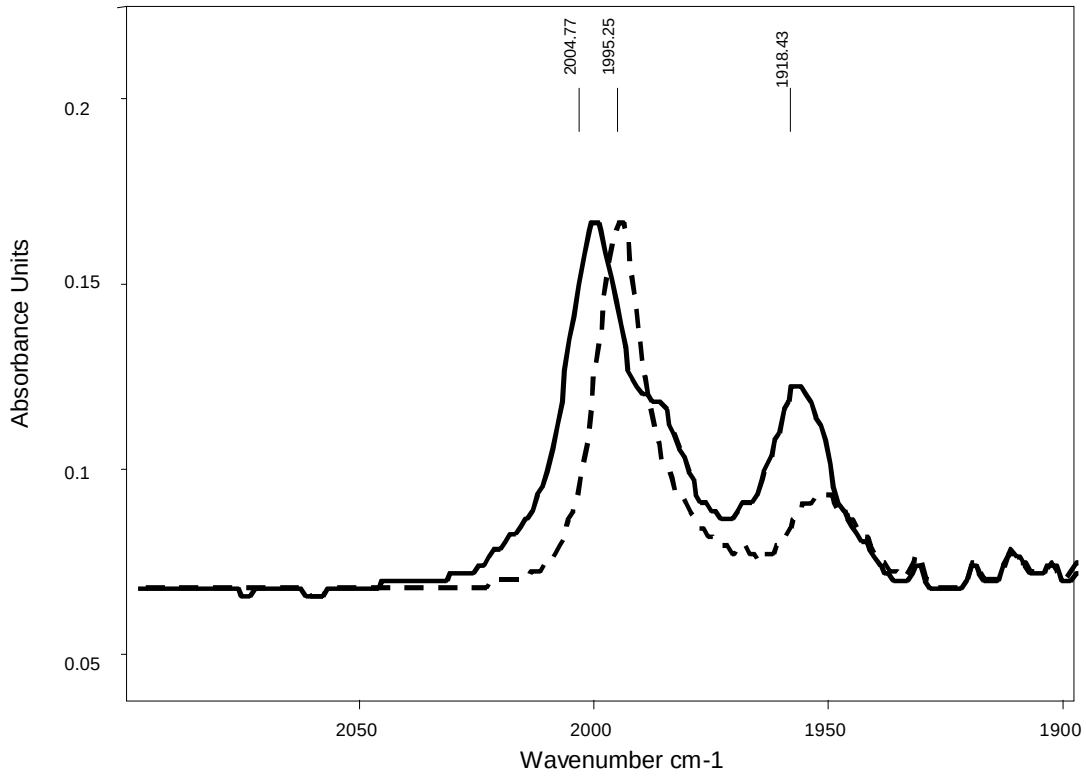

Figure 3.2. IR spectra of $[RhH(CO)(PPh_3)_3]$ (solid) and that of grown crystals of $[RhH(CO)(PPh_3)Xp]$ (dashed))] recorded in CH_2Cl_2 with a M:L ratio of 1:1.1 at room temperature.

$[RhH(CO)(PPh_3)(xantphos)]$ gave two υ (CO) values of 1995.3 and 1918.4 cm^{-1}. These observed frequencies were in agreement with those obtained in the literature,[1] confirming that the crystals grown were indeed those of the mixed phosphine species, $[RhH(CO)(PPh_3)(xantphos)]$. Crystals were then obtained and data collected that showed a decomposition product in CH_2Cl_2. This is presented in Section 3.2 below.

3.2 Crystallographic characterisation of studied rhodium complexes

3.2.1 Introduction

A thorough understanding of the phosphine modified rhodium catalyst employed in these studies is of crucial importance. As illustrated in Section 4.3.3.2 ([$RhH(CO)_2(PPh_3)_2$]) and Section 4.3.3.5 ([$RhH(CO)_2$(xantphos)]), active catalyst species bearing two CO ligands could not be obtained due to stability reasons. These complexes require a syngas atmosphere to remain stable against dimer formation or higher clusters. The stability of these complexes has also not been confirmed at low temperatures (lower than room temperature), which is the temperature that is normally favourable for crystals collection. Following these reasons, it was decided that crystals of [$RhH(CO)(PPh_3)$(xantphos)] be subjected to crystallographic data collection since this complex can be obtained at room temperature and atmospheric pressure without the need of syngas atmosphere. The work-up of this complex was performed in CH_2Cl_2 because it was the solvent that gave the best results in terms of solubility of product and crystal isolation. Other solvents such as toluene, hexane, methanol and acetone failed to either dissolve the product or aid in crashing the crystals out of the solvent at low temperatures. CH_2Cl_2, however, is a co-ordinating solvent through the Cl that may result in the formation of other Cl containing species. This behaviour would then help in shedding crucial information on the stability of the catalyst in the presence of Cl containing compounds.

Crystals suitable for crystallography were collected for analysesThe following were used for crystallographic data collection:

3.2.2 Results and Discussion: X-ray structure of *trans*-[$RhCl(CO)(PPh_3)_2$]

Crystallographic data collected revealed that the complex formed was *trans*-[$RhCl(CO)(PPh_3)_2$].[4] This observation suggests that Cl-containing compounds or solvents may act as catalyst inhibitors whereby the catalyst may decompose into complexes of the form *trans*-[$RhCl(CO)(L)_2$] where L may be any ligand of choice.

Table 3.1. Crystallographic data and refinement parameters for *trans*-[$RhCl(CO)(PPh_3)_2$]·Ch_2Cl_2.

	[$Rh(Cl)(CO)(PPh_3)_2$]
Empirical formula	$RhC_{37}\ H_{30}\ Cl\ O\ P_2$
Formula weight	690.3
Crystal system	Orthorhombic
Space group	P_{bca}
a/ Å	20.320(5)
b/ Å	7.911(5)
c/ Å	23.045(5)
α/ °	90.000(5)
β/ °	90.000(5)
γ/ °	90.000(5)
V/ $Å^3$	3705(3)
Z	4
D_c/ $g.cm^{-3}$	1.348
μ/ mm^{-1}	0.689
Tmax/ Tmin	0.920/ 0.510
F(000)	1548
θ limit/ °	5.15 to 28.28
Index ranges	$-23 \le h \le 26$ $-10 \le k \le 9$ $-18 \le l \le 30$
Collected reflections	15590
Independent reflections	4524
R_{int}	0.0803
GooF	0.989

The compound crystallises as discrete disordered *trans*-[$RhCl(CO)(PPh_3)_2$] complexes and dichloromethane solvate molecules (see Figure 3.5). There is a weak intramolecular hydrogen interaction between the ortho proton and the chloride (2.854(24) (Å)), as well as a weak intermolecular hydrogen bond between a dichloromethane-hydrogen and the carbonyl-oxygen atom with a distance of 2.334(10) (Å) between the atoms.

A fraction of the unit cell diagram of the complex collected, *trans*-$[RhCl(CO)(PPh_3)_2]\cdot Ch_2Cl_2$ is shown in Figure 3.3 below.

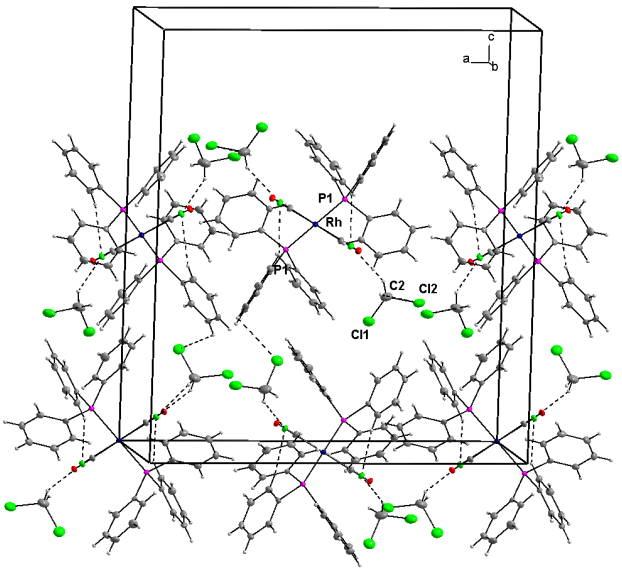

Figure 3.3. Fraction of the unit cell diagram of *trans*-$[RhCl(CO)(PPh_3)_2]\cdot Ch_2Cl_2$, aligned along the b-axis.

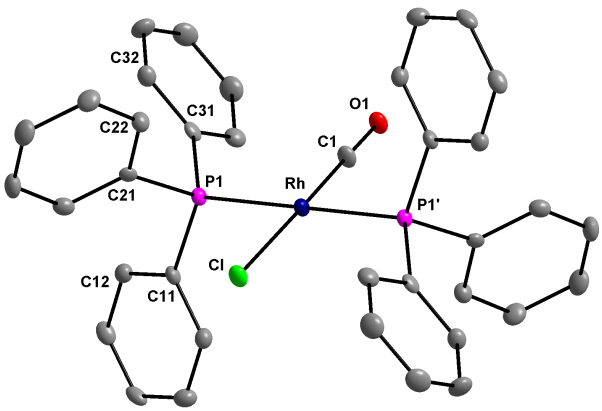

Figure 3.4. Molecular diagram of $[RhCl(CO)(PPh_3)_2]$ showing the numbering scheme. With 30 % proability for the C atoms, the first digit indicates the ring number and the second digit the position of the atom in the ring. Primed atom denotes atom that is generated by inversion centre.

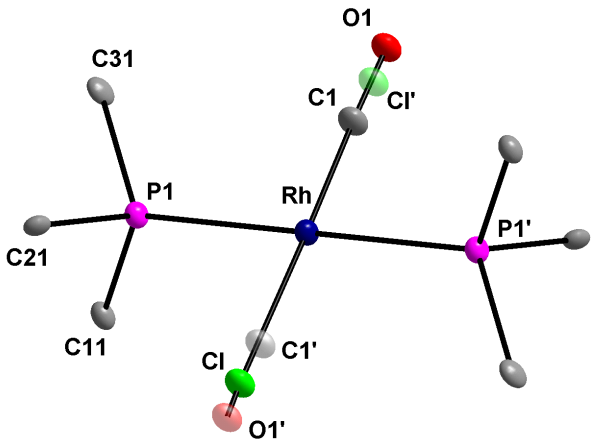

Figure 3.5. A diagram of two *trans*-[RhCl(CO)(PPh_3)$_2$] moieties displaying the disorder along the Cl-Rh-CO axis. For simplicity sake, only the first carbon of each phenyl ring is shown.

The Rh atom resides on an inversion centre and the molecule is square planar. Selected bond lengths and angles are given in Table 3.1 below. The refinement of the molecule involves a disorder of the *trans* CO and Cl groups related through an inversion centre. Examples of this disorder for [RhCl(CO)(PPh_3)$_2$] have been studied in detail[5] including the determination of the orthorhombic CH_2Cl_2 solvate.[6]

Table 3.2. Selected bond lengths (Å) and angles (°) of *trans*-[RhCl(CO)(PPh_3)$_2$].[a]

	Bond lengths (Å)		**Bond lengths (Å)**
Rh – C1	1.747(9)	P1 – C21	1.817(4)
Rh – Cl	2.376(2)	P1 – C31	1.831(3)
Rh – P1	2.3129(10)	C – O	1.156(10)
P1 – C11	1.830(3)		

Table 3.3. Selected bond angles (°) of *trans*-[RhCl(CO)(PPh_3)$_2$].

	Bond angles (°)		Bond angles (°)
C1 – Rh – Cl	178.8(4)	C11 – P1 – C31	102.16(15)
P1 – Rh – Cl	93.85(6)	C21 – P1 – Rh	111.07(11)
C21 – P1 – C 11	106.55(16)	C31 – P1 – Rh	118.85(12)
C21 – P1 – C 31	103.25(16)		

A literature search was conducted to investigate crystals obtained of related complexes. Compound formulae, names and crystallographic data collected were highlighted in this search. Parameters like bond distances and angles were also recorded. Below are a few selected complexes for comparison purposes.

Table 3.4. A comparison between different complexes' (**A** to **C**, **I** to **L**) and ligand's distances and angles.[a]

	Rh – P (Å)	P – P (Å)	P – Rh – P (°)
A[7]	2.155	3.143	93.752
B[8]	2.252	3.595	105.629
C[9]	2.243		87.790
I[10]			120.991
J[8]			129.103
K	2.3129		180.00
L[11]	2.322		180.00

[a.] See Figure 3.6 for structures of complexes.

Table 3.5. A comparison between different complexes' (**D** to **H**) and ligand's distances and angles.[a]

	P – P (Å)	C3 – O – C4 (°)
D[12]	4.025	124.363
E[13]	4.059	116.841
F[14]	4.876	118.835
G[15]	4.693	118.022
H[16]	5.422	117.575

[a.] See Figure 3.6 for structures of complexes.

ESD's of the given data were not available. Longer P – P distance is observed in **B** compared to that of **A**. This observation is accompanied by a wider P – Rh – P angle of 105.63 °(**B**) vs. 93.752 °(**A**). It was speculated that this was due to steric effects resulting from the phosphine ligands. The oxygen atom of the phosphite ligand in **A** may allow for some flexibility of the ligand thereby reducing the steric congestion between the two ligands. This is, however, not the case with the more rigid complex **B** where the PCy_3 does not allow for any flexibility. The much smaller P – Rh – P angle (87.790 °) of the less sterically hindered complex **C** (CO vs. PCy_3 and $P(OPh)_3$) confirms this speculation. The same steric effect reasoning may be assumed when comparing **H** with the other free ligands (**D**, **E**, **F** and **G**). Due to the two phosphine oxide ligands higher steric effect is experienced with **H** resulting in longer P – P distance (5.422 Å).

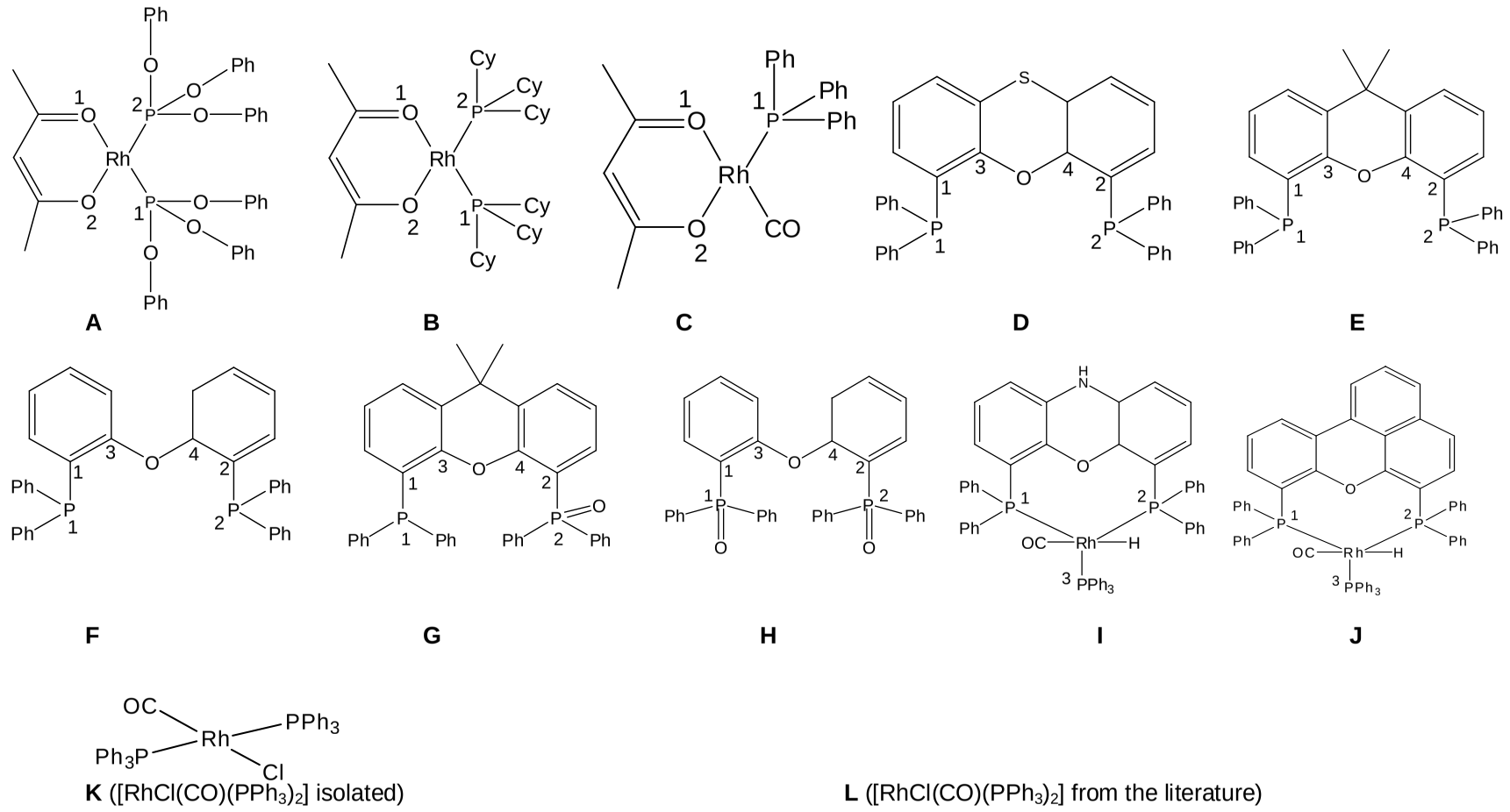

Figure 3.6. Summary of structures described in Table 3.4 and Table 3.5.

A table below highlights comparisons between the isolated and the literature ([RhCl(CO)(PPh_3)$_2$]).

Table 3.6. Comparisons of selected bond lengths and angles between the isolated and the literature (*trans*-[RhCl(CO)(PPh_3)$_2$]·Ch_2Cl_2).

	Isolated	**Literature[10]**	**Literature[17]**
Rh – C	1.747(9) (Å)	1.77(1) (Å)	1.74(3) (Å)
Rh – Cl	2.376(2) (Å)	2.382(1) (Å)	2.38(11) (Å)
Rh – P	2.3129(10) (Å)	2.322(1) (Å)	2.313(7) (Å)
C – O	1.156(10) (Å)	1.14(2) (Å)	1.20(5) (Å)
P – Rh – C	92.6(4) (°)	95(1) (°)	92.1(12) (°)
P – Rh – Cl	93.85(6) (°)	93.6(1) (°)	97.3 (4) (°)

Table 3.4 above displays a strong correlation between the isolated and the literature complexes. Similar to literature[16] results, an unusually long Rh – Cl distance of 2.376(2) Å was obtained. This was speculated to be due to the compensation of the chlorine atom for the electron density of the oxygen atom of the CO ligand.

Supporting information for the crystallographic data can be obtained in the appendix.

References

1. Kranenburg, M.; van der Burgt, Y. E. M.; Kamer, P. C. J.; van Leeuwen, P. W. N. M. *Organometallics* **1995**, *14*, 3089.

2. McCleverty, Wilkinson, G. *Inorganic Syntheses*, **1966**, *8*, 211.

3. Van Rooy, A.; Kamer, P. C. J; van Leeuwen. P. W. N. M. ; Goubitz, K.; Fraanje, J.; Veldman, N.; Spek, A. L. *Organometallics* **1996**, *15*, 835.

4. Crystallographic data was collected as follows: APEX2 (Bruker, 2005), cell refinement: SAINTPlus (Bruker, 2004); data reduction: SAINT-Plus and XPREP (Bruker, 2004); program(s) used to solve structure: SIR97 (Altomare, 1999); program(s) used to refine structure: SHELXL97 (Sheldrick, 1997); molecular graphics: DIAMOND (Brandenburg & Berndt, 2001); software used to prepare material for publication: WinGX (Farrugia, 1999).

5. Chen, Y. –J; Wang, J. –C; Wang, Y. *Acta Crystallogr*. **1991**, *C47*, 2441.

6. Chaloner, P. A.; Claver, C.; Hitchcock, P. B.; Masdeu, A. M; Ruiz, A. *Acta Crystallogr*. **1991**, *C47*, 1307.

7. Leipoldt, J.G.; Lamprecht, G.J.; Van Zyl, G.J. *Inorg. Chim. Acta* **1985**, *96*, L31.

8. Esteruelas, M. A.; Lahoz, F. J.; Onate, E.; Oro, L. A.; Rodriguez, L.; Steinert, P.; Werner, H. *Organometallics,***1996***, 15*, 3436.

9. Leipoldt, J. G.; Basson, S. S.; Bok, L. D. C.; Gerber, T. I. A. *Inorg. Chim. Acta* **1978**, *26*, L35.

10. van der Veen, L. A.; Keeven, P. H.; Schoemaker, G. C.; Reek, J. N. H.; Kamer, P. C. J.; van Leeuwen, P. W. N. M.; Lutz, M.; Spek, A. L. *Organometallics* **2000**, *19*, 872.

11. Dunbar, K. R.; Haefner, S. C. *Inorg. Chem.* **1992**, *31*, 3676.

12. Goertz, W.; Keim, W.; Vogt, D.; Englert, U.; Boele, M. D. K.; van der Veen, L. A.; Kamer, P. C. J.; van Leeuwen, P. W. N. M., *J. Chem. Soc. Dalton Trans.* **1998***,* 2981.

13. Kranenburg, M.; van der Burgt, Y. E. M.; Kamer, P. C. J.; van Leeuwen, P. W. N. M.; Goubitz, K.; Fraanje, J. *Organometallics* **1995***, 14*, 3081.

14. Pintado-Alba, A.; de la Riva, H.; Nieuwhuyzen, M.; Bautista, D.; Raithby, P. R.; Sparkes, H. A.; Teat, S. J.; Lopez-de-Luzuriaga, J. M.; Lagunas, M. C. *Dalton Trans.* **2004***,* 3459.

15. Ellis, D. D.; Spek, A. L. *Acta Crystallogr. Sect. E.* **2001**, *E. 57*, o94.

16. Kovalevsky, A. Yu.; Coppens, P. *Private Communication ,* **2003**.

17. Kemp, G.; Roodt, A.; Purcell, W. Rhodium Express **1995**, *1*, 21.

CHAPTER 4.....50
NMR and IR Spectroscopic Investigations on Rhodium PPh_3 and Xantphos Catalyst: Inhibition and Stability Studies.....50
4.1 Introduction.....50
4.2 NMR Studies.....50
4.2.1 Introduction.....50
4.2.2 Experimental.....55
4.2.3 Results and Discussion.....58
4.3 *In situ* HP-IR spectroscopy studies.....82
4.3.1 Introduction.....82
4.3.2 Experimental.....83
4.3.3 Results and Discussion.....85
References.....106

CHAPTER 4

NMR and IR Spectroscopic Investigations on Rhodium PPh_3 and Xantphos Catalyst: Inhibition and Stability Studies

4.1 Introduction

In this chapter, spectroscopic investigations involving rhodium catalyst are reported. Characterization of different species have been performed using both NMR and IR spectroscopy. Stability studies demonstrate the benefit of employing additional PPh_3 in combination with the rhodium xantphos catalyst system.

Equally important, the stability of the catalyst against inhibition by methyl vinyl ketone (MVK) is reported using $[RhH(CO)_2(PPh_3)_2]$, $[RhH(CO)_2$(xantphos)] and the mixed $[RhH(CO)_2(PPh_3)$(xantphos)] system. The power of spectroscopy as an *in situ* characterization technique is demonstrated by the strong correlations which can be drawn between autoclave and spectroscopy studies.

4.2 NMR Studies

4.2.1 Introduction

4.2.1.1 The Wilkinson Catalyst $[RhX(PPh_3)_3]$

One of the most widely applied characterisation techniques is Nuclear Magnetic Resonance (NMR) spectroscopy, with proton, carbon and phosphorus NMR routinely applied in hydroformylation studies. Rhodium NMR (^{103}Rh) has also gained a lot of interest due to the widespread application of the metal in catalysis. For example, rhodium is widely

employed in hydroformylation, hydrogenation,[1] dehydrogenation,[2] carbonylation[3] and hydroacylation[4] catalytic systems. Unfortunately, due to its small magnetic moment, ^{103}Rh has a low sensitivity with a 17 % receptivity relative to ^{13}C. It's spin number I = ½ with 100 % natural abundance.[5] Rh has such a low sensitivity that ^{13}C, also with a spin number of ½, and a natural abundance of only 1.1 %, is more NMR sensitive than ^{103}Rh. However, it can be used in induced NMR experiments. It was for this reason that Freeman and co-workers employed the double-resonance "tickling" (decoupling) experiment to determine rhodium's chemical shifts.[6] In this experiment, the lines in the rhodium spectrum are irradiated with a small radio frequency field while simultaneously observing another nucleus to which it is coupled. Where complexes $[RhX(PPh_3)_3]$ and $[RhX(CO)(PPh_3)_2]$ were investigated, phosphorus is the observed nucleus.[7] In order to improve on the sensitivity and resolution of the spectra obtained, the protons in the phosphine ligands were decoupled.

A very useful NMR study conducted on rhodium(I) and rhodium(III) complexes is the dependence of phosphorus chemical shifts on the electronegativity of the neighbouring atoms.[8] For rhodium(I) studies, complexes of the form $[RhX(PPh_3)_3]$ and $[RhX(CO)(PPh_3)_2]$ were studied where X = Cl, Br or I. In the case of rhodium(III), complexes of the form $[RhX_3(PPh_3)_3]$ were investigated. The phosphorous spectra of the rhodium(I) complexes supported a square-planar structure. The phosphorous spectra of $[RhX(PPh_3)_3]$ consisted of a doublet of doublets at high field due to the mutually *trans* phosphorous atoms (labelled P1 in Figure 4.1) as well as a doublet of triplets observed at a low field due to the *cis* phosphorous atom (labelled P2 in Figure 4.1). For example, in the case of $[RhCl(PPh_3)_3]$, $\delta P1 = -31.5$ ppm while $\delta P2 = -48.0$ ppm). A negative chemical shift for either nucleus indicates that the phosphorous

or the rhodium resonance occurs at a higher frequency and therefore the nucleus is more shielded than in the reference. The structure of the lines arises from a large rhodium-phosphorous coupling superimposed upon the smaller phosphorous-phosphorous coupling of the non-equivalent phosphorous atoms.

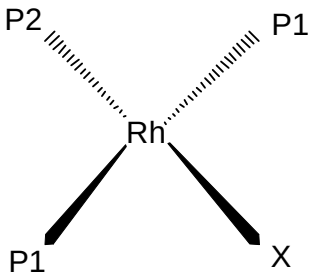

Figure 4.1. Notation for square planar rhodium(I) complex as studied by NMR spectra.

Increasing the temperature or adding excess triphenylphosphine (PPh_3) to the solution resulted in the disappearance of the multiplet patterns and a subsequent appearance of a single phosphorous resonance. Unlike the chloro complex, the bromo and the iodo complexes had to be cooled down to 283 and 263 K respectively before the multiplet splittings could be well resolved. These observations suggest the dissociation of the *tris*-PPh_3 complex into a three co-ordinated (unsaturated) rhodium species and unassociated PPh_3 that will be in equilibrium with the four co-ordinated species as shown below.

$$[Rh(PPh_3)_3X] \rightleftharpoons [Rh(PPh_3)_2X] + PPh_3 \qquad 4.1$$

4.1

The ^{31}P phosphorous NMR spectrum of $[RhX(CO)(PPh_3)_2]$ consisted of a doublet due to rhodium-phosphorous coupling, consistent with magnetically equivalent phosphorous ligands.

In the case of rhodium(III) complexes as shown in Figure 4.2, the phosphorous spectra consisted of a doublet of doublets at high field (δP1 = 0.5 ppm) and doublet of triplets (δP1 = – 15.1 ppm), the coupling scheme of which was analogous to that found for $[RhX(PPh_3)_3]$ with the same labelling scheme.[8]

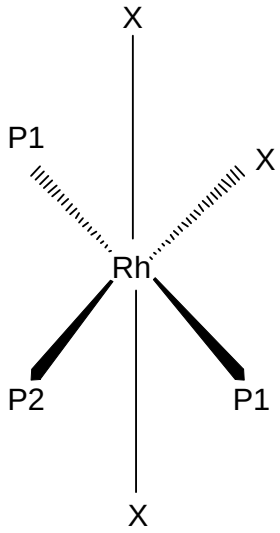

Figure 4.2 Notation for octahedral rhodium(III) complex as confirmed by NMR spectra.

To illustrate the *trans* influence, the rhodium-phosphorous coupling constant was always larger for the phosphorous *trans* to the halogen. In contrast to this, the substitution of a carbonyl for a phosphine group displayed a marked decrease in the coupling constants of the phosphorous atoms *cis* to the carbonyl group. A deeper look into chemical shifts revealed that the phosphorous shielding is mainly sensitive to the electronegativity of the neighbouring atom. Phosphorous resonances shifted to a higher field as various halogens with less electronegativity were substituted.

4.2.1.2 Wilkinson hydride derivative [$RhH(CO)(PPh_3)_3$]

The Wilkinson catalyst, [$RhX(PPh_3)_3$], has proven to be a very efficient catalyst for the homogenous hydrogenation where it was also realised that the PPh_3, pyridine and stannous chloride complexes can afford hydroformylation reactions of alkenes at 70 ℃ and 100 bar syngas.[9] This catalyst reacts rapidly with CO to give *trans*-[$RhX(CO)(PPh_3)_2$], being the carbonyl species that appears to be the actual active catalyst during the hydroformylation reaction. Studies have shown that there is an inhibition period involved in the formation of the catalytically active hydride species, [$RhH(CO)(PPh_3)_2$], through hydrogenolysis from the dimer, [$RhX(CO)(PPh_3)_2]_2$.[10] This inhibition period could be eliminated in the presence of a base. Isolation of [$RhH(CO)(PPh_3)_3$][11] can be afforded in the presence of excess PPh_3. The solutions of [$RhH(CO)(PPh_3)_3$] are highly active for hydroformylation reactions (under conditions as mild as 25 ℃ and 1 bar), where an equilibrium exists betwe en [$RhH(CO)(PPh_3)_3$] and [$RhH(CO)_2(PPh_3)_2$].

Recent advances in spectroscopic techniques allowed for the confirmation of the still accepted general mechanistic concepts proposed in early years. Moreover, in depth understanding of different catalytic species involved under the reaction conditions (elevated pressures and temperatures in the case of hydroformylation) could be attained.[12] *In situ* characterisation of different catalytic species includes stability and exchange processes of active intermediates or resting states of the catalyst. A study has been conducted where hydroformylation of 1-hexene with syngas (CO/H_2 = 1:1 at 40 bar) was investigated using high pressure ^{31}P NMR (HP-NMR) spectroscopy.[13] Having established the background of hydroformylation with [$RhH(CO)(PPh_3)_3$], factors influencing the formation, inter-conversion

as well as the inhibition of different rhodium resting states formed during a catalytic cycle were then identified. In agreement with the previous literature elucidations, a five coordinated species $[RhH(CO)_2(PPh_3)_2]$ was observed to form from $[RhH(CO)(PPh_3)_3]$ upon the introduction of syngas (H_2/CO = 1:1). Addition of the olefin and a subsequent carbonylation of the resulting species resulted in the formation of an acyl species of the form $[Rh(COR)(CO)_2(PPh_3)_2]$ after CO migratory insertion (this mechanism is briefly illustrated in the introduction chapter). While $[RhH(CO)(PPh_3)_3]$ gave a doublet at 41.3 ppm with P-Rh coupling constant, $J_{Rh\text{-}P}$ = 153.9 Hz, $[RhH(CO)_2(PPh_3)_2]$ gave a doublet at 37.3 ppm, a $J_{Rh\text{-}P}$ of 138.7 Hz. A singlet at – 4.8 ppm arising from the free PPh_3 was also recorded. Upon carbonylation, $[Rh(COR)(CO)_2(PPh_3)_2]$ was characterised by a doublet at δ 27.5 with $J_{P\text{-}Rh}$ of 78.0 Hz.

Following these studies, a series of NMR experiments was proposed where a bidentate ligand, xantphos, was incorporated.

4.2.2 Experimental

$[RhH(CO)(PPh_3)_3]$ (98 %), $[Rh(acac)(CO)_2]$ (98 %), xantphos (97 %) and methyl vinyl ketone (MVK) (99 %) were purchased from Aldrich while PPh_3 (99.9 %) was obtained from BASF. These reagents were used as purchased. $CDCl_3$ (98 %) was obtained from Aldrich and was also used as purchased. Argon (99 %) and CO (99 %) were obtained from Afrox while syngas (49.9 % CO, balanced with H_2) was obtained from Air-Liquide.

4.2.2.1 Ambient pressure NMR studies

^{31}P and ^{1}H NMR experiments were carried out in a Varian 500 MHz Mercury NMR spectrometer operating at 202.47 and 500.13 MHz respectively, using a BBO BB-1 probe. ^{31}P NMR spectra were obtained using a 30 ° pulse and a 2 s T_1 delay with a Waltz 16 ^{1}H decoupling sequence while the ^{1}H NMR spectra were obtained with a 30 **°** pulse and a 5 s T_1 delay. Chemical shifts are reported in ppm and referenced to tetramethylsilane (^{1}H) and 85 % H_3PO_4 (^{31}P) at 0 ppm. These experiments were performed in 5 mm NMR tubes.

During the stability studies of the hydride, $[RhH(CO)(PPh_3)_3]$ (0.016 mmol; 15.14 mg) was dissolved in $CDCl_3$ (1.0 mL) and placed in the NMR instrument to record spectra. To investigate the effect of extra added PPh_3, a solution of $[RhH(CO)(PPh_3)_3]$ (0.016 mmol; 15.1 mg) and PPh_3 (0.48 mmol; 125.9 mg) was prepared in $CDCl_3$ (1.0 mL) and spectra recorded. Both solutions were allowed to stand for 72 hours before the next spectra were recorded to evaluate stability over time. To investigate the mixed catalyst system, xantphos (0.16 mmol; 95.4 mg) was added to a mixture of $[RhH(CO)(PPh_3)_3]$ and PPh_3 (same amounts as above) and the contents dissolved in $CDCl_3$ (1.0 mL) before spectra could be recorded. This solution was allowed to stand for 72 hours for stability comparisons to other prepared solutions. The reactions of MVK and the hydride were performed using the same quantities of $[RhH(CO)(PPh_3)_3]$ and PPh_3. After recording a spectrum of the cooled $[RhH(CO)(PPh_3)_3]$ (–60 ℃) and added PPh_3 solution, MVK (0.16 mmol; 0.013 mL) was added and another spectrum recorded. Syngas 1:1 was then bubbled through the solution before recording another spectrum to investigate the effect of syngas on the $[RhH(CO)(PPh_3)(xantphos)]$/MVK system.

4.2.2.2 HP-NMR studies

^{31}P and ^{1}H NMR experiments were carried out in a 500 MHz Bruker Avance NMR spectrometer operating at 202.47 and 500.13 MHz respectively, using a BBO BB-1 probe. ^{31}P NMR spectra were obtained using a 30° pulse and a 2 s T_1 delay with a Waltz 16 ^{1}H decoupling sequence while the ^{1}H NMR spectra were obtained with a 30° pulse and a 5 s T_1 delay. Chemical shifts are reported in ppm and referenced to tetramethylsilane (^{1}H) and 85 % H_3PO_4 (^{31}P) at 0 ppm. These experiments were performed in a 10 mM high-pressure Roe cell[14] and spectra were recorded without spinning.

With mixed system studies, samples were prepared by dissolving $[Rh(acac)(CO)_2]$ (0.033 mmol; 8.42 mg) with PPh_3 (1.92 mmol; 0.504 g) and xantphos (0.035 mmol; 20.37 mg) in degassed toluene (0.865 mol; 1 mL) and toluene-d_8 (0.943 mol; 1 mL). For pure/single ligand catalysts individual ligands were employed separately. The cell was then pressurised to 17 bar syngas (H_2:CO 1:1) and vigorously shaken for 10 minutes. After inserting the cell into the instrument, parameters were tuned for the selected experiment and a spectrum recorded. The catalytically active hydride was preformed by increasing the temperature to 87 °C thereby increasing the pressure to 20 bar syngas. The cell was then cooled to room temperature before introducing the MVK (12.8 mmol; 0.86 g/mL; 1.1 mL) and the experiment carried out as described above.

4.2.3 Results and Discussion

4.2.3.1 The stability of $[RhH(CO)(PPh_3)_3]$ at ambient pressure

$[RhH(CO)(PPh_3)_3]$ was chosen as the catalyst precursor of choice over $[Rh(acac)(CO)_2]$, since the latter requires syngas pressure and PPh_3 to be added before an active catalyst can be formed, while the former can be used as is without the need for syngas pressure. Omitting syngas increased the flexibility of the studies as the substitution reactions could be carried out without multiple complications arising from the formation of other catalytic species such as $[RhH(CO)_2(PPh_3)_2]$.

A 16 mM solution of $[RhH(CO)(PPh_3)_3]$ (0.016 mmol, 0.015 g) was prepared in a mixture of degassed toluene and toluene-d_8 after which a spectrum was recorded as shown in Figure 4.3.

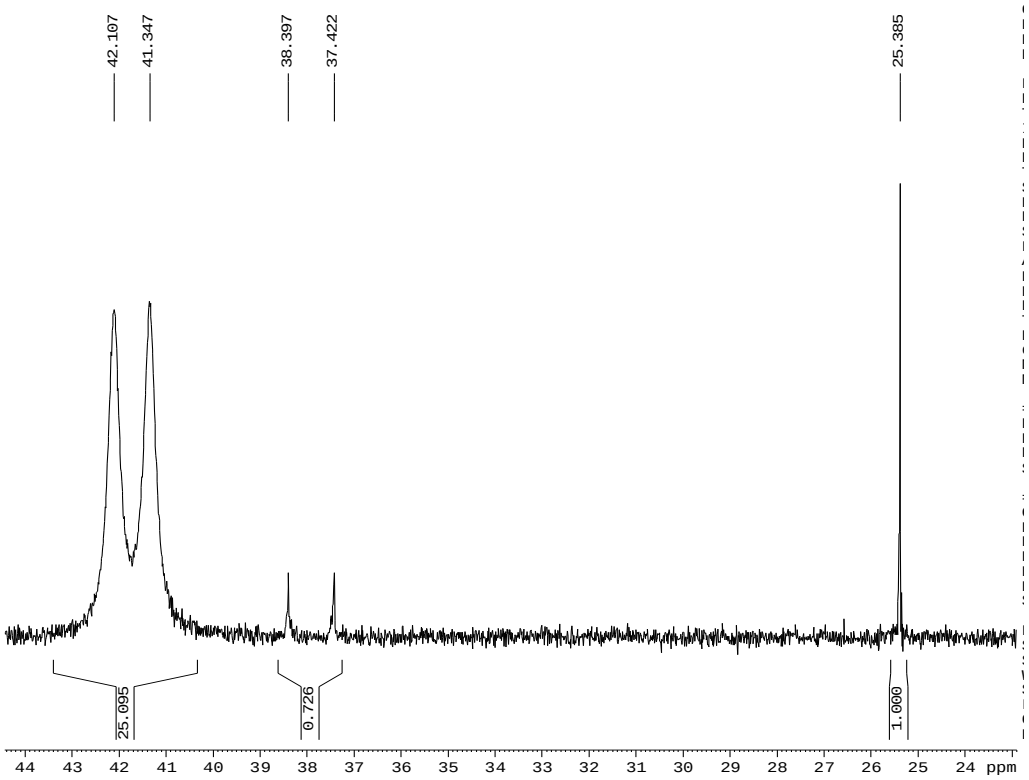

Figure 4.3. A ^{31}P NMR spectrum of $[RhH(CO)(PPh_3)_3]$ at 30 ℃ in toluene (0.8 mL) and toluene-d_8 (1 mL).

The spectrum obtained was acceptably close to that reported in the literature[12] where a symmetrical doublet was recorded at 41.7 ppm with P-Rh coupling constant, J_{Rh-P} of 151.6 Hz. However, a singlet at 25.4 ppm was also obtained which was assigned to the phosphine oxide due to unavoidable oxidation. A very small doublet at 37.9 ppm and a coupling constant of 197 Hz was also observed. Under these conditions, a possibility of rhodium dimers should also not be ruled out and this doublet was assumed to be due to dimer formation.[13] The solution was allowed to stand at room temperature for 72 hours and a spectrum recorded to establish the stability of the complex (Figure 4.4).

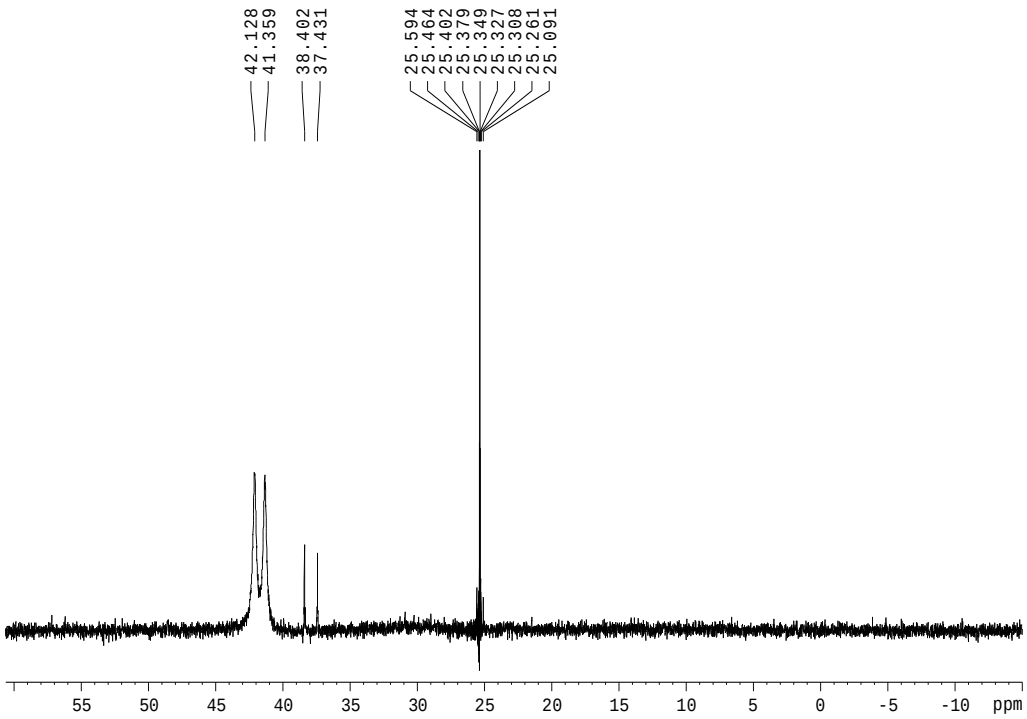

Figure 4.4. A ^{31}P NMR spectrum of $[RhH(CO)(PPh_3)_3]$ at 30 ℃ in toluene (0.8 mL) +-++and toluene-d_8 (1 mL): stability study after 72 hours.

An increase in intensity of the doublet at 37.9 ppm is seen with an increase in intensity of the oxidised phosphine singlet at 25.4 ppm at the expense of the hydride at 41.7 ppm.

The effect of additional PPh_3 was then evaluated where similar procedures were followed and PPh_3 (L:M molar ratio of 30:1) was added to $[RhH(CO)(PPh_3)_3]$ as illustrated in Figure 4.5.

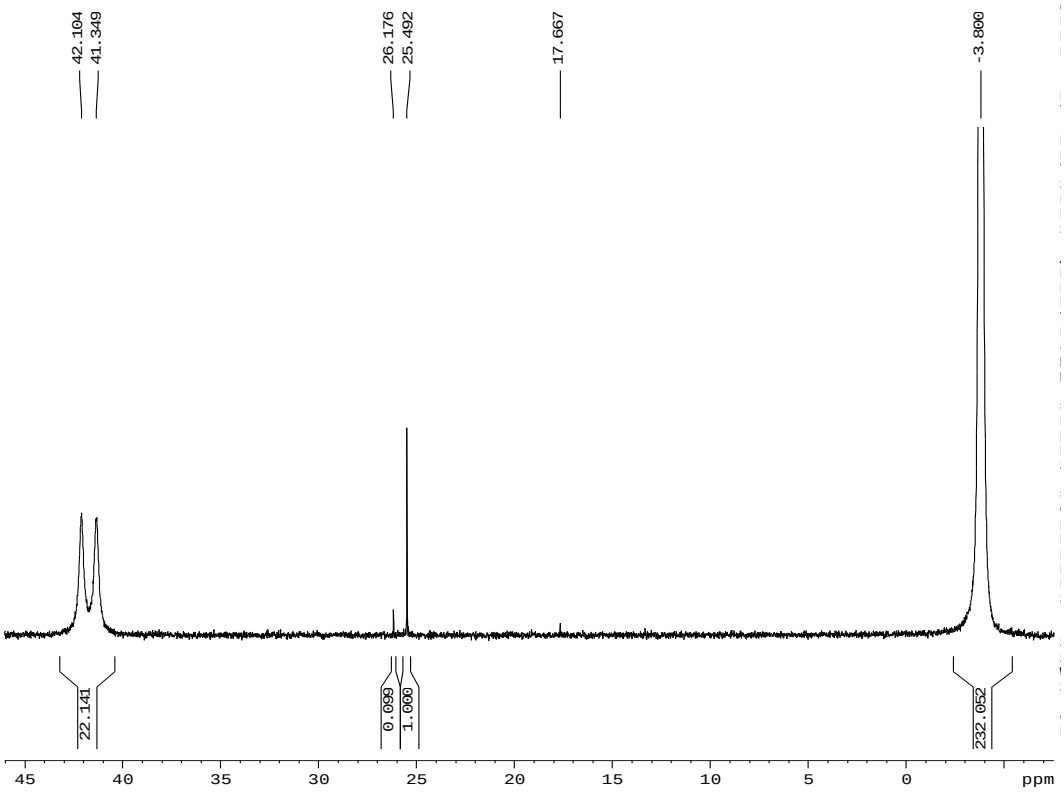

Figure 4.5. The effect of extra PPh_3 (Rh:PPh_3 = 1:30) on the stability of $[RhH(CO)(PPh_3)_3]$ at 30 ℃ in toluene (0.8 mL) and toluene-d_8 (1 mL).

A doublet at 37.9 ppm is not observed but only a doublet at 41.7 ppm, which is characteristic of the starting catalyst as well as a singlet at – 3.8 ppm assigned to the free PPh_3. This observation brought attention to the equilibrium between the five and the four co-ordinated species similar to the one shown below.

$$[RhH(CO)(PPh_3)_3] \rightleftharpoons [RhH(CO)(PPh_3)_2] + PPh_3 \qquad 4.2$$

The doublet at 37.9 pm was therefore thought to be possibly due to the four co-ordinated species when the equilibrium is shifted towards the right-hand side. The coupling constant ($J_{Rh\text{-}P}$ = 197 Hz) of this doublet was consistent with the coupling constant of the square planar complex,

$[RhCl(PPh_3)_3]$, as observed from the literature.[7] PPh_3 is observed to stabilise the five co-ordinated hydride species by preventing decomposition through either dimer formation or dissociation of PPh_3. There was also some oxidation of the ligand, evident from the singlet at 25.4 ppm. This stabilising effect of extra added PPh_3 was investigated over an extended period of time and a spectrum recorded as shown in Figure 4.6 below.

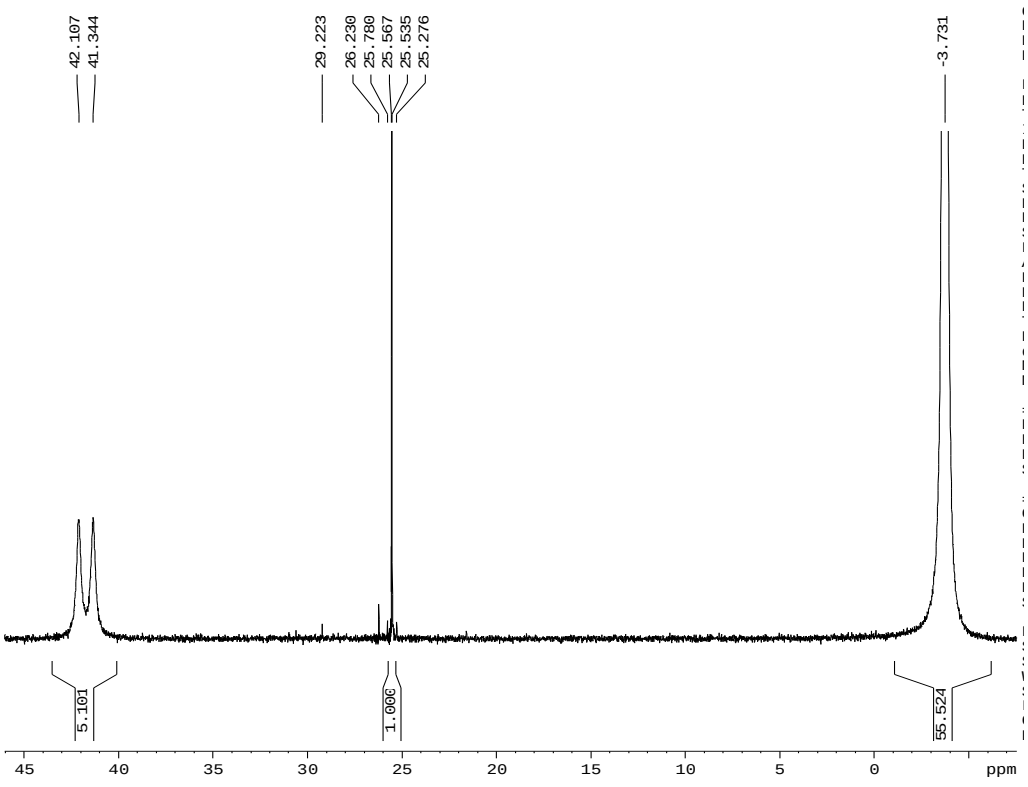

Figure 4.6. A ^{31}P NMR spectrum of $[RhH(CO)(PPh_3)_3]$ with excess PPh_3 ($Rh:PPh_3$ = 1:30) at 30 ℃ in toluene (0.8 mL) and toluene-d_8 (1 mL): Stability study after 72 hours.

The stabilising effect of added PPh_3 could still be observed even after 72 hours despite the loss of some PPh_3 through oxidation as witnessed by an increase of the oxide peak at 25.4 ppm. The benefit of employing additional PPh_3 is displayed here, where PPh_3 populates the

$[RhH(CO)(PPh_3)_3]$ species by shifting the equilibrium 4.2 more to the left hand side. The literature[13] has also shown that the presence of extra PPh_3 inhibits the formation of dimers of the form $Rh_2(CO)_{4+x}(PPh_3)_{4-x}$ where $0 \leq x \leq 4$, although none of this kind are observed in the spectra.

4.2.3.2 Reactions of $[RhH(CO)(PPh_3)_3]$ with xantphos at ambient pressure

The substitution reaction was studied where the solution of $[RhH(CO)(PPh_3)_3]$ and PPh_3 with xantphos (Rh:PPh_3:Xp ratio of 1:30:10) was prepared. Extra PPh_3 was added for stability reasons as discussed in Section 4.1.3.1 above. The substitution reaction can be briefly illustrated in the scheme below.

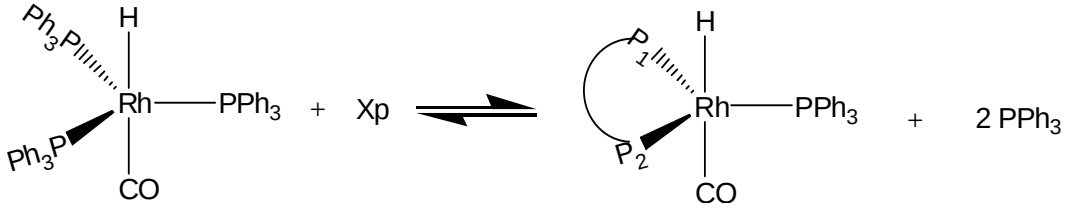

Scheme 4.1. A substitution reaction between $[RhH(CO)(PPh_3)_3]$ and a bidentate ligand, xantphos.

Stoichiometrically, a L:M molar ratio of 1:1 is sufficient to perform the desired substitution as both PPh_3 ligands can be substituted by the phosphines of the bidentate ligand. An excess of 10 molar equivalences relative to the metal was, however, used in order to push the equilibrium to the right hand side. The amount of unsubstituted and/or monosubstituted complex will therefore be negligible, if at all present, and this would simplify characterisation of the fully substituted complex. After a careful preparation of the solution under inert atmosphere a spectrum was

recorded. Below in Figure 4.7 is the spectrum displaying only the complex region at a higher chemical shift (> 20 ppm). The other part of the spectrum (< 20 ppm) consisted of only the free PPh_3 and the $O=PPh_3$.

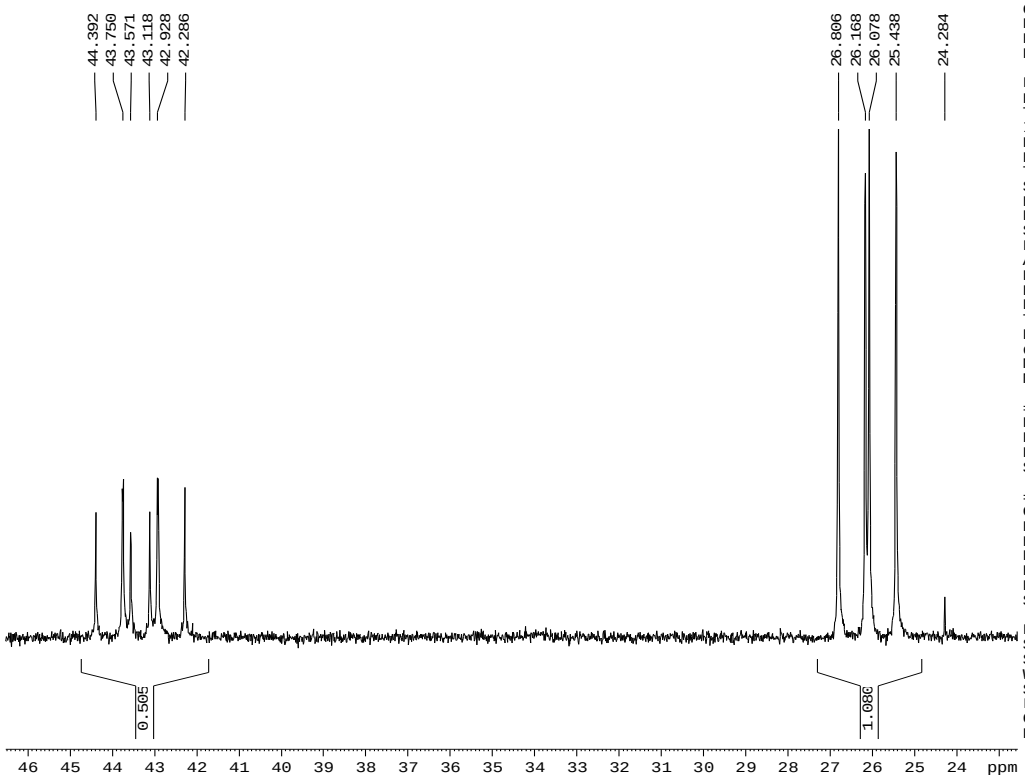

Figure 4.7. A ^{31}P NMR spectrum of $[RhH(CO)(PPh_3)_3]$ reacted with xantphos (Rh:Xp = 1:10) at 30 ℃ in toluene (0.8 mL) and toluene-d_8 (1 mL).

The spectrum of the reaction between $[RhH(CO)(PPh_3)_3]$ and xantphos gave a doublet of doublets at 26.13 ppm with the coupling constant, $^1J_{Rh\text{-}P}$, of 147.80 Hz, and $^2J_{P\text{-}P}$, of 129.28 Hz corresponding to the xantphos phosphines. Another set of peaks, a doublet of triplets, was observed at

43.12 ppm with $^1J_{Rh-P}$, of 162.00 Hz, and $^2J_{P-P}$, of 127.26 Hz. Although the coupling constants were not too far off from those reported in the literature[15], they were consistently ~ 10 Hz higher. This was assumed to be due to a change in the reaction mixture matrix brought about the excess xantphos employed in these experiments. Note that no time period was given for the reaction to occur, this species was formed at room temperature and was observed immediately after introducing the sample into the NMR instrument. No change of spectrum was observed even after 72 hours, not even a doublet at 37.9 ppm as was observed where additional PPh_3 was omitted.

4.2.3.3 Reaction of $[RhH(CO)(PPh_3)_3]$ with MVK at ambient pressure

The reactions with methyl vinyl ketone (MVK) were investigated using NMR techniques. A spectrum of $[RhH(CO)(PPh_3)_3]$ was recorded at room temperature before the addition of MVK (10 molar equivalences relative to rhodium). Additional PPh_3 (30 molar equivalences) was employed for stability reasons as explained in the stability studies in Section 4.1.3.1. Excess MVK was added to maximise the effect of this unsaturated ketone on the catalyst and to ensure that the reaction with the inhibitor is driven to completion. Spectra obtained were, however, unsatisfactory as a result of many poorly resolved peaks recorded. This was thought to be due to the fast and messy reaction(s) between the complex and the MVK under these conditions. To eliminate this problem, the catalyst $[RhH(CO)(PPh_3)_3]$ was first pre-cooled in the NMR tube to – 60 ℃ before introducing the MVK as shown in Figure 4.8.

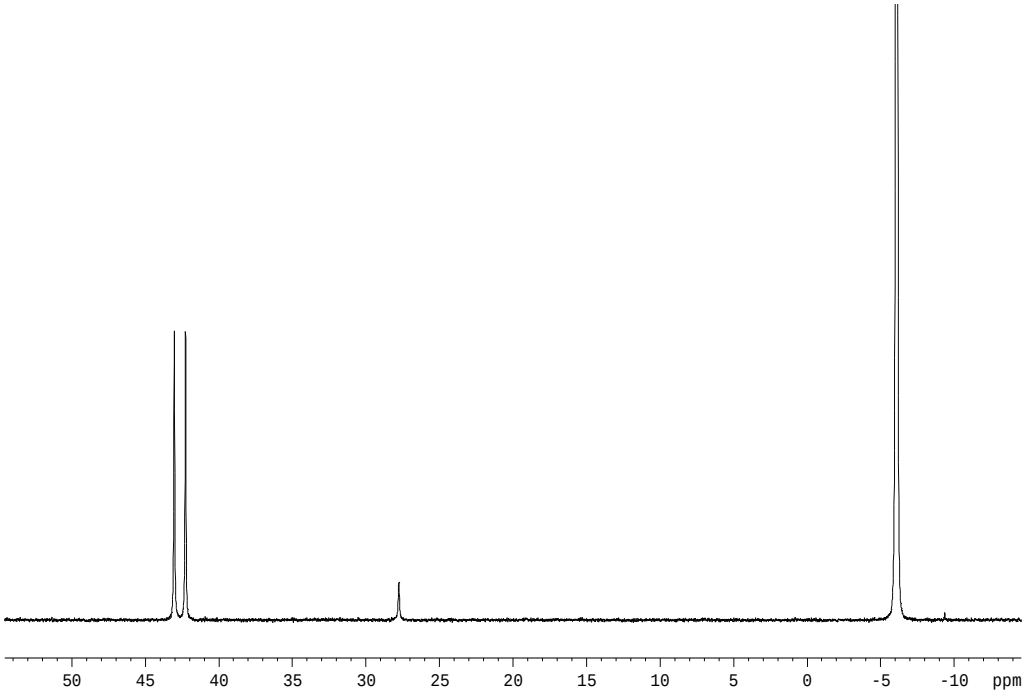

Figure 4.8. A ^{31}P NMR spectrum of $[RhH(CO)(PPh_3)_3]$ and excess PPh_3 ($Rh:PPh_3$ = 1:30) at – 60℃ in toluene (0.8 mL) and toluene- d_8 (1 mL).

Sharper peaks were recorded as compared to those recorded at room temperature suggesting a fast exchange of species at room temperature that is being slowed down or eliminated at low temperatures.

MVK was then introduced and a spectrum recorded, Figure 4.9.

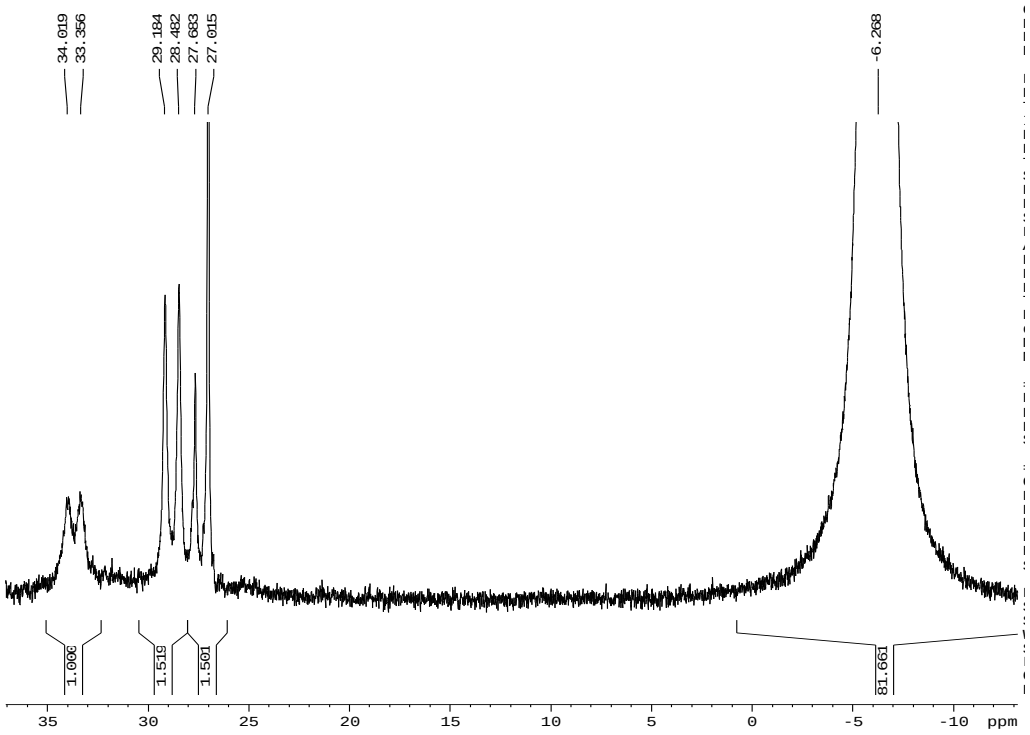

Figure 4.9. A ^{31}P NMR spectrum of $[RhH(CO)(PPh_3)_3]$ and excess PPh_3 ($Rh:PPh_3$ = 1:30) at – 60℃ in toluene (0.8 mL) and toluene-d_8 (1 mL) with 10 molar equivalents of MVK.

A doublet of doublets was observed at 28 ppm, which was consistent with two enolate isomers (E/Z) as previously described in the literature[16] and in Figure 4.10 (Also see Scheme 2.7) where the two methyl groups on the enolate may either be *cis* or *trans* to each other. Likewise, the two PPh_3 groups may also be *cis* or *trans* to each other relative to the rhodium centre.

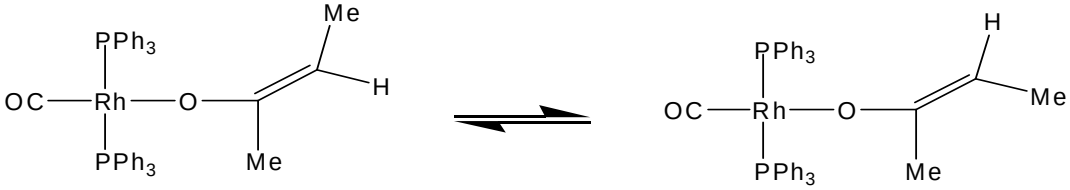

Scheme 4.2. The E/Z enolate isomers formed from the reaction between $[RhH(CO)(PPh_3)_3]$ and MVK.

To investigate the effect of MVK concentration on the catalyst, excess MVK (50 molar equivalences) was added to a pre-cooled solution of $[RhH(CO)(PPh_3)_3]$. A spectrum was then recorded for comparison purposes (Figure 4.10).

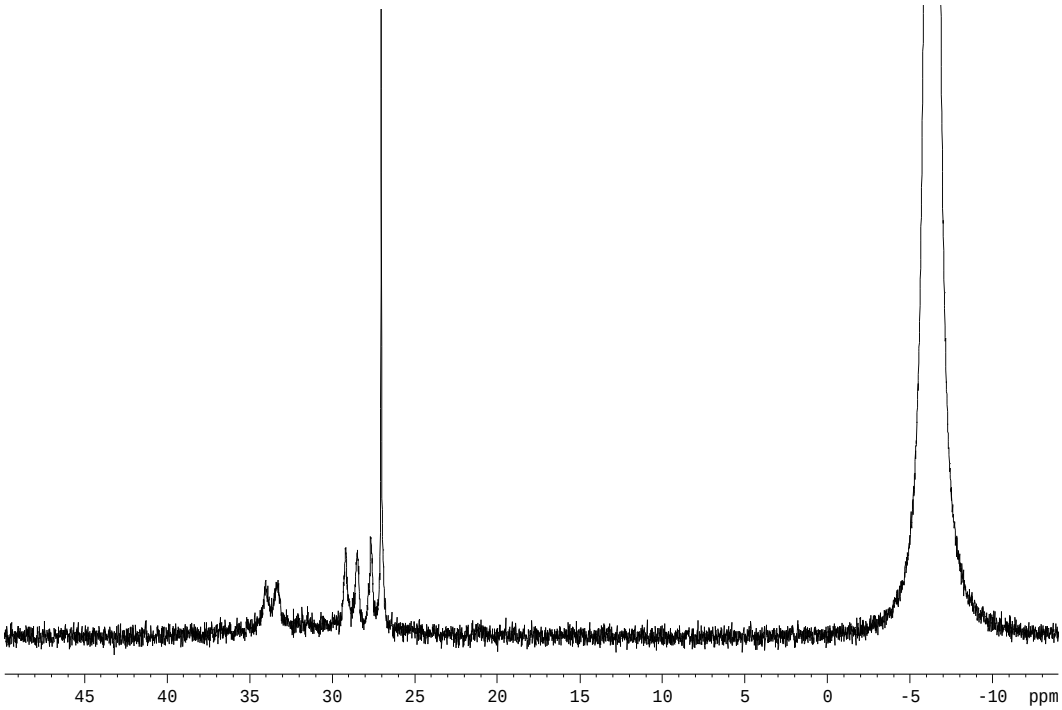

Figure 4.10. A ^{31}P NMR spectrum of $[RhH(CO)(PPh_3)_3]$ and excess PPh_3 ($Rh:PPh_3$ = 1:30) at – 60℃ in toluene (0.8 mL) and toluene- d_8 (1 mL) with excess MVK (50 molar eq.).

No significant difference was observed between the two experiments with different MVK concentration. This observation suggests that the amount of MVK employed is enough to push the reaction to completion.

After the confirmation that the reaction between $[RhH(CO)(PPh_3)_3]$ and MVK reached completion, the effect of CO was investigated. Upon

obtaining an enolate solution as described above, the NMR cell was ejected from the instrument and CO bubbled through the reaction mixture for 6 min (Figure 4.11).

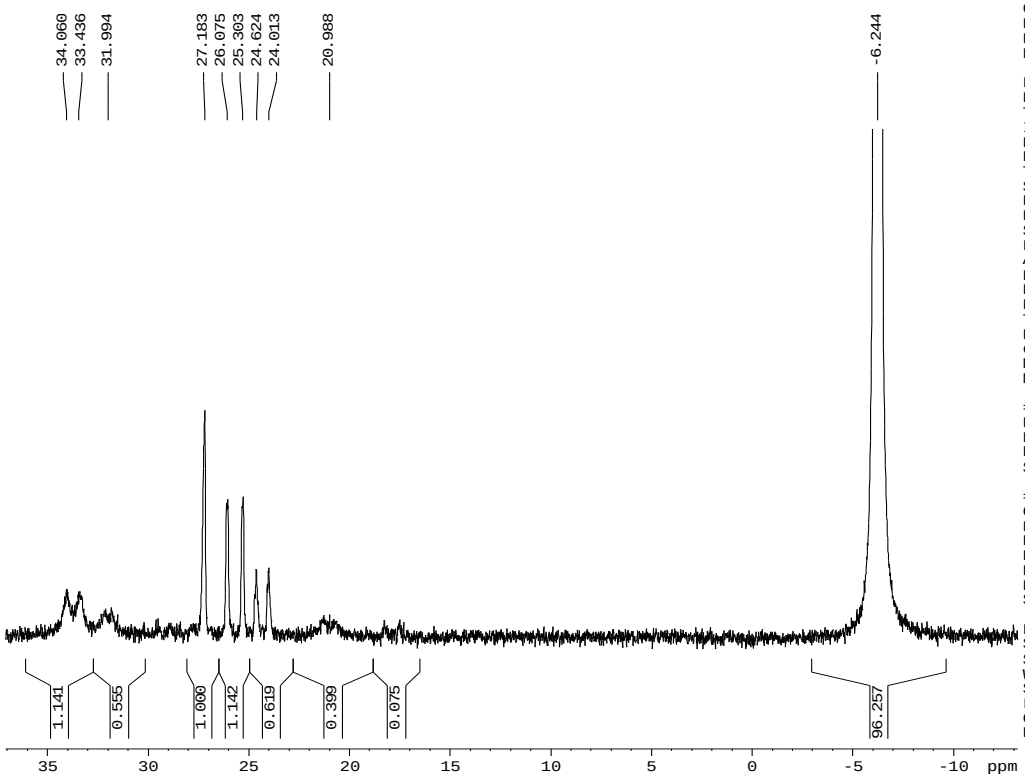

Figure 4.11. A ^{31}P NMR spectrum of $[RhH(CO)(PPh_3)_3]$ and excess PPh_3 ($Rh:PPh_3$ = 1:30) at – 60℃ in toluene (0.8 mL) and toluene- d_8 (1 mL) with 10 molar equivalents of MVK after bubbling CO for 6 min.

In the presence of CO, migratory insertion may occur where the CO may initially be associatively bonded to the metal centre and thereafter be migratory inserted between the enolate and the rhodium centre yielding the complex shown in Scheme 4.3.

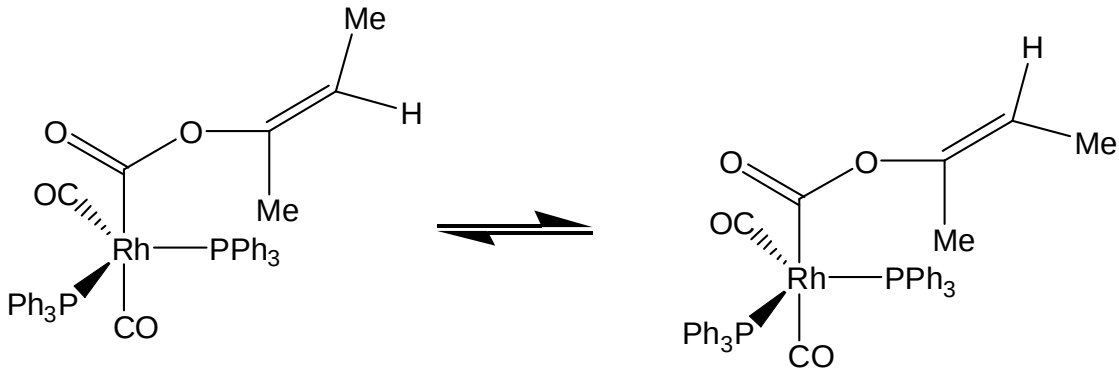

Scheme 4.3. The CO insertion product on the E/Z enolate isomers after the syngas introduction.

4.2.3.4 MVK inhibition studies on $[RhH(CO)_2(PPh_3)_2]$ by *in situ* HP-NMR Spectroscopy.

The conditions reported thus far have been at ambient pressure and low temperatures. This is however not the case during hydroformylation reactions. It was thus decided that high pressure NMR experiments (HP-NMR) be carried out with MVK addition to study the catalyst under actual hydroformylation conditions. The mixed $[RhH(CO)(PPh_3)(xantphos)]$ as well as individual $[RhH(CO)_2(PPh_3)_2]$ and $[RhH(CO)_2(xantphos)]$ catalysts were investigated at 87 °C and 17 bar syngas (H_2/CO 1:1). As the pressure increases with temperature, it was realised during HP-IR experiments that increasing the temperature from 30 to 87 °C the pressure will have increased from 17 to 20 bar.

The first catalyst to be investigated was the $[RhH(CO)_2(PPh_3)_2]$ catalyst. A ^{31}P NMR spectrum of a solution of 16 mM $[Rh(acac)(CO)_2]$ and 60 molar equivalences PPh_3 was recorded at 30 ℃ before heating the reaction mixture to 87 °C as shown in Figure 4.12. Only a maximum Rh:PPh_3:Xp ratio of 1:60:1.1 could be employed due to solubility reasons at the high concentrations required for NMR experiments.

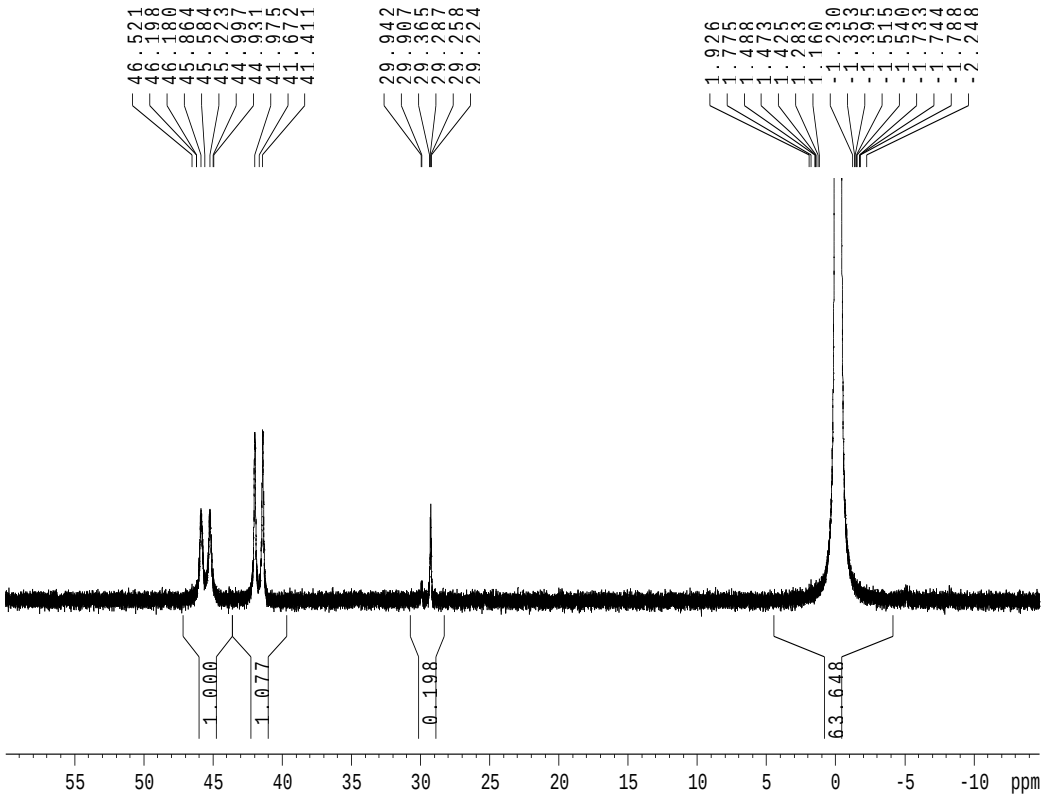

Figure 4.12. A ^{31}P NMR spectrum of the mixture of $[Rh(acac)(CO)_2]$ and PPh_3 (Rh:PPh_3 = 1:60) under 17 bar syngas (H_2:CO = 1:1) pressure at 30 ℃ in toluene (0.8 mL) and toluene-d_8 (1 mL).

A doublet indicative of the active hydride, $[RhH(CO)(PPh_3)_3]$, was observed at 46.1 ppm suggesting that the hydride was formed even before heating the reaction mixture. A doublet observed at 41.6 ppm was assumed to be due to the other hydride species, $[RhH(CO)_2(PPh_3)_2]$. No significant change was observed upon heating the reaction mixture to the reaction temperature. 200 molar equivalences of MVK were then added to investigate the effect the inhibitor has on the $[RhH(CO)_2(PPh_3)_2]$ catalyst. Excess MVK was employed with the aim of amplifiying the effect of inhibition on the catalyst and subsequently driving the conversion to the

inhibited species as close to 100 % as possible. This excess amount of the inhibitor was also employed to ensure conditions that were as close to autoclave conditions as possible. The cell was then repressurised to 17 bar with syngas and shaken vigorously to allow for gas dissolution into the reaction solution before recording another spectrum (Figure 4.13).

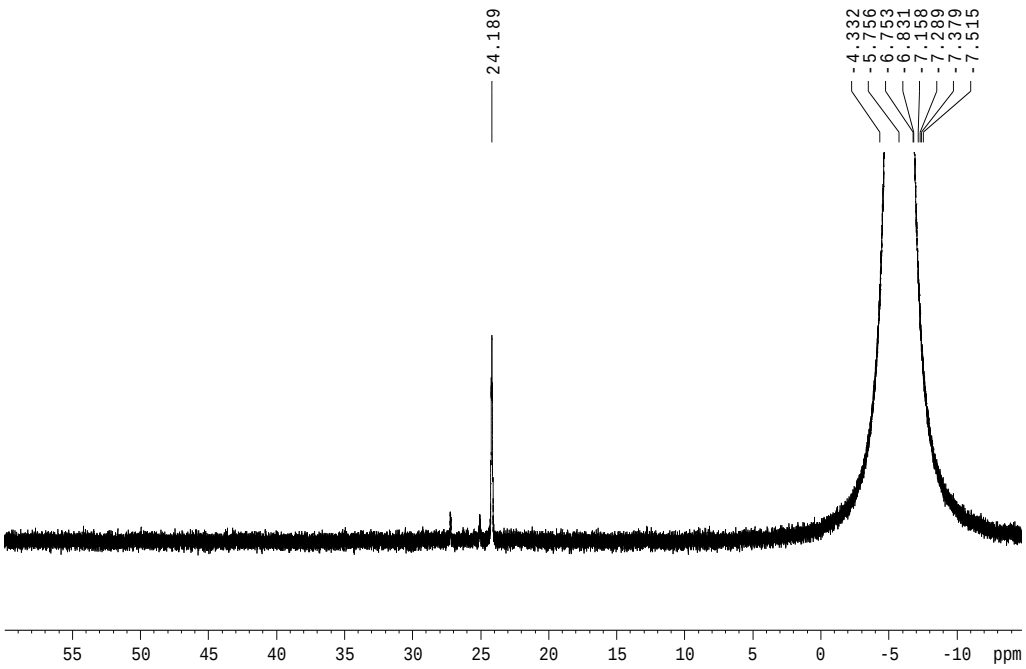

Figure 4.13. A ^{31}P NMR spectrum of the mixture of $[Rh(acac)(CO)_2]$ and PPh_3 (Rh:PPh_3 = 1:60) under 17 bar syngas (H_2:CO = 1:1) pressure and at 30 ℃ in toluene (0.8 mL) and toluene-d_8 (1 mL) with excess MVK (200 molar equivalents).

The severe deleterious effect of MVK on the $[RhH(CO)_2(PPh_3)_2]$ catalyst species is evident from the absence of a rhodium hydride species in the spectra recorded, even after heating the solution at 87 °C for 30 minutes. The solution was then heated for another 10 minutes and cooled to room temperature before another spectrum was recorded. Taking the reaction temperature to – 60 ℃ resulted in the spectrum ill ustrated below in Figure 4.14.

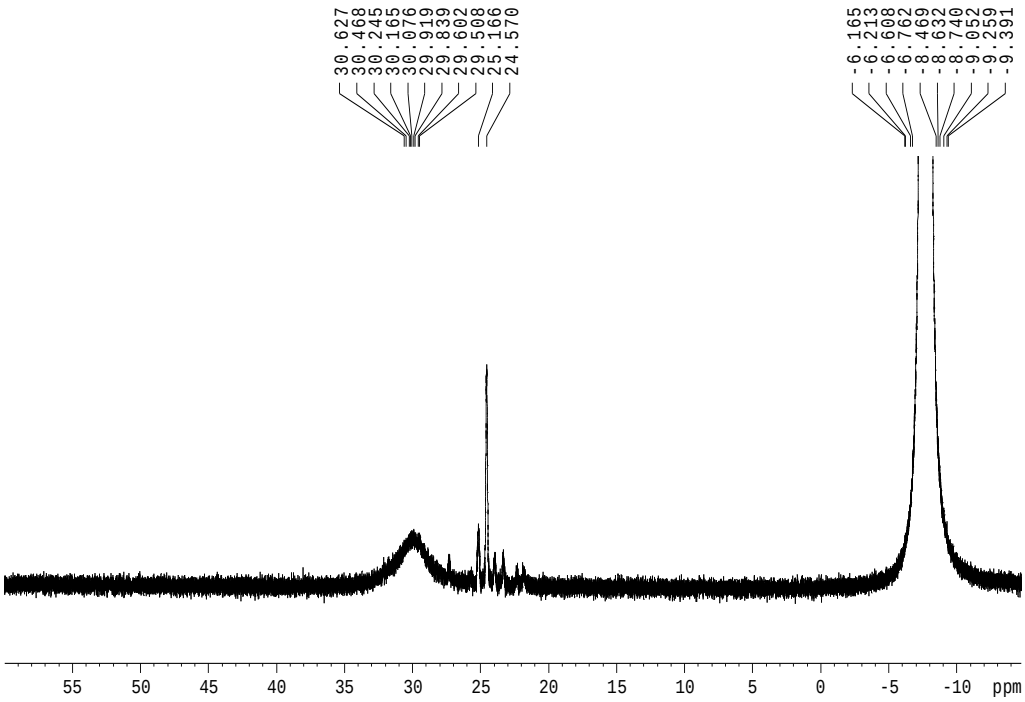

Figure 4.14. A ^{31}P NMR spectrum of the mixture of $[Rh(acac)(CO)_2]$ and PPh_3 (Rh:PPh_3 = 1:60) under 17 bar syngas (H_2:CO = 1:1) pressure at 30 ℃ in toluene (0.8 mL) and toluene-d_8 (1 mL) with 200 molar equivalents of MVK after heating the reaction mixture for 10 minutes at 87 ℃ and cooling down to –60 ℃.

A multiplet of peaks was observed at 23.7 ppm and was thought to be due to the inhibited species as well as dimers that might have formed under these conditions. A broad peak (hump) at 30 ppm was attributed to dimer formation. No further changes were observed in spectra recorded at this temperature suggesting that no active hydride could be regenerated under these conditions.

4.2.3.5 MVK inhibition studies on [$RhH(CO)_2$(xantphos)] by *in situ* HP-NMR Spectroscopy.

Xantphos studies were then carried out for comparison purposes with a Rh:Xp ratio of 1:1.1. Similar procedures were followed and a spectrum recorded at 30 ℃ and 17 bar syngas as shown below in Figure 4.15.

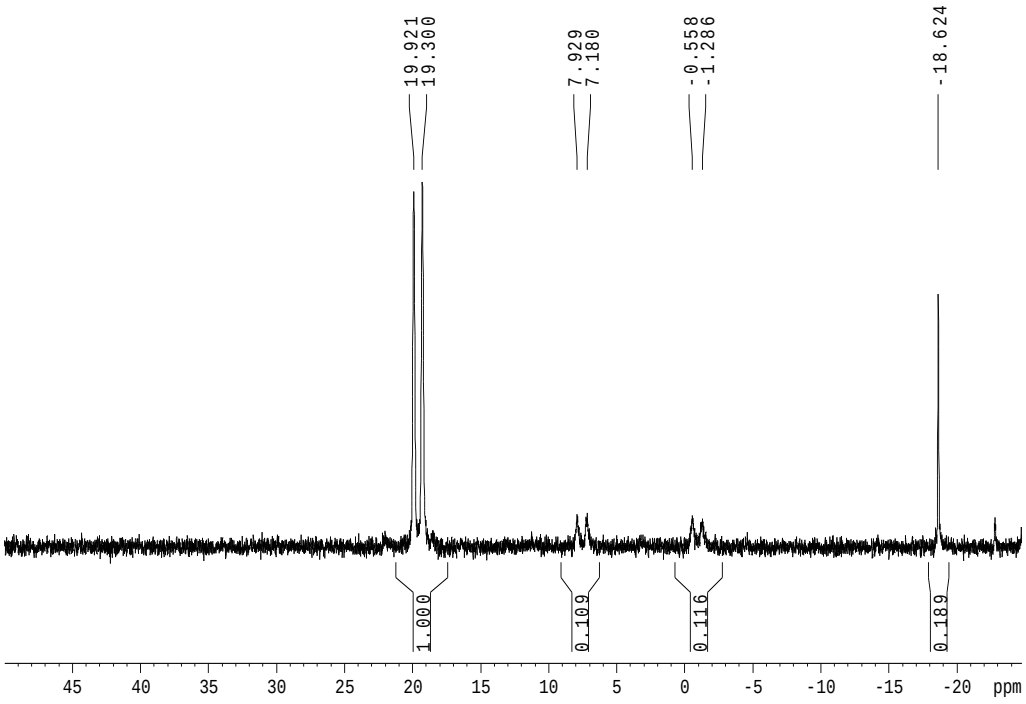

Figure 4.15. A ^{31}P NMR spectrum of the fully preformed [$RhH(CO)_2$(xantphos)] catalyst from a mixture of [$Rh(acac)(CO)_2$] and xantphos (Rh:Xp = 1:1.1) under 17 bar syngas (H_2:CO = 1:1) pressure at 30 ℃ in toluene (0.8 mL) and toluene-d_8 (1 mL) after heating to 87 ℃ for 10 minutes.

A doublet at 19.9 ppm with $^1J_{Rh\text{-}P}$ = 125.53 Hz confirmed the fully preformed active hydride, with the free xantphos ligand at –18.6 ppm.

Uncharacterised doublets were observed at 7.9 ppm and – 0.6 ppm with $^1J_{Rh\text{-}P}$ = 149.83 Hz and $^1J_{Rh\text{-}P}$ = 159.95 Hz respectively. These doublets were assumed to be due to dimers formed. MVK (200 molar equivalences relative to Rh) was added and a spectrum recorded at 30 ℃ after heating the reaction mixture for 10 minutes at 87 ℃ (Figur e 4.16).

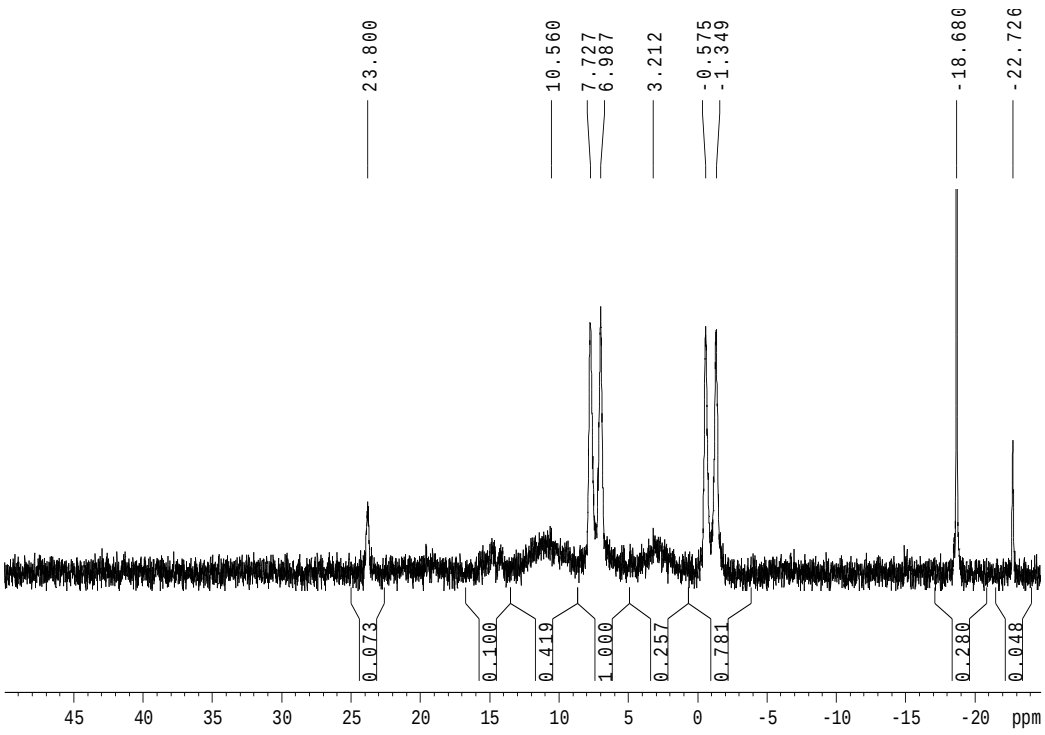

Figure 4.16. A ^{31}P NMR spectrum of [$RhH(CO)_2$(xantphos)] with Rh:Xp ratio of 1:1.1 under 17 bar syngas (H_2:CO = 1:1) pressure at 30 ℃ in toluene (0.8 mL) and toluene-d_8 (1 mL) after adding 200 molar equivalents of MVK and heating to 87 ℃ for 10 minutes.

A complete disappearance of the hydride was observed with an increase in the doublets at 7.9 and – 0.6 ppm. The reaction mixture was then heated for 45 minutes at 87 ℃ and 20 bar syngas in an attempt to regenerate the active hydride.

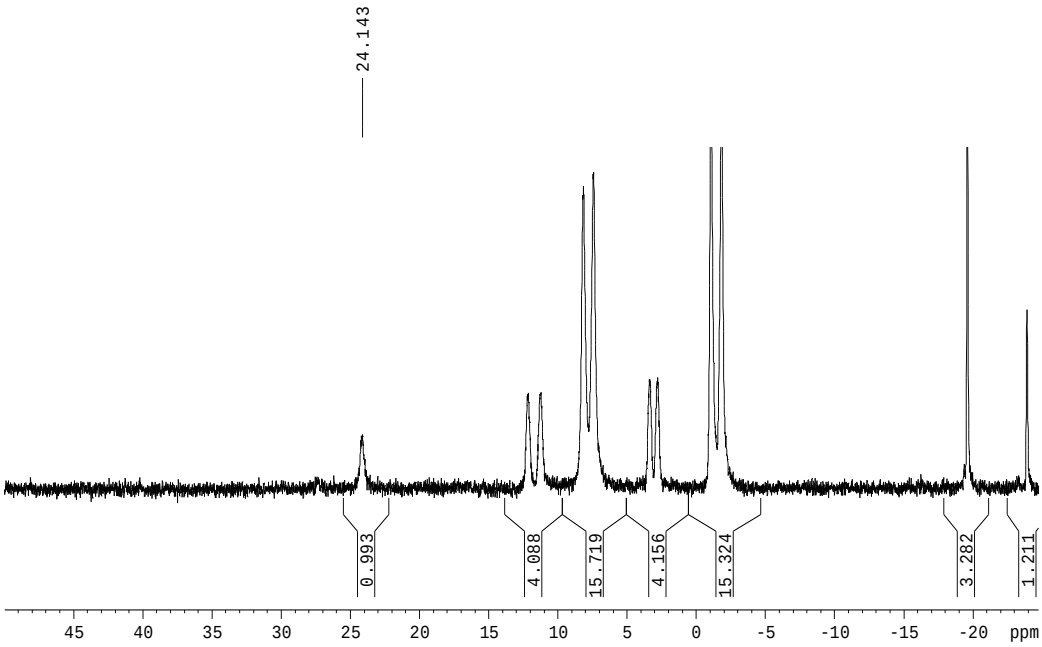

Figure 4.17. A ^{31}P NMR spectrum of $[RhH(CO)_2(xantphos)]$ with Rh:Xp ratio of 1:1.1 under 17 bar syngas (H_2:CO = 1:1) pressure at 30 ℃ in toluene (0.8 mL) and toluene-d_8 (1 mL) after adding 200 molar equivalents of MVK and heating to 87 ℃ for 45 minutes and cool ing down to –20 ℃.

Unlike with $[RhH(CO)_2(PPh_3)_2]$ where no significant reformation of peaks was observed, the $[RhH(CO)_2(xantphos)]$ catalyst inhibition experiment displayed reformation of new peaks and an increase in intensity of existing peaks. An increase in intensity of the doublets at 7.9 ppm and – 0.6 ppm was observed with more doublets forming at 12 ppm and 3 ppm with $J_{Rh\text{-}P}$ = 147.59 Hz and $J_{Rh\text{-}P}$ = 148.20 Hz respectively. These results were, however, contrary to those obtained earlier with autoclave studies (Section 4.3.2) where MVK had little to no effect on the $[RhH(CO)_2(xantphos)]$. The reason for this discrepancy was attributed to dimer formation during the MVK addition with NMR experiments. MVK addition necessitated the cell to be completely depressurised to allow for the inhibitor to be syringed into the reaction mixture, which may have resulted in dimer formation at an expense of the active hydride. It is worth noting that the M:L ratio was

considerably lower than that employed during autoclave studies due to the poor solubility of the Xp at higher concentrations. Mass transfer limitations experienced with the NMR technique were also thought to contribute to this observation, which were aggravated by the high concentrations employed.

4.2.3.6 MVK inhibition studies on [RhH(CO)(PPh_3)(xantphos)] by *in situ* HP-NMR Spectroscopy

The mixed catalyst system was investigated for comparison purposes while using similar procedures and quantities as above. Below in Figure 4.18 is the spectrum indicating the catalyst species formed after heating the reaction mixture and cooling to 30 °C.

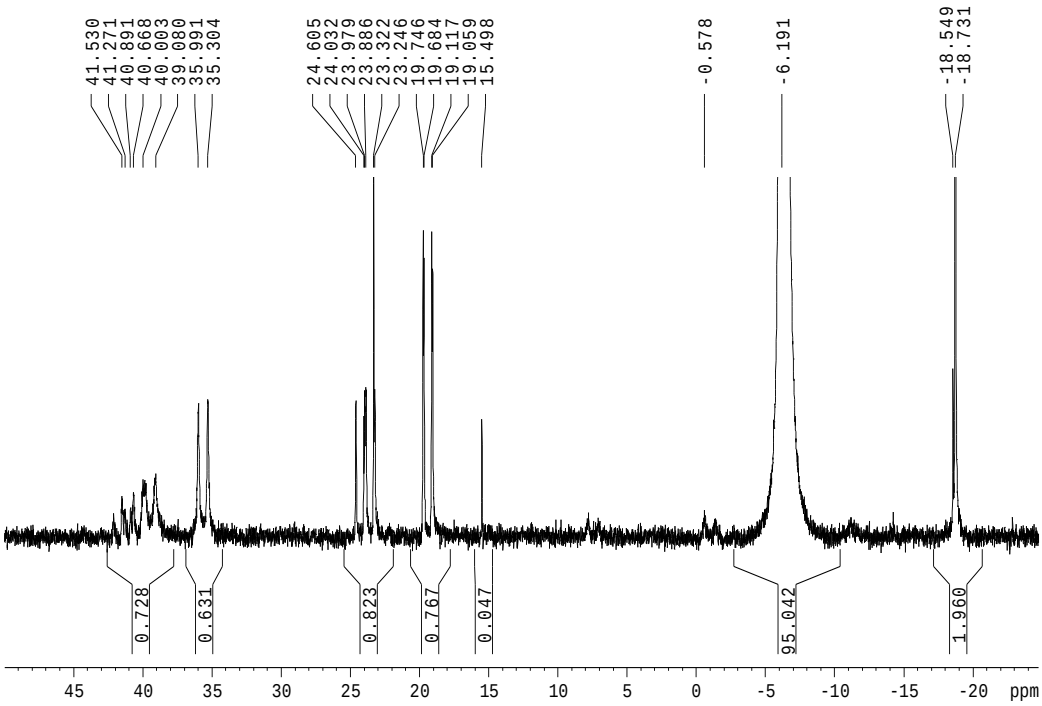

Figure 4.18. A ^{31}P NMR spectrum of RhH(CO)(PPh_3)(xantphos)] catalyst with Rh:PPh_3:Xp ratio of 1:60:1.1 under 17 bar syngas (H_2:CO = 1:1) pressure at 30 ℃ in toluene (0.8 mL) and toluene-d_8 (1 mL).

Table 4.1. Labelling of catalytic species formed

Species	**NMR spectra (ppm)**
$[RhHCO(PPh_3)Xp]$	40.8 and 23.9
$[RhH(CO)(PPh_3)_3]$	40.0
$[RhH(CO)_2(PPh_3)_2]$	35.9
$[RhH(CO)_2Xp]$	19.6
Free PPh_3	– 6
PPh_3 Oxide	23.3
xantphos	– 18
xantphos oxide	– 22.7/23.8

MVK (200 molar equivalences relative to rhodium) was then added and a spectrum recorded (Figure 4.19). The excess MVK was employed with the aim of operating at conditions that were as close as possible to the autoclave studies conditions.

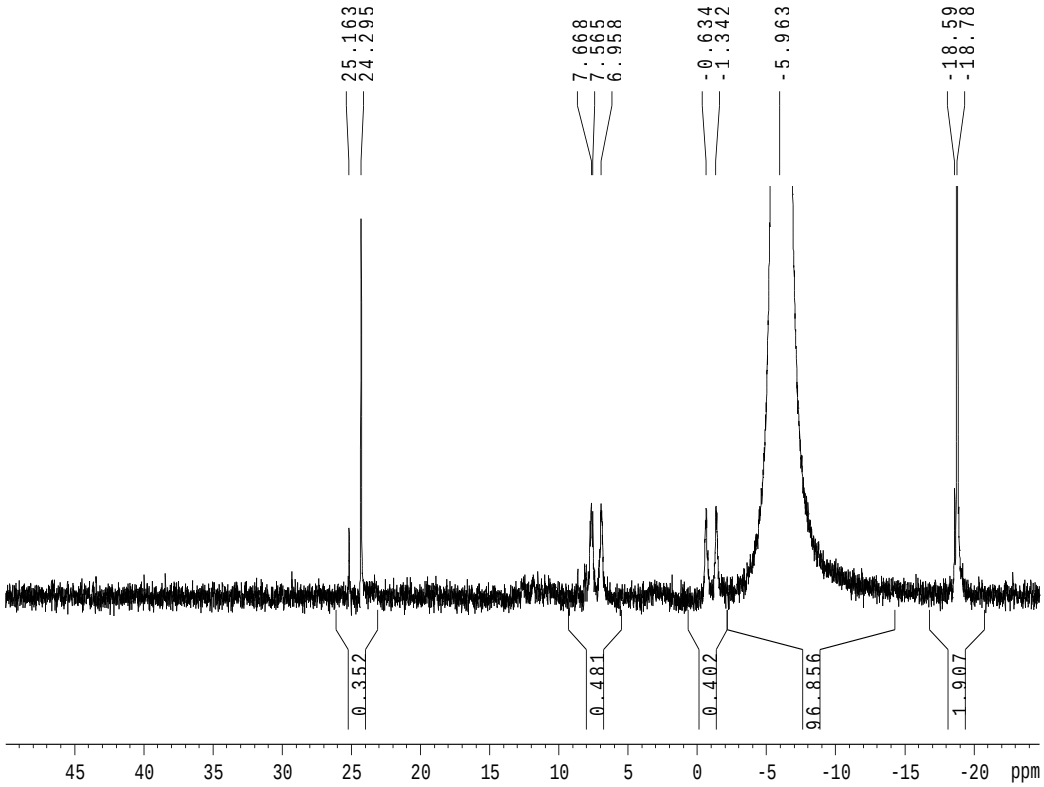

Figure 4.19. A ^{31}P NMR spectrum of [RhH(CO)(PPh_3)(xantphos)] catalyst with Rh:PPh_3:Xp ratio of 1:60:1.1 under 17 bar syngas (H_2:CO = 1:1) pressure at 30 ℃ in toluene (0.8 mL) and toluene-d_8 (1 mL) after adding 200 molar equivalents of MVK and heating to 87 ℃ for 10 minutes.

A spectrum similar to that of inhibited [RhH$(CO)_2$(xantphos)] was observed with no indication of the inhibited [RhH$(CO)_2(PPh_3)_2$]. This observation is in agreement with previous results obtained where the Rh-PPh_3 species were seen to be more inhibited than the [RhH$(CO)_2$(xantphos)].

The reaction mixture was heated for 45 minutes and the effect of MVK investigated over time as shown in Figure 4.20.

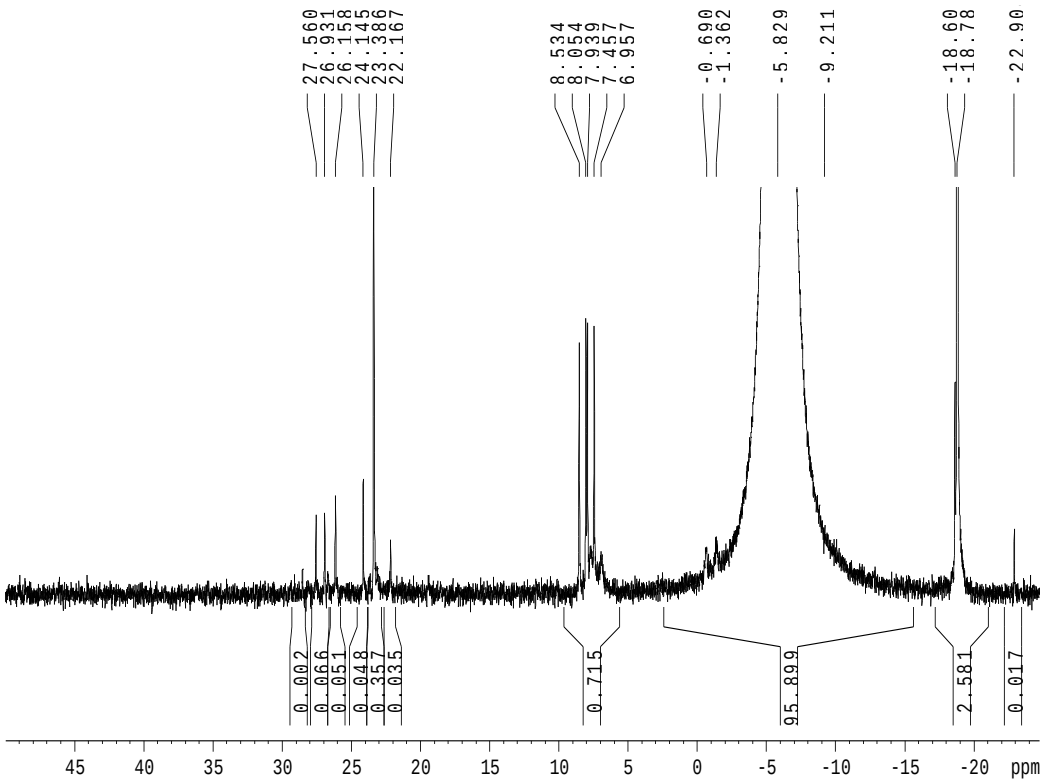

Figure 4.20. [A ^{31}P NMR spectrum of $RhH(CO)(PPh_3)$(xantphos)] catalyst with $Rh:PPh_3$:Xp ratio of 1:60:1.1 under 17 bar syngas (H_2:CO = 1:1) pressure at 30 ℃ in toluene (0.8 mL) and toluene-d_8 (1 mL) after adding 200 molar equivalents of MVK and heating to 87 ℃ for 45 minutes.

The only Rh-PPh_3 catalyst that was regeneration was the tris-PPh_3 species ([$RhH(CO)(PPh_3)_3$]) with no indication of the bis-PPh_3 species ([$RhH(CO)_2(PPh_3)_2$]) reforming, even after heating the reaction mixture for 45 minutes. This species was witnessed by a set of peaks at 24 ppm. Both the [$RhH(CO)_2$(xantphos)] and the [$RhH(CO)(PPh_3)$(xantphos)] species regenerated as observed from the following set of peaks:

- [$RhH(CO)(PPh_3)$(xantphos)]: A triplet of doublets at 26 ppm and a doublet of doublets at 8 ppm.
- [$RhH(CO)_2$(xantphos)]: A doublet at – 1 ppm with J_{Rh-P} = 135.65 Hz.

There was a consistent shift of chemical shifts towards lower field with all Rh complexes that were regenerated. This shift was attributed to a change in the polarity of the reaction matrix from the added MVK and its hydrogenated product, 2-butanone.

4.2.3.7 Conclusions

The stabilising effect of additional PPh_3 on the $[RhH(CO)_2(PPh_3)]$ catalyst was highlighted in this section. In cases where no additional PPh_3 was added, formation of other peaks was observed at an expense of the active hydride. These peaks were assumed to be mainly due to dimer formation. Additional to this observation, excess PPh_3 is required as some ligand will be lost through oxidation as observed with a peak at 23.3 ppm as illustrated in Table 4.1. Similar results can be observed in Section 5.4.2.

Advantages highlighted earlier of using xantphos as a secondary ligand in the aim of conferring some inhibitor resistance to the active catalyst were again confirmed by these results. The difference between the mixed and the pure system is that in the pure system, as observed with the $[RhH(CO)_2(xantphos)]$ and $[RhH(CO)_2(PPh_3)_2]$ species, dimer formation is enhanced when the reaction mixture is degassed, whilst the monomeric species are formed in the mixed system.

4.3 *In situ* HP-IR spectroscopy studies

4.3.1 Introduction

Many advances in spectroscopic studies, related to the field of homogeneous catalysis, have been made over the past years. Techniques such as high pressure IR and NMR (HP-IR and HP-NMR) have, for example, been employed, with great success, for the *in situ* characterisation of catalytic species. The study of diphosphite modified rhodium catalyst is one example, amongst many, where these techniques were in a complementary manner used to study the factors influencing the rates and selectivities of the catalyst in hydroformylation reactions.[17] The data collected from both IR and NMR spectroscopic studies pointed towards the same catalytic species where the five co-ordinated Rh(I) complex was formed containing a hydrido ligand and the diphosphite co-ordinated in a bidentate fashion. Bulky and bis-equatorially (*ee*) co-ordinating diphosphites, induced by a natural bite angle of approximately 120°, were observed to be responsible for high regioselectivity towards the linear aldehyde. However, these rigid diphosphite ligands gave slower rates in comparison to their flexible counterparts. Conversely, flexible and equatorially-axially (*ea*) co-ordinating diphosphites lead to the enhancement of the formation of branched aldehyde and higher rates comparable to those of a PPh_3-modified system. Many other studies have furthermore confirmed the value of using both the NMR and IR spectroscopy in obtaining a better understanding of catalytic species involved in catalytic reactions.[18] In the latter study, van Leeuwen and colleagues employed bidentate phosphine ligands to demonstrate the effect of ligand properties on the selectivity and activity of hydroformylation reactions using HP-NMR and HP-IR spectroscopy for characterisation.

Unfortunately, high concentrations are normally required in NMR experiments in order to obtain satisfactory signal to noise ratios. Equilibria involved under these high concentrations, however, deviate considerably from those obtained under actual catalytic conditions (may be a hundred fold higher). It is furthermore worthy to note inherent mass transfer limitations of the NMR technique (although this shortcoming might be advantageous as kinetic products may be intercepted). The IR is for these reasons a better alternative. Rhodium-carbonyl complexes have strong absorptions for the CO stretching vibrations; consequently, low concentrations that approach real catalytic conditions can be employed. Studies have been carried out where HP-IR conditions were almost perfectly similar to those applied in the actual catalytic reactions.[19] This can be attained as the HP-IR cell is itself an autoclave. HP-IR assisted in distinguishing the *ee* and the *ea* geometric isomers of the hydride-dicarbonyl resting state with various bisphosphine ligands. Moreover, the HP-IR provided valuable information on the decomposition of Rh species into non-phosphine containing complexes that would not have been satisfactorily detected using the HP-NMR technique (due to a fast exchange between the isomers, only an average between the two is observed in the NMR). Since HP-IR spectroscopic studies can be carried out under real catalytic conditions, activities and selectivities obtained during hydroformylation reactions can be related to the observed species.[20]

4.3.2 Experimental

HP-IR experiments were carried out in an EQUINOX55 Bruker IR instrument equipped with a 55 mL stainless steel autoclave and ZnS windows. The autoclave was fitted with a mechanical stirrer, two dip-

tubes, a vent line connected to the fume hood, a rapture valve (RV), a pressure transducer and a thermocouple. A control-box was used to control and indicate the temperature while the pressure was controlled by a high-pressure regulator.

$[Rh(acac)(CO)_2]$ (98 %), xantphos (97 %) and MVK (99 %) were purchased from Aldrich while PPh_3 (99.9 %) was obtained from BASF. These reagents were used as purchased. DHN (98 %) was obtained from Aldrich and was degassed with argon before use. Syngas (49.9 % CO balanced with H_2) was obtained from Air-liquide while argon (99 %) was obtained from Afrox.

All spectra were collected with a resolution of 4 cm^{-1} with 32 scans. Procedures followed for all HP-IR experiments were analogous, so only one typical procedure will be described.

HP-IR experiments were carried out using decahydronaphthalene (DHN) as a solvent of choice. The reasons for this are as follows:

- DHN does not absorb in the CO region thereby minimising errors during subtraction of background spectra.
- The rhodium precursor and the ligand are soluble in the solvent. Although the solubility of the reagents in other solvents such as toluene is significantly better, they have the disadvantage of absorbing strongly in the carbonyl region. This introduces errors during subtraction of solvent backgrounds.
- The lower votality of DHN over other solvents like cyclohexane allowed for the reactor to be depressurised at high temperatures and pressures during pressure effect studies without losing a significant amount of the solvent.

Before HP-IR experiments could be carried out, background spectra of the solvent were collected under reaction conditions. After flushing the HP-IR cell with argon, a background spectrum was collected at 30 ℃ and 10 bar argon. The reactor was then evacuated, flushed with syngas (H_2:CO 1:1) and pressurised to ~18 bar syngas before collecting spectra at 10 ℃ intervals until the temperature reached 100 ℃. When the temperature reached 80 ℃, the pressure reached 20 bar.

In order to have an inert atmosphere at the commencement of the reaction, the HP-IR cell was flushed with argon before introducing the reagents. [Rh(acac)$(CO)_2$] (0.024 mmol; 6.19 mg) was dissolved in DHN (7.5 mL) and introduced into the reactor *via cannula* under argon atmosphere. After recording the spectrum at 30 ℃ and 10 bar argon, a solution of xantphos (0.0048 mol; 28.60 mg) in DHN (7.5 mL) was introduced and the reagents allowed to react for about 5 min before recording a spectrum at 30 ℃ and 10 bar argon. For monodentate experiments, xantphos was replaced with PPh_3 (4.08 mmol; 1070.14 mg) and the same procedure followed. The reactor was then flushed with syngas, pressurised to ~18 bar and heated to the reaction temperature (90 ℃) to preform the catalyst. Spectra were recorded at 10 ℃ intervals. During inhibition studies, MVK (4.8 mmol; 0.40 mL) was added through a dip tube after the catalyst was fully preformed. These conditions were chosen as they most closely resemble those employed in autoclave studies.

4.3.3 Results and Discussion

A study of the literature has shown that extremely valuable information may be obtained from *in situ* spectroscopic studies, especially those involving IR.[21] This prompted us to carry HP-IR spectroscopic studies on

the $[RhH(CO)_2(xantphos)]$ catalyst system and $[RhH(CO)_2(PPh_3)_2]$ for comparison purposes. This study will not only contribute to understanding the different catalytic species involved in hydroformylation reactions but also allow for comparisons to work already published in the open literature.

4.3.3.1 $[RhH(CO)_2(PPh_3)_2]$ preforming studies by *in situ* HP-IR Spectroscopy

The traditional monodentate ligand, PPh_3, was studied for benchmark and comparisons with the bidentate xantphos ligand. Initially, the IR spectrum of the catalyst precursor $[Rh(acac)(CO)_2]$ and PPh_3 dissolved in DHN was recorded under 17 bar syngas pressure before heating the reaction mixture to allow preforming. Figure 4.21 below illustrates the comparison between the starting and the fully preformed catalyst.

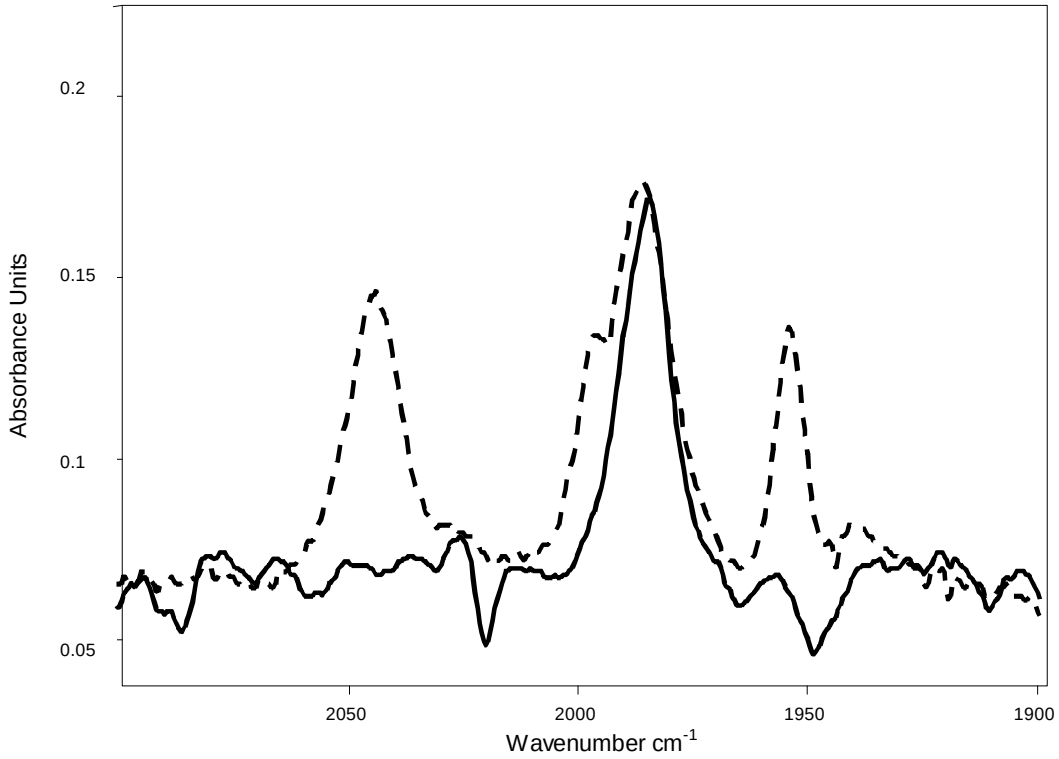

Figure 4.21. A comparison between the HP-IR spectrum of starting $[RhH(CO)_2(PPh_3)_2]$ catalysts and the fully preformed one. Solid: $[Rh(acac)(CO)_2]$: $P(Ph)_3$ 1:90 at 30 ℃ and 17.5 bar syngas. Dashed: $[Rh(acac)(CO)_2]$: $P(Ph)_3$ 1:90 at 90 ℃ and 20 bar syngas for 5 minutes.

A single peak at 1985 cm^{-1} was recorded during preforming before the fully preformed catalyst was obtained at 90 ℃. The fully preformed catalyst was witnessed by four absorption bands at 2043, 1997, 1986 and 1953 cm^{-1}. These observed carbonyl bands were consistent with those observed in the literature.[14,22] Appearance of these peaks, characteristic of the Rh hydride, during preforming was slightly delayed relative to their formation when bidentate ligands were employed. Peaks characteristic of the hydride only appeared at temperatures higher than 50 ℃ while they

would normally appear at temperatures as low as 30 ℃ with bidentate ligands.

4.3.3.2 $[RhH(CO)_2(PPh_3)_2]$ stability studies by *in situ* HP-IR Spectroscopy

The effect of temperature on the hydride was investigated. After preforming the catalyst, the temperature was decreased to 40 ℃. No change was observed on the spectrum recorded even after an extended period of time (200 min). The effect of pressure on the hydride was also investigated where the reactor was depressurised to 5 bar. A drifting baseline was observed possibly due to subtraction errors at low pressures. However, no change in the catalytic species was observed until the reactor was depressurised to 0 bar, with the aim of depleting syngas from the reaction mixture. After the depletion of syngas, a complete absence of the active catalyst was observed with no peak present in the spectrum recorded. The reactor was then flushed with syngas and re-pressurised to 20 bar in an attempt to re-generate the catalyst. Illustrated below in Figure 2.22 is the comparison between the freshly preformed catalyst and the re-generated one at 90 ℃ and 20 bar syngas.

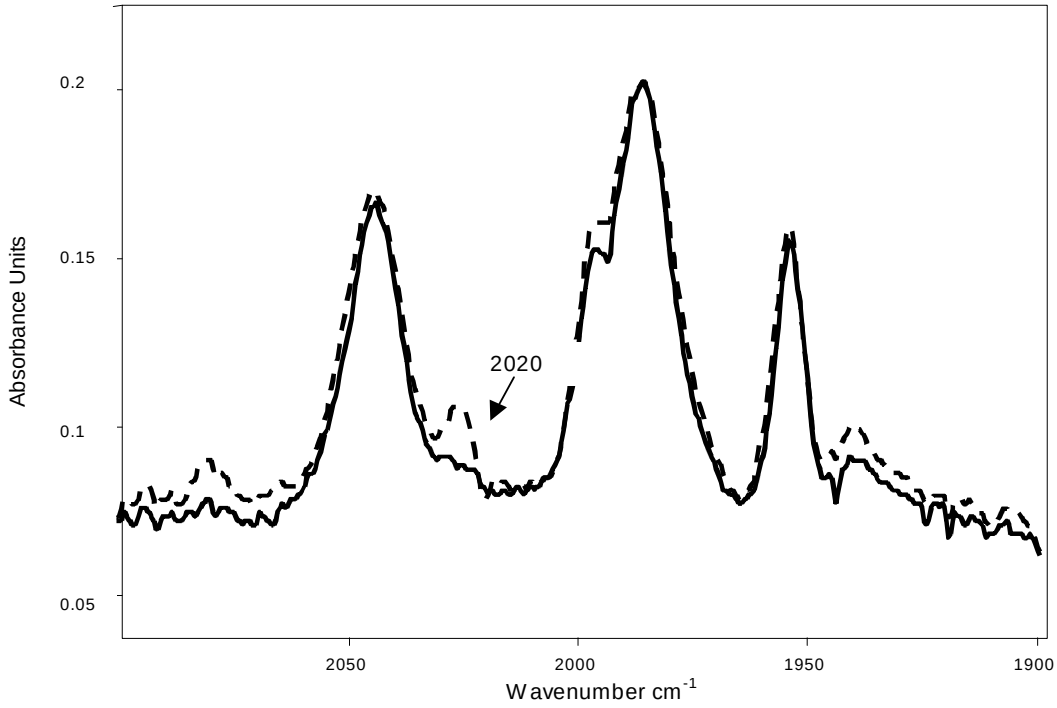

Figure 4.22. A comparison between the HP-IR spectrum of a freshly preformed catalyst and that of the regenerated one. Solid: $[Rh(acac)(CO)_2]$: PPh_3 1:90 at 90 ℃ and 20 bar syngas. Dashed: $[Rh(acac)(CO)_2]$: PPh_3 1:90 at 90 ℃ and 20 bar syngas after total syngas depletion and re-pressurising.

The regeneration of the active catalyst was afforded at 40 ℃ and 20 bar syngas with a peak appearing at 2020 cm^{-1}. This peak was thought to be due to dimers formed upon depleting the reaction solution from syngas. Syngas is seen to have a major effect on the stability of the hydride. It is, however, only after completely depleting the reaction mixture from syngas that this effect is realised. Depressurising the reactor to 5 bar did not have an effect on the catalyst stability since enough syngas is still present in the reaction mixture.

4.3.3.3 MVK inhibition of $[RhH(CO)_2(PPh_3)_2]$ studied by *in situ* HP-IR Spectroscopy

The inhibition effect of MVK on $[RhH(CO)_2(PPh_3)_2]$ was investigated. Following results obtained during autoclave studies (Section 5.3.2) where the $[RhH(CO)_2(PPh_3)_2]$ was inhibited even when Rh:PPh_3 ratios as high as 1:170 were employed, it was decided that this inhibition should be evaluated spectroscopically using HP-IR at similar conditions to those employed when $[RhH(CO)_2(PPh_3)_2]$ inhibition was studied. To avoid complications and uncertainties in characterising the species, only pure ligand systems were considered during inhibition studies.

After preforming the $[RhH(CO)_2(PPh_3)_2]$ hydride at 90 ℃ and 20 bar syngas, a spectrum was recorded and MVK (200 molar equivalences relative to rhodium) subsequently added to study it's inhibition effect on the $[RhH(CO)_2(PPh_3)_2]$ hydride. A spectrum was then recorded and comparisons made as shown in Figure 5.23 below.

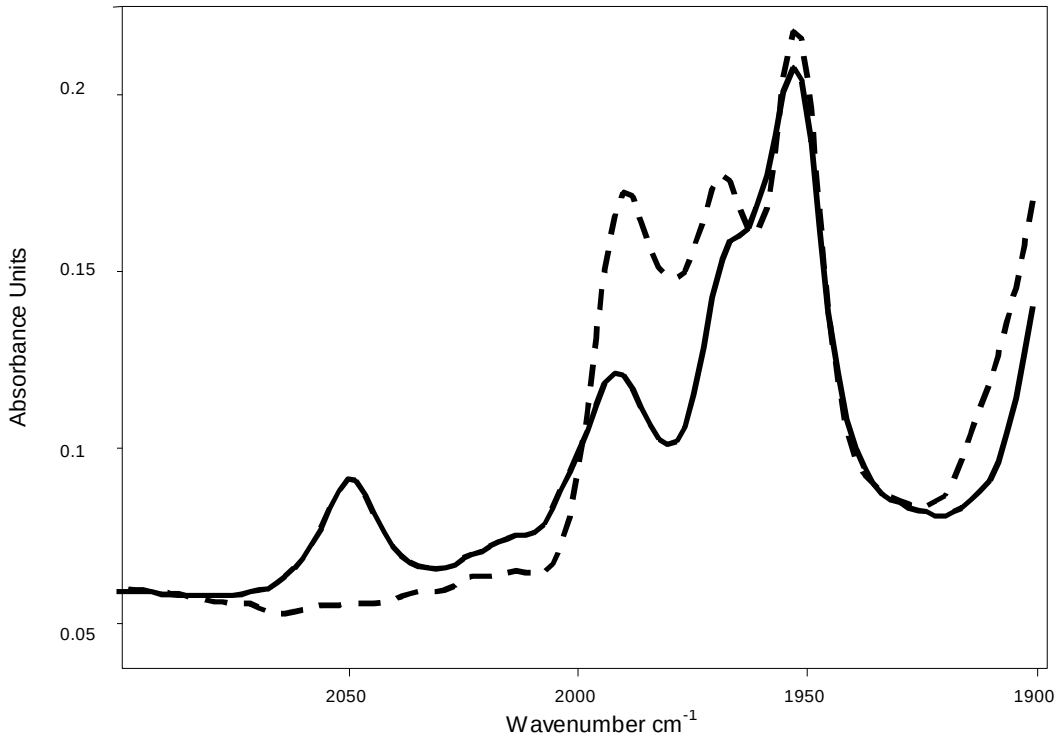

Figure 4.23. A comparison between the HP-IR spectrum of the freshly preformed $[RhH(CO)_2(PPh_3)_2]$ ($Rh:PPh_3$ = 1:170) catalyst (solid) and the MVK (Rh:MVK = 1:200) inhibited one (dashed) at 90 °C and 20 bar syngas.

A different spectrum of the preformed catalyst was recorded in comparison to the ones recorded earlier (Figure 5.23). The reason for this is the excess PPh_3 employed with the former compared to the latter where the PPh_3 concentration was almost doubled ($Rh:PPh_3$ = 1:170 vs. 1:90). Not only will the excess PPh_3 change the reaction matrix, but it will also populate the higher PPh_3 substituted species ($[RhH(CO)(PPh_3)_3]$) that will cause discrepancies between the two preformed hydrides. This observation is explained in Section 4.3.3. Inhibition was witnessed by the

disappearance of a peak 2044 cm^{-1} and an increase of the peak at 1986 and 1962 cm^{-1}.

The reaction was left to stir at 90 ℃ and 20 bar s yngas to allow for regeneration of the active catalyst to occur. Figure 5.24 below illustrates the comparison between the freshly preformed and the regenerated catalyst at the reaction conditions, *i.e.* 90 ℃ and 20 bar syngas (H_2:CO = 1:1) .

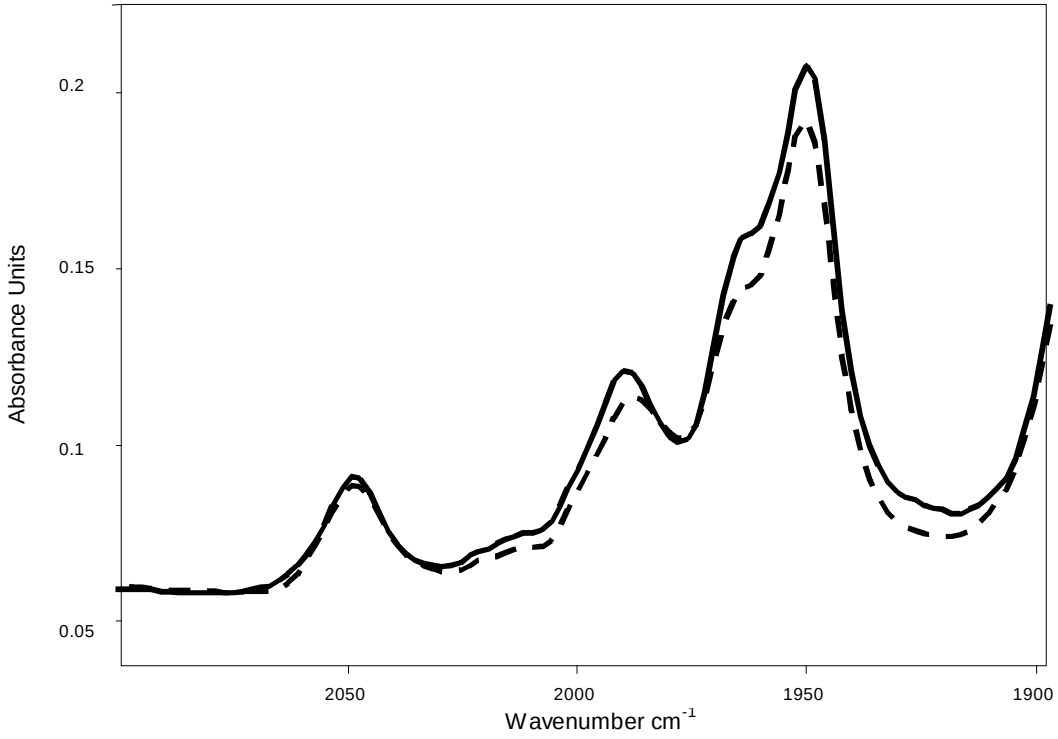

Figure 4.24. A comparison between the HP-IR spectrum of the freshly preformed [$RhH(CO)_2(PPh_3)_2$] (Rh:PPh_3 = 1:170) catalyst (solid) and the regenerated one (dashed) after 120 minutes of MVK inhibition at 90 ℃ and 20 bar syngas.

Regeneration of the active catalyst was afforded after 190 minutes upon the MVK addition. This was in agreement with autoclave studies (Section 4.3.2) where the inhibition of the $[RhH(CO)_2(PPh_3)_2]$ catalyst ($Rh:PPh_3$ = 1:170) was observed for 190 minutes after which hydroformylation of the olefin commence as witnessed by a normal gas uptake.

4.3.3.4 $[RhH(CO)_2(xantphos)]$ preforming studied by *in situ* HP-IR Spectroscopy

Similar to $[RhH(CO)_2(PPh_3)_2]$ studies, DHN was the solvent of choice during $[RhH(CO)_2(xantphos)]$ studies for reasons already stated. Initially, the IR spectrum of the catalyst precursor $[Rh(acac)(CO)_2]$ in DHN was recorded under an argon atmosphere before the introduction of the ligand of choice which in this case was xantphos. After recording a spectrum of the rhodium precursor, the ligand was introduced under an argon atmosphere and another spectrum recorded for comparison purposes as illustrated in Figure 4.25 below.

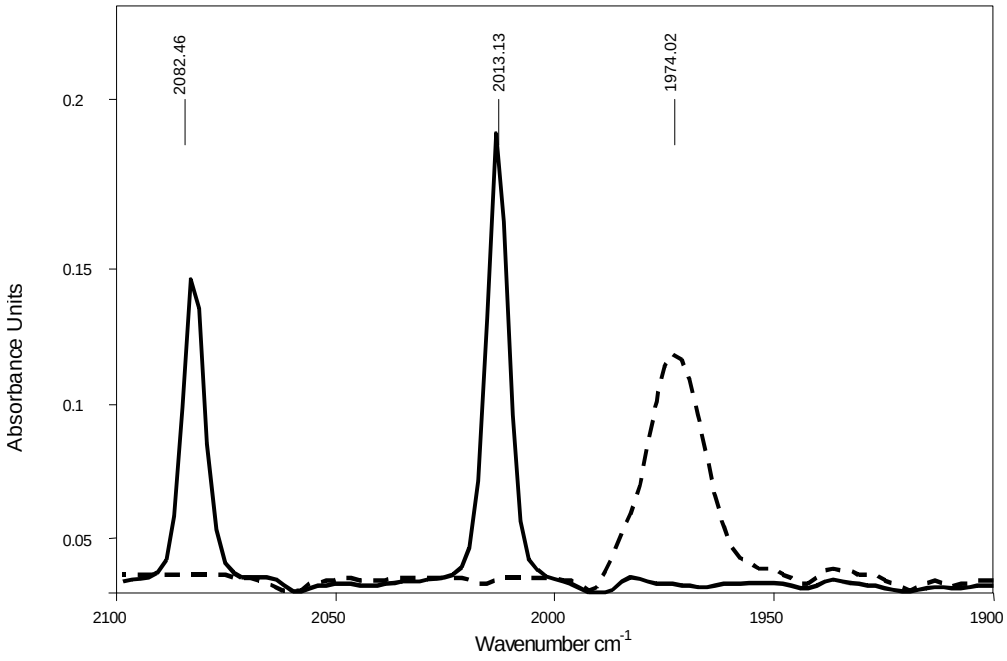

Figure 4.25. An illustration of Rh precursor HP-IR spectrum before and after xantphos addition. Solid: [Rh(acac)$(CO)_2$] at 30 ℃ and 10 bar Argon; Dashed: [Rh(acac)$(CO)_2$]:Xp 1:2 at 30 ℃ and 10 bar Argon.

[Rh(acac)$(CO)_2$] displayed two peaks at 2082 cm^{-1} and 2013 cm^{-1} representative of the symmetric and asymmetric stretching frequencies of the two CO ligands on the Rh centre. Absorption bands obtained were in agreement with those obtained in the literature.[15]

Upon the addition of xantphos, one CO ligand was replaced by the least sterically hindered phosphorus to form a mono-substituted complex **(B)** in Scheme 4.4. This substitution was confirmed by the disappearance of the two peaks and a formation of one peak at 1974 cm^{-1}. Flushing the reactor with syngas and pressuring it to 20 bar with syngas (H_2:CO = 1:1) lead to the formation of the catalytically active hydride as illustrated in Scheme 4.4 below.

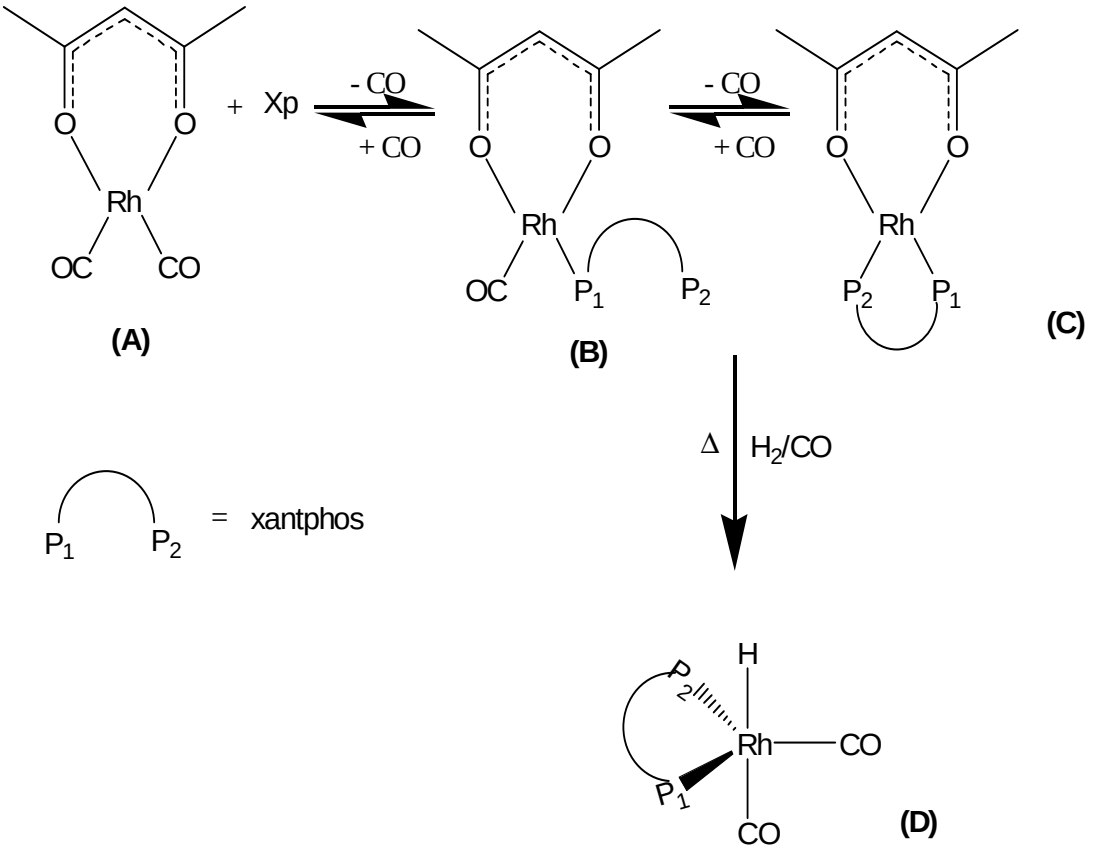

Scheme 4.4. Substitution reaction between $[Rh(acac)(CO)_2]$ and xantphos to allow preforming of the active hydride under a syngas atmosphere.

The existence of **(C)**, with both mono- and bidentate ligands, has only been proven with phosphite ligands after heating or evacuating the mixture.[15,23] Since this species does not contain any CO ligand, it does not absorb in the carbonyl region and thus other techniques apart from HP-IR will have to be used to characterise it. Detailed characterisation and in-depth investigations of this species, including its mono- and bidentate phosphine ligands derivatives, warrants a valuable study on its own. Under these conditions, only **(B)** may be formed.

After heating the reaction mixture to 90 °C, the fully preformed catalyst **(D)** was observed as witnessed by four absorption bands in the figure below.

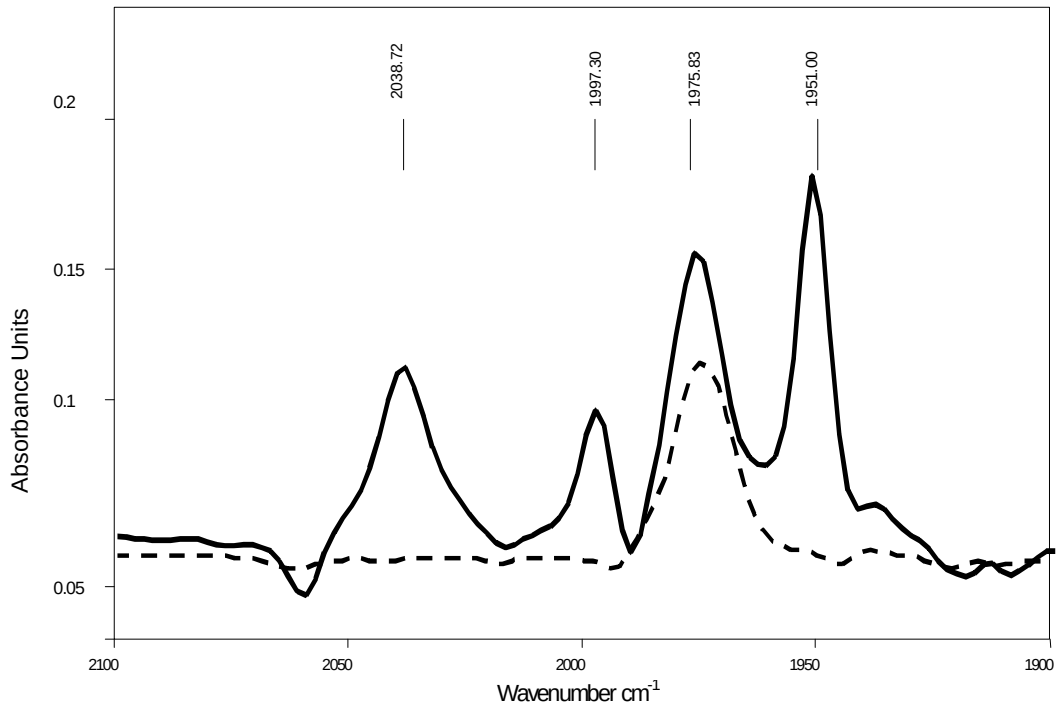

Figure 4.26. A comparison between the HP-IR spectrum of the mono-substituted catalyst and a fully preformed Rh-Xp. Solid: $[RhH(CO)_2Xp]$ at 90 ℃ and 20 bar syngas (H_2:CO 1:1). Dashed: [Rh(acac)(CO)Xp] at 30 ℃ and 10 bar Argon.

A peak at 1974 cm^{-1} that was observed before the introduction of syngas disappears with the formation of other four bands. The four absorption bands observed at 2038, 1997, 1975 and 1951 cm^{-1} representing the fully preformed catalyst were consistent with those obtained in the literature.[24] These bands are assigned to the equatorial-equatorial (*ee*) and equatorial-axial (*ea*) isomers of the preformed catalyst that contains two CO ligands, a hydride and a bidentate phosphine ligand.

Below is the comparison between the fully preformed $[RhH(CO)_2(xantphos)]$ and $[RhH(CO)_2(PPh_3)_2]$ catalysts.

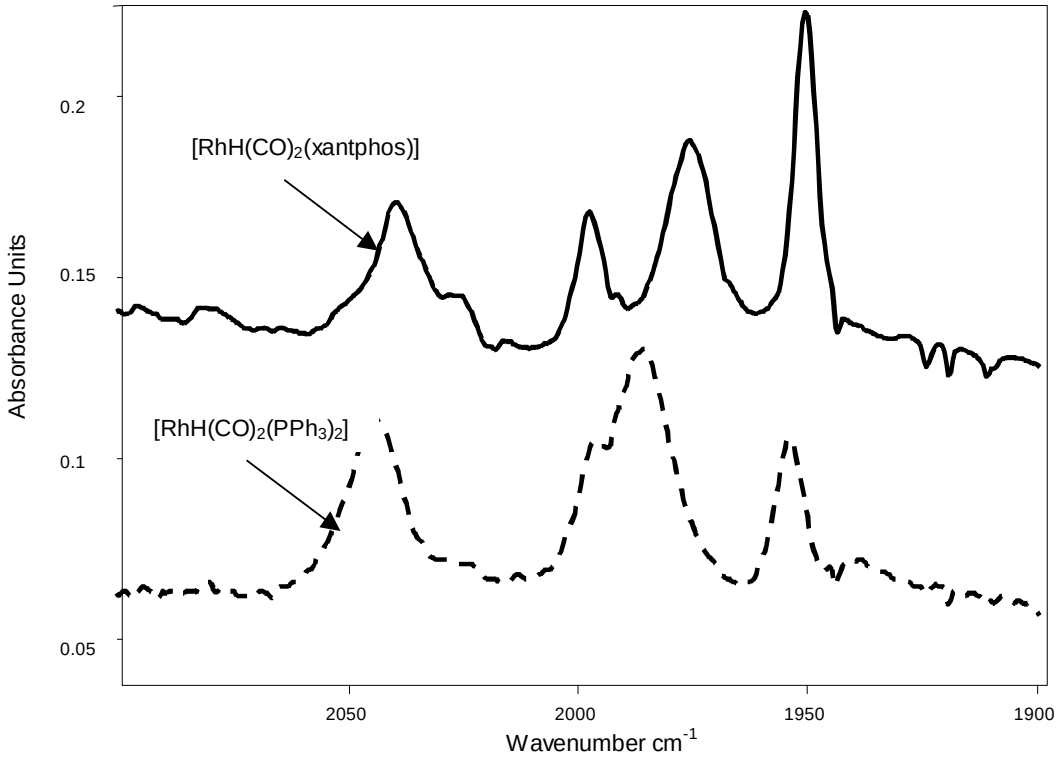

Figure 4.27. A comparison between the HP-IR spectrum of the fully preformed $[RhH(CO)_2(xantphos)]$ and $[RhH(CO)_2(PPh_3)_2]$ catalysts at 90 °C and 20 bar syngas after 5 minutes.

4.3.3.5 $[RhH(CO)_2(xantphos)]$ stability studied by *in situ* HP-IR Spectroscopy

To determine whether it would be possible to obtain single crystals of the $[RhH(CO)_2(xantphos)]$ species in the absence of syngas, the stability of

the hydride species first had to be determined at low synthesis gas pressures. These experiments are necessary as it is known that these Rh-bidentate phosphine ligands form dimeric Rh species in the absence of synthesis gas.[13] Moreover, if the catalyst is relatively stable at ambient pressures and temperatures, other studies such as stopped-flow, kinetic studies would be easier to carry out.

During catalyst stability studies, the catalyst was initially preformed at 90 ℃ and 20 bar syngas as illustrated in Section 4.2. 3.2. Due to the tendency of these bidentate ligands to stabilise the preferred bisequatorial coordination in the trigonal bipyramidal complexes,[25] a M:L ratio of only 1:1.1 was employed in an attempt to confer minimal protection to the metal centre and hence maximise the deleterious effect on the active hydride formed. The fully preformed catalyst was witnessed by four absorption bands characteristic of the $[RhH(CO)_2(xantphos)]$ hydride.

Upon preforming the catalyst, the reactor was depressurized to 5 bar to investigate the effect of pressure on the active hydride. The spectra recorded at 5 bar syngas was similar to that recorded at 20 bar syngas even after 120 min, suggesting a negligible change on the catalytic species under these conditions. These results suggest that the conditions are still favourable for the stability of the hydride as sufficient syngas is still present in the reaction mixture. Minor deviations observed could be attributed to subtraction errors at low pressures. This was because the background spectra were recorded at a higher pressure than the sample pressure and this could causes discrepancies in the concentration of syngas as well as differences in the separation of the IR-cell windows (i.e. pathlength changes). The reaction temperature was then allowed to cool down to at least 40 ℃ while keeping the pressure constant (20 bar) to investigate the effect of temperature on the active catalyst. No significant change was observed suggesting a negligible effect of temperature on the

active catalyst under these conditions. To push the limits even further, the reactor was then depressurised to ~0 bar and flushed with argon to eliminate/minimise syngas dissolved in the reaction mixture. The catalyst was significantly affected as illustrated in Figure 4.28 below.

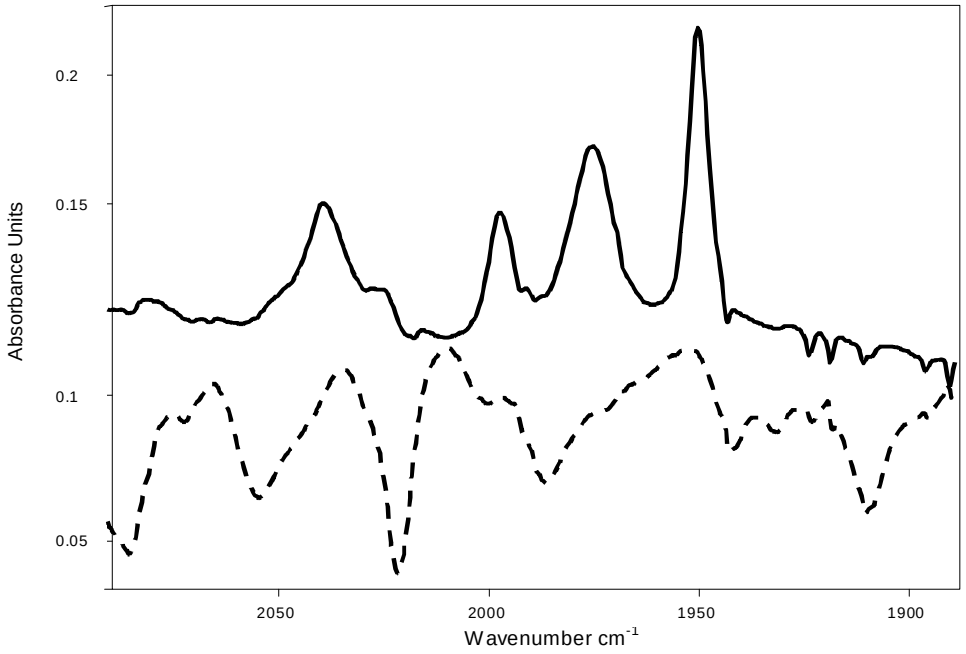

Figure 4.28. Illustration of a HP-IR spectrum of the totally deteriorated catalyst at 90 ℃ and 0 bar syngas. Solid: [Rh(acac)$(CO)_2$]: Xantphos 1:1 at 90 ℃ and 20 bar syngas. Dashed: [Rh(acac)$(CO)_2$]:Xantphos 1:1 at 40 ℃ and ~0 bar syngas.

The spectrum recorded showed a completely decomposed/transformed catalyst with no distinct peak observed. This observation was thought to be due to dimeric species formed under these.[12] The above experiment suggests that in order to keep the hydride intact, the solution should always be saturated with syngas. Studies such as stopped-flow kinetic experiments can therefore not be carried out to study the Rh species

formed during hydroformylation reactions as the Rh hydride, $[RhH(CO)_2(xantphos)]$, is not retained under the conditions suitable for these studies.

In a continuous operation, the catalyst will likely be exposed to low syngas pressures and will thus change its form as illustrated in Figure 4.29. For a hydroformylation process to be economically feasible, the catalyst has to be re-cycled making catalyst re-formation and stability imperative. Re-generation of the catalyst was therefore investigated. Important observations to take note of during this exercise were not only the formation of new peaks and shoulders, but also peaks that might have shifted or completely diminished. In an attempt to fully re-generate the catalyst, the reaction mixture was flushed with syngas and the reactor pressurized to 20 bar before recording a spectrum (Figure 4.29).

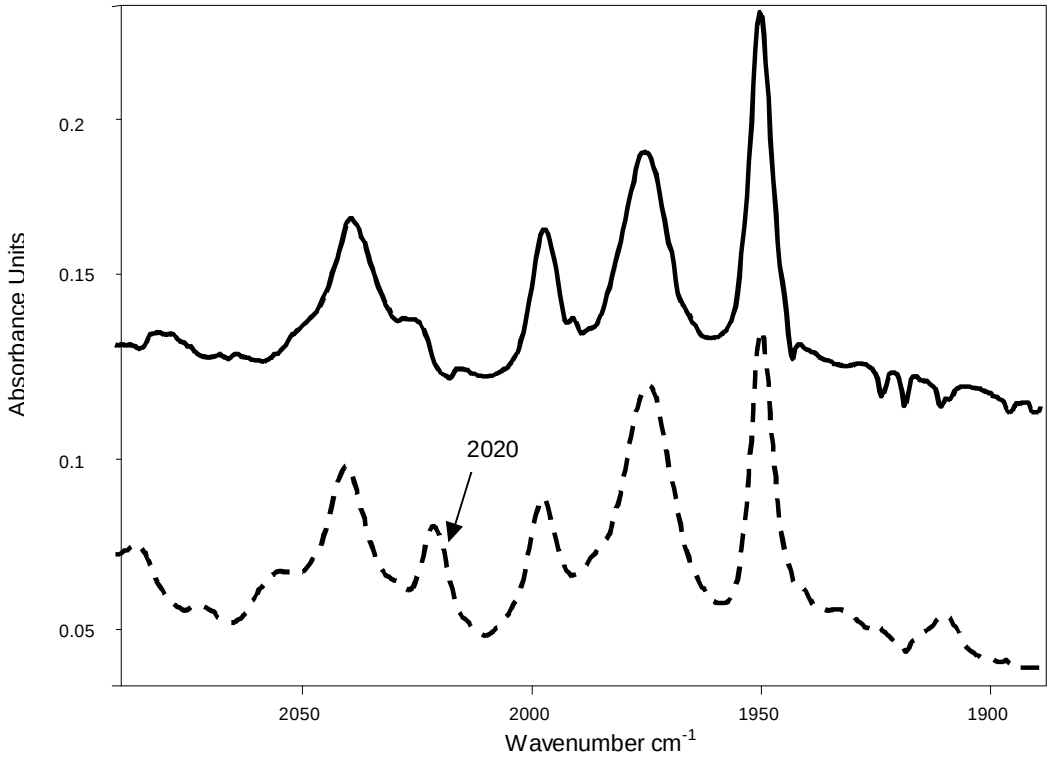

Figure 4.29. Regeneration of the catalyst ([$RhH(CO)_2$(xantphos)]) after depressurising to 0 bar and flushing with argon. Solid: Freshly preformed catalyst. Dashed: Regenerated catalyst at 90 ℃ and 20 bar syngas.

Upon re-pressurizing the reactor to 20 bar, the active catalyst was regenerated with the same peak intensity and position. However, there was an additional peak that formed at 2020 cm^{-1}. To investigate the stability of this species formed, the reactor was opened to expose the reaction mixture to air at room temperature. The reactor was then closed and flushed with syngas before recording a spectrum at 5 bar syngas. The active catalyst was observed at 40 ℃ and 5 bar with the peak at 2020 cm^{-1} still present as observed earlier (See Figure 4.30). This peak was assumed to be due to dimer formation, similar to that observed during NMR experiments without extra PPh_3 added.

In conclusion, the active hydride is unstable in the absence of syngas but can be easily re-generated by re-pressurizing the reaction mixture. This observation has also been evident in the literature where Rh dimers were fragmented by the reaction with CO to form the mononuclear hydride species.[26] However, other CO containing dimers/clusters that formed (absorption at 2020 cm^{-1}) under these conditions could not be fragmented upon the introduction of syngas.

4.3.3.6 MVK inhibition studies on $[RhH(CO)_2(xantphos)]$ by *in situ* HP-IR Spectroscopy

The reaction of the inhibitor, MVK, with the $[RhH(CO)_2(xantpos)]$ catalyst was investigated using HP-IR spectroscopy. The catalyst was preformed following similar procedures as in Section 4.2.3.2. After allowing the temperature to stabilize at 90 ℃ and 20 bar syngas, a spectrum was recorded and excess amounts of an inhibitor of choice (methylvinyl ketone: MVK) added to evaluate its effect on the active catalyst. The α,β-unsaturated ketone was chosen due to its pronounced inhibition effect on the Rh catalyst as indicated during autoclave studies (see Section 5.3.2). Excess amounts were added in order to enhance the inhibition effect on the catalyst. After the reactor was depressurised, MVK (200 mol eq) was added by syngas pressure as the reactor was pressurized to 20 bar. A spectrum was recorded at 90 ℃ and 20 bar syngas for comparison purposes.

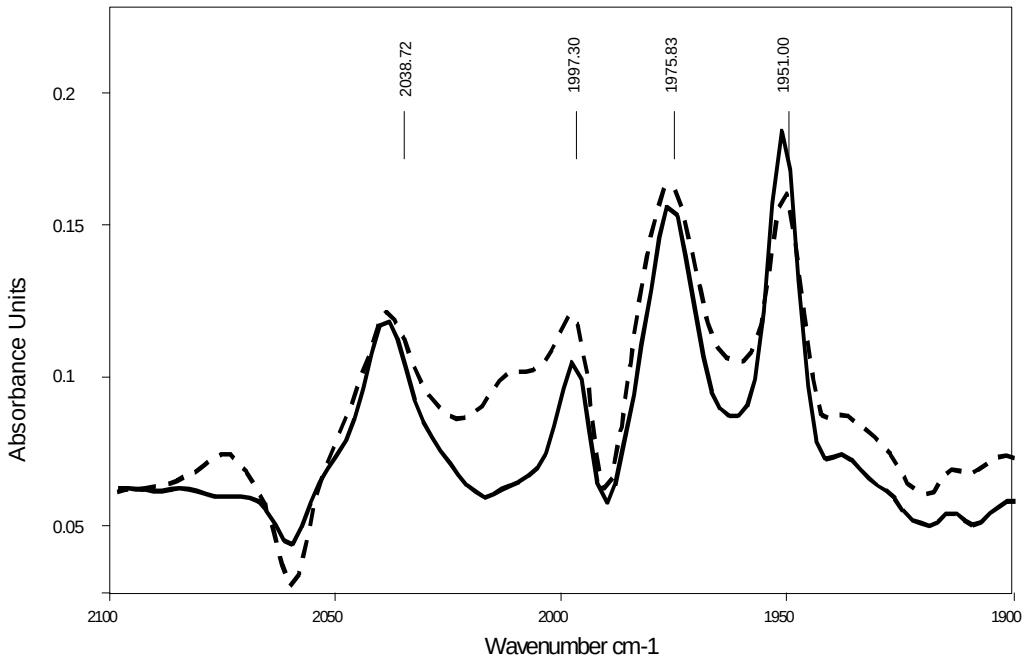

Figure 4.30. Illustration of the HP-IR spectrum of the fully formed catalyst ([$RhH(CO)_2$(xantphos)]), before and after MVK addition. Solid: Rh-Xp catalyst before MVK addition. Dashed: Rh-Xp catalyst after MVK addition.

The resistance of the xantphos catalyst to MVK inhibition is yet again displayed. The addition of MVK did not lead to any formation or depletion of any distinct peak from the original spectrum. The only difference observed was a shoulder at 2010 cm^{-1} that was not at an expense of any original peak. The spectrum remained unchanged for the entire duration of the experiment (120 min). This shoulder was assumed to be due to a change in the solvent matrix resulting from the addition of MVK. A change in the solvent matrix introduces errors during the subtraction of the solvent background.

In conclusion, it can be noted that the [$RhH(CO)_2(PPh_3)_2$] catalyst is inhibited by MVK where the inhibitor is reacted away after some time to liberate the active catalyst to perform a hydroformylation reaction.

[$RhH(CO)_2$(xantphos)] catalyst is not affect by the inhibition under the conditions investigated *i.e.* M:L:MVK ratio of 1:5:200 at 90 ℃ and 20 bar syngas.

4.3.3.7 Conclusions

Table 4.2. Labelling of catalytic species formed with HP-IR

Species	CO frequency (cm^{-1})
[$Rh(acac)(CO)(PPh_3)$]	1985
[$RhH(CO)_2(PPh_3)_2$]	2043, 1997, 1986 and 1953
[Rh(acac)(CO)(xantphos)]	1974
[RhH(CO)(xantphos)]	2038, 1997, 1975 and 1951
Poisoned species[a]	2020

a) This species was observed after the regeneration of both the [$RhH(CO)_2(PPh_3)_2$] and [$RhH(CO)_2$(xantphos)] hydrides during stability studies. Respective CO frequencies of active hydrides were also present.

In conclusion:

- Active hydrides of both catalysts ([$RhH(CO)_2(PPh_3)_2$] and [$RhH(CO)_2$(xantphos)]) were characterized where both the *ee* and *ea* isomers were observed under 20 bar syngas pressure .
- Syngas atmosphere is vital for the stability of the active hydride. Depleting syngas from the solution led to the deactivation of the catalyst that regenerated, together with the unknown species, under syngas atmosphere (at least 5 bar). Dimers are likely to form under syngas deficient atmosphere.
- In agreement with previous studies conducted (autoclave and NMR studies), the [$RhH(CO)_2(PPh_3)_2$] hydride was inhibited by MVK where it was later liberated for the regeneration of the active species.
- No negative effect of MVK was observed on the [$RhH(CO)_2$(xantphos)] catalyst under the selected conditions (90 ℃ and 2 0 bar syngas).

- This observation is in agreement with conclusions drawn in Section 5.3.2.1 with the aid of Scheme 5.2 displaying postulated equilibria and species formed during hydroformylation of 1-octene in the presence of an inhibitor, MVK. These equilibria suggest that the more the $[RhH(CO)_2(xantphos)]$ catalyst is formed, the less the inhibition there will be while the reverse is true where an increase in $[RhH(CO)_2(PPh_3)_2]$ species will lead to increased inhibition periods.

References

1. Barbaro, P.; Bianchini, C.; Meli, A.; Moreno, M.; Vizza, F. *Organometallics* **2002**, *21*, 1430.

2. Chen Y.; Fulton J. L.; Linehan J.C.; Autrey T. *J. Am. Chem. Soc.* **2005**, *127*, 3254.

3. Gonsalvi, L.; Adams, H.; Sunley, G. J.; Ditzel, E.; Haynes, A. *J. Am. Chem. Soc.* **1999**, *121*, 11233.

4. Chang, D.-H.; Lee, D.-Y.; Hong, B.-S.; Choi, J.-H.; Jun, C.-H. *J. Am. Chem. Soc.* **2004**, *126*, 424.

5. Brevard, C.; Granger, P. *Handbook of High Resolution Multinuclear NMR, Wiley J. & Sons, New York*, **1981**.

6. Freeman, R.; Whiffen, D. H. *Mol. Phys.* **1961**, *4*, 321.

7. Brown, T. H.; Green, P. J. *J. Am. Chem. Soc.* **1969**, *91*, 3378.

8. Brown, T. H.; Green, P. J; *J. Am. Chem. Soc*. **1970**, *92*, 2359.

9. Osborn, J. A.; Young, J. F.; Wilkinson, G. *Chem. Commun.* **1965**, 17.

10. Evans, D.; Osborn, J. A.; Wilkinson, G. *J. Am. Chem. Soc* (A) **1968**, *90*, 3133.

11. Bath, S. S.; Vaska, L. *J. Am. Chem. Soc*. **1963**, *85*, 3500.

12. Moasser, B.; Gladfelter, W. L.; Roe, D. C. *Organometallics* **1995**, *14*, 3832.

13. Bianchini, C.; Lee, H. M.; Meli, A.; Vizza, F. *Organometallics* **2000**, *19*, 849.

14. Roe, D. C. *J. Magn. Res*. **1985**, *63*, 388.

15. Kranenburg, M.; van der Burgt, Y. E. M.; Kamer, P. C. J.; van Leeuwen, P. W. N. M. *Organometallics* **1995**, *14*, 3089.

16. Walczuk, E. B.; Kamer, P. C. J.; van Leeuwen, P. W. N. M. *Angew. Chem. Int. Ed.* **2003**, *42*, 4665.

17. Van Rooy, A.; Kamer, P. C. J.; van Leeuwen, P. W. N. M.; Goubitz, K.; Fraanje, J.; Veldman, N.; Spek, A. L. *Organometallics* **1996**, *15*, 835.

18. Nettekoven, U.; Kamer, P. C. J.; Widhalm, M.; van Leeuwen, P. W. N. M. *Organometallics* **2000**, *19*, 4596.

19. Bianchini, C.; Oberhauser, W.; Orlandini, A. *Organometallics* **2005**, *24*, 3692.

20. Diéguez, M.; Claver, C.; Masdeu-Bultó, A. M.; Ruiz, A. *Organometallics* **1999**, *18*, 2107.

21. (a) Nozaki, K.; Matsuo, T.; Shibahara, F.; Hiyama, T. *Organometallics* **2003**, *22*, 594. (b) Castellanos-Páez, A.; Castillón, S.; Claver, C.; van Leeuwen, P. W. N. M.; de Lange, W. G. J. *Organometallics* **1998**, *17*, 2543. (c) van der Slot, S. C.; Kamer, P. C. J.; van Leeuwen, P. W. N. M.; Iggo, J. A.; Heaton, B. T. *Organometallics* **2001**, *20*, 430.

22. Van der Veen, L. A.; Boele, M. D. K.; Bregman, F. R.; Kamer, P. C. J.; Van Leeuven, P. W. N. M.; Goubitz, K.; Fraanje, J.; Schenk, H.; Bo, C.; *J. Am. Chem. Soc* **1998**, *120*, 11616.

23. Aigen, S.; van Eldik, R. *Organometallics* **1987**, *6*, 1080.

24. van der Veen, L. A.; Keeven, P. H.; Schoemaker, G. C.; Reek, J. N. H.; Kamer, P. C. J.; Van Leeuwen, P. W. N. M.; Lutz, M.; Spek, A. L.; *Organometallics* **2000**, *19*, 872.

25. van Leeuwen, P. W. N. M.; Kamer, P. C. J.; Reek, J. N. H. *Pure Appl. Chem* **1999**, *71*, 1443.

26. Burch, R. R.; Muetterties, E. L.; Schultz, A. J.; Gebert, E. G.; Williams, J. M. *J. Am. Chem. Soc.* **1981**, *103*, 5517.

CHAPTER 5 108
5 Rhodium Triphenyl- and Bidentate Phosphine based Hydroformylation Catalysts: Kinetics, Selectivity and Inhibition Studies 108
5.1 Introduction 108
5.2 Experimental: Autoclave studies 110
5.2.1 General 110
5.2.2 Reproducibility studies and method validations 112
5.3 Results and Discussion: Autoclave studies 120
5.3.1 Dual catalyst system: $[RhH(CO)_2(PPh_3)_2]$ and $[RhH(CO)_2(xantphos)]$ studies 120
5.3.2 Inhibition studies on the dual catalyst system 129
5.3.3 Effect of PP bidentate ligand bite angle on inhibition 136
5.3.4 Effect of PPh_3 concentration on selectivity and inhibition for the hydroformylation of 1-octene 138
5.4 Kinetics of the formation of $[RhH(CO)(PPh_3)(xantphos)]$ from $[RhH(CO)(PPh_3)_3]$ and subsequent catalytic hydroformylation of 1-octene 141
5.4.1 Introduction to kinetics studies 141
5.4.2 Stability studies of $[RhH(CO)(PPh_3)_3]$ in the presence of PPh_3 142
5.4.3 Kinetics of the substitution reaction between $[RhH(CO)(PPh_3)_3]$ and xantphos studied by Stopped-flow spectrophotometry 144
5.4.4 Kinetics of catalytic hydroformylation of 1-octene with the Rh-PPh_3-Xp system 148
5.4.5 Concluding remarks 156
References 158

CHAPTER 5

Rhodium Triphenyl- and Bidentate Phosphine based Hydroformylation Catalysts: Kinetics, Selectivity and Inhibition Studies

5.1 Introduction

In an economically viable catalytic process, a homogeneous catalyst should not only give acceptable rates and selectivities, but also, and perhaps more important, be resistant to deactivation processes in all sections of the plant. This was for example highlighted in Section 2.5. For this reason, optimisation of the reaction conditions is imperative. Parameters commonly considered when optimising reaction conditions are temperature, pressure, metal and ligand concentration. The objective is to attain economically viable rates and product selectivities under the mildest conditions possible, with the latter aimed at reducing operating costs.

There are some instances when the above-mentioned parameters, *i.e*. temperature, pressure, metal concentration as well as ligand concentration, are not sufficient in ensuring a workable process. One such example arises when there are impurities in the feed. A distinct advantage of homogeneous catalysis is the ability to considerably alter the behaviour of the catalyst by altering the ligand environment. Ligand modification involves altering the ligand steric and/or electronic properties to suit the needs of the process. This flexibility may aid in addressing aspects beyond normal reaction parameters, such as the stability of the catalyst towards impurities in the feed. Not only will impurities unnecessarily take up reactor volume, but more importantly, they can inhibit/poison the catalyst rendering it unable to enter the reaction cycle.

From studies undertaken in the van Leeuwen laboratories, it was shown that α,β-unsaturated ketones have a more severe inhibition effect compared to

dienes.[1] There are, however, ligands that impart some resistance to a hydroformylation system. One such ligand is 4,5-bis(diphenylphosphino)-9,9-dimethylxanthene (xantphos; Xp).[2]

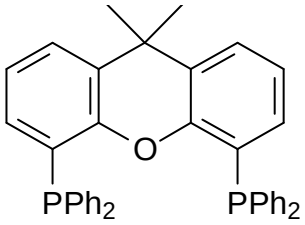

Figure 5.1. Xantphos, 4,5-bis(diphenylphosphino)-9,9-dimethylxanthene (Xp).

This study was therefore directed towards catalysts derived from such bidentate ligand systems in greater depth. Using such a ligand would likely derive the following benefits:

- It may be possible to do away with a costly feed preparation section.
- The linearity and yield of the product would increase.
- Possible increased stability imparted to the rhodium metal by the chelating ligand.
- Rh-Xantphos type of complexes have been reported to be capable of hydroformylating internal olefins inaccessible to the Rh-triphenylphosphine ($[RhH(CO)_2(PPh_3)_2]$) system under standard operating conditions (for example, T = 90 ℃, P = 20 bar).

The one drawback of using these ligand systems, however, is the very slow rates at which olefins are hydroformylated. The use of a dual catalyst system where xantphos and PPh_3 co-ordinated catalysts would operate in the same reactor was therefore proposed. This would hopefully result in some of the above listed benefits from the use of a bidentate ligand being incorporated without too great a loss in activity.

In this chapter the investigations into hydroformylation reactions involving $[RhH(CO)_2(PPh_3)_2]$, Rh-bidentate (PP ligands) as well as a mixed Rh-PPh_3-

bidentate ligand systems are discussed, with particular reference to their behaviour in the presence of catalyst inhibitors such as α,β-unsaturated ketones and dienes.

5.2 Experimental: Autoclave studies

5.2.1 General

Autoclave experiments were carried out in a Parr autoclave reactor (100 mL) equipped with the following: a dip tube to introduce the feed as well as a second dip tube to introduce the syngas into the reaction solution, a vent line and a rupture valve (RV) as a safety measure. A cooling loop to ensure a well-controlled temperature (within a 1 °C temperature window) during the reaction was also installed on the reactor. Observed rate constants (k_{obs}) for gas consumption were calculated by measuring a drop in pressure of ballast vessel filled with synthesis gas (H_2:CO = 1:1). Section 5.2.2 below illustrates the calculation of k_{obs} values. Unless otherwise specified, all reactions were carried out with a H_2:CO 1:1 syngas ratio.

[Rh(acac)$(CO)_2$], Xp and 1-octene were purchased from Aldrich at 98 % purity while PPh_3 was obtained from BASF with a purity of 99.9 %. Toluene was obtained from Merck with a purity of 98.5 %. Syngas (minimum purity of H_2:CO = 49.8:49.8) was obtained from Air-Liquide at a purity of >99.5%.

The baseline reaction conditions were as follows:
Unless otherwise specified, a [Rh] = 1.65 mM (~ 180 ppm) was employed with a high Rh:PPh_3 ratio of 1:170 at 100 ℃ and 15 bar syngas (H_2:CO = 1:1). In a typical Rh-PPh_3 system, a Rh-PPh_3 reaction solution was prepared by dissolving [Rh(acac)$(CO)_2$] (25.55 mg; 0.099 mmol) and PPh_3 (4.41 g; 0.0168 mol) in degassed toluene (50 mL) before transferring it into the reactor, *via cannula,* under an argon atmosphere. All these values were chosen as they closely resemble or represent averages of conditions normally used in rhodium hydroformylation processes.[3]

Upon flushing the reactor with synthesis gas, it was heated to 90 °C at 15 bar synthesis gas (CO/H_2 1:1). At the reaction temperature, the reactor was depressurised to at least 5 bar syngas and 1-octene (10 mL; 0.059 mol) introduced by overpressure on a connected sample bomb, bringing the reactor pressure to 20 bar. The sample bomb valve was closed and the ballast vessel valve opened from which gas was fed to the reactor on demand. The reaction progress was monitored by a drop in the ballast vessel pressure. The temperature of the ballast vessel was incorporated in the calculations of the rates so as to account for any temperature fluctuations in the laboratory that might affect the pressure drop of the ballast vessel. For example, a decrease in temperature may lead to a decrease in pressure that may be mistaken for a decrease resulting from the reaction consuming gas.

In the case of inhibition studies, methyl vinyl ketone (MVK; 200 molar equivalents to Rh) was added with the feed to the preformed catalyst.

The duration of the reactions was 240 min, at the end of which samples were drawn for selectivity analyses by GC and the data analyzed to obtain the rates. Due to slower rates recorded with the MVK studies, reactions were allowed to proceed for 21 hours.

Selectivity analyses were conducted using an Agilent 6890N GC with the following specifications: Oven temperature: Initial temperature = 40 ℃, hold for 20 min, First Ramp = 5 ℃/min to 200 ℃, second ra mp = 30 ℃/min and hold for 10 min at 300 ℃. Inlet temperature = 250 ℃ with a split ratio of 25:1. A capillary Pona column of 50 m length, 200 μm internal diameter, 0.50 μm film thickness and a maximum temperature limit of 325 ℃ was used.

UV-visible and kinetic measurements were obtained on a Varian Cary 100 spectrometer equipped with cooling water bath accurate to 0.1 ℃ in a double-sided 1 cm tandem quartz cell with teflon cap.

5.2.2 Reproducibility studies and method validations

To determine the reliability of obtained autoclave experimental data, reproducibility runs were carried out to compare the rates and selectivities of a chosen set of experiments. For this purpose, three $[RhH(CO)_2(PPh_3)_2]$ runs were performed under the same conditions and the rates (k_{obs} determination) and selectivities (determined by GC analyses of the reaction product) were compared to determine the deviation between the runs.

A Rh-PPh_3 reaction solution was prepared by dissolving selected amounts of $[Rh(acac)(CO)_2]$ and PPh_3 in degassed toluene (50 mL) before transferring it into the reactor, *via cannula,* under an argon atmosphere. Quantities chosen resembled, as close as possible, those normally used in the rhodium hydroformylation processes.[3] The reaction was then allowed to proceed by feeding syngas, on demand, from a ballast vessel.

The ballast vessel pressure drop of individual runs was recorded and the curves fitted into the first order equation using the "Scientist"[4] program to obtain k_{obs} values (the fitting of the experimental data is described in Section 5.4.4). Below is only an illustration of the first-order fits obtained from these calculations since detailed results are discussed in Section 5.3.

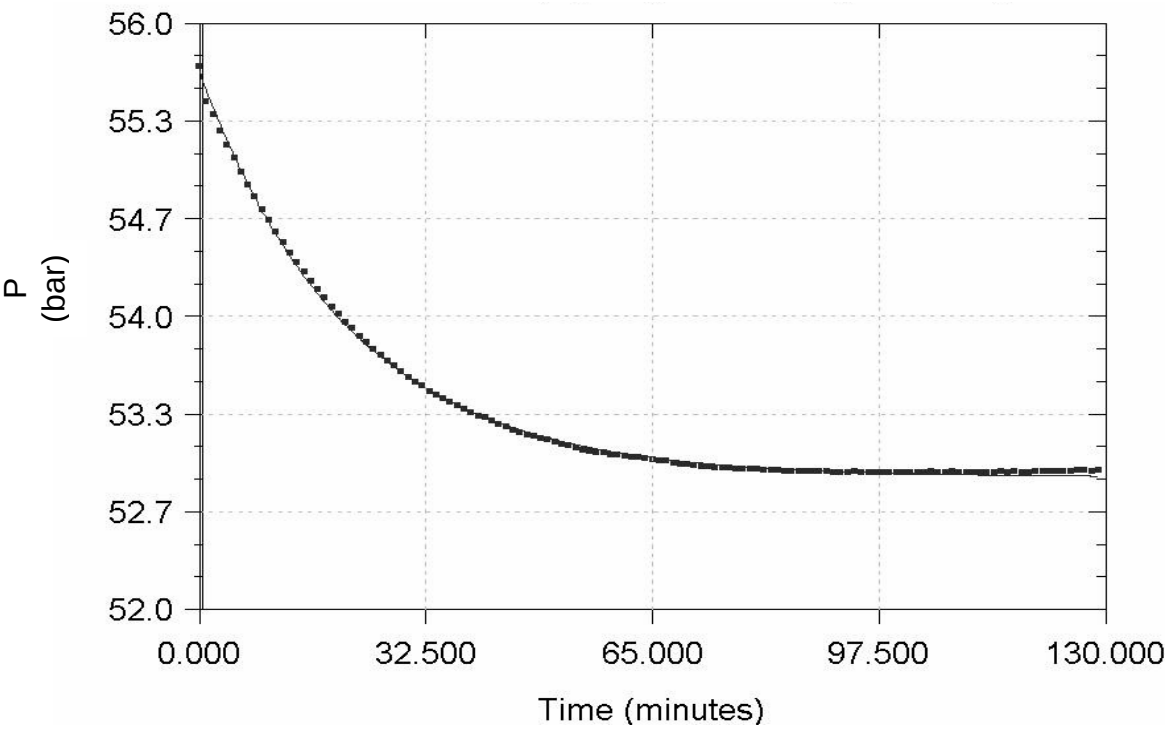

Figure 5.2. A graph of ballast vessel pressure drop over time for the calculation of k_{obs} values at (90 °C and 20 bar syngas) using Scientist. Dots: Experimental values, Line: calculated values using Eq 5.10)

Table 5.1 below summarises results (rates and selectivities) obtained with reproducibility runs.

Table 5.1. Reproducibility runs of 1-octene hydroformylation performed under the same conditions while following same procedures to establish window of accuracy.[a]

Rxn ID	T/ ℃	P / bar	PPh_3:M[b]	n:iso[c]	L / %[d]	I / %[e]	H / %[f]	k_{obs} (min^{-1})
Rxn A	90	20	170	3.9	78.0	1.0	0.7	0.0467(3)
Rxn B	90	20	170	3.8	79.1	1.0	0.7	0.0452(4)
Rxn C	90	20	170	3.8	78.8	0.9	0.6	0.0458(2)

[a] Reaction conditions given in Section 5.2.1.
[b] The molar ratio of ligand to rhodium.
[c] n:iso = normal:iso aldehyde product ratio.
[d] Amount of linear aldehyde produced during the reaction expressed as a percentage relative to the total aldehyde produced.
[e] Amount of isomerised octene produced during the reaction expressed as a percentage relative to the amount of 1-octene consumed.
[f] Amount of octene hydrogenated during the reaction expressed as a percentage relative to the amount of octene consumed.

The deviation between the three reproducibility runs was very low, with an error bar of less than 0.002 min^{-1}. The baseline run gave a rate of 0.0467(3) min^{-1} while reproducibility runs under the same conditions gave rates of 0.0452(4) min^{-1} and 0.0458(2) min^{-1}. The product selectivity deviation was just as low for all the reproducibility runs with an error bar of only 0.1 for the n:iso ratio (3.9 *vs*. 3.8). The deviations between the linearities in all the runs were less than 1.2 % with a minimum at 78.0 % and a maximum at 79.1 %. Isomerisation and hydrogenation were virtually the same. This high correlation not only validated the procedures followed in carrying out the experiments, but also the methods employed to calculate the reaction rates.

Selectivity analyses were performed immediately after every run by injecting a product sample into an Agilent 6890N series GC fitted with a Pona column, which separates products according to their boiling points. Details on this method were given in the experimental section earlier (Section 5.2.1). Decane was used as an internal standard in the feed, which enables one to compare the ratios of components in the feed (e.g. internal octenes and octane) before and after the hydroformylation experiments. The GC trace in Figure 5.3 displays the composition of the feed before being hydroformylated with toluene used to dilute the feed to a toluene:octene ratio of around 1:1.

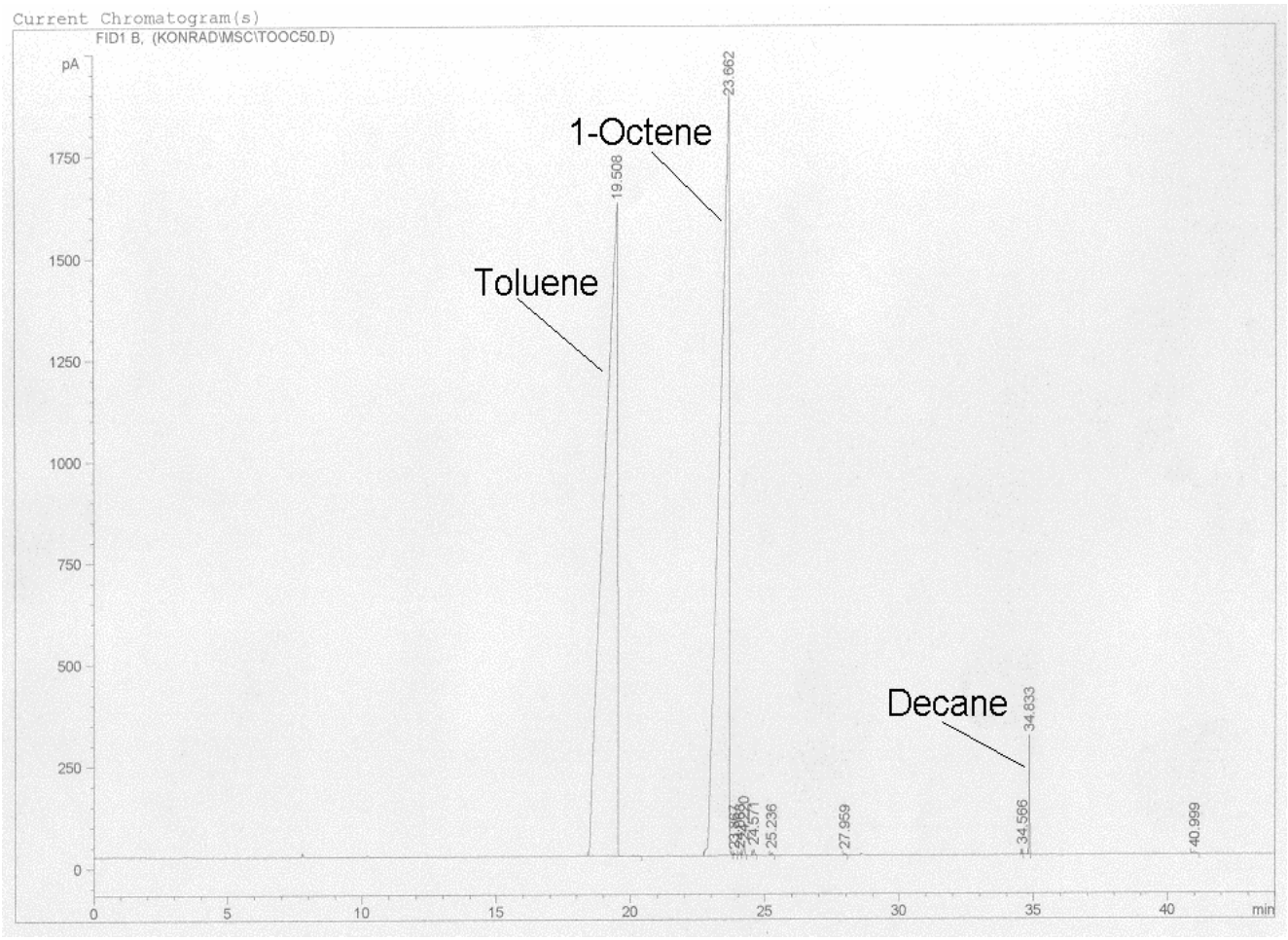

Figure 5.3. A GC chromatogram of decane standardized feed (octene) diluted to 50 % with toluene. X-axis represent retention time in minutes and y-axis the intensity of the peaks.

The products from the hydroformylation reaction were analysed using the same GC method as that used in the feed analyses. Figure 5.4 illustrates the GC trace of the product region displaying the normal product (aldehyde) and the corresponding isomers. The methyl branched product will be referred to as the *iso* product as will be seen during the selectivity analyses.

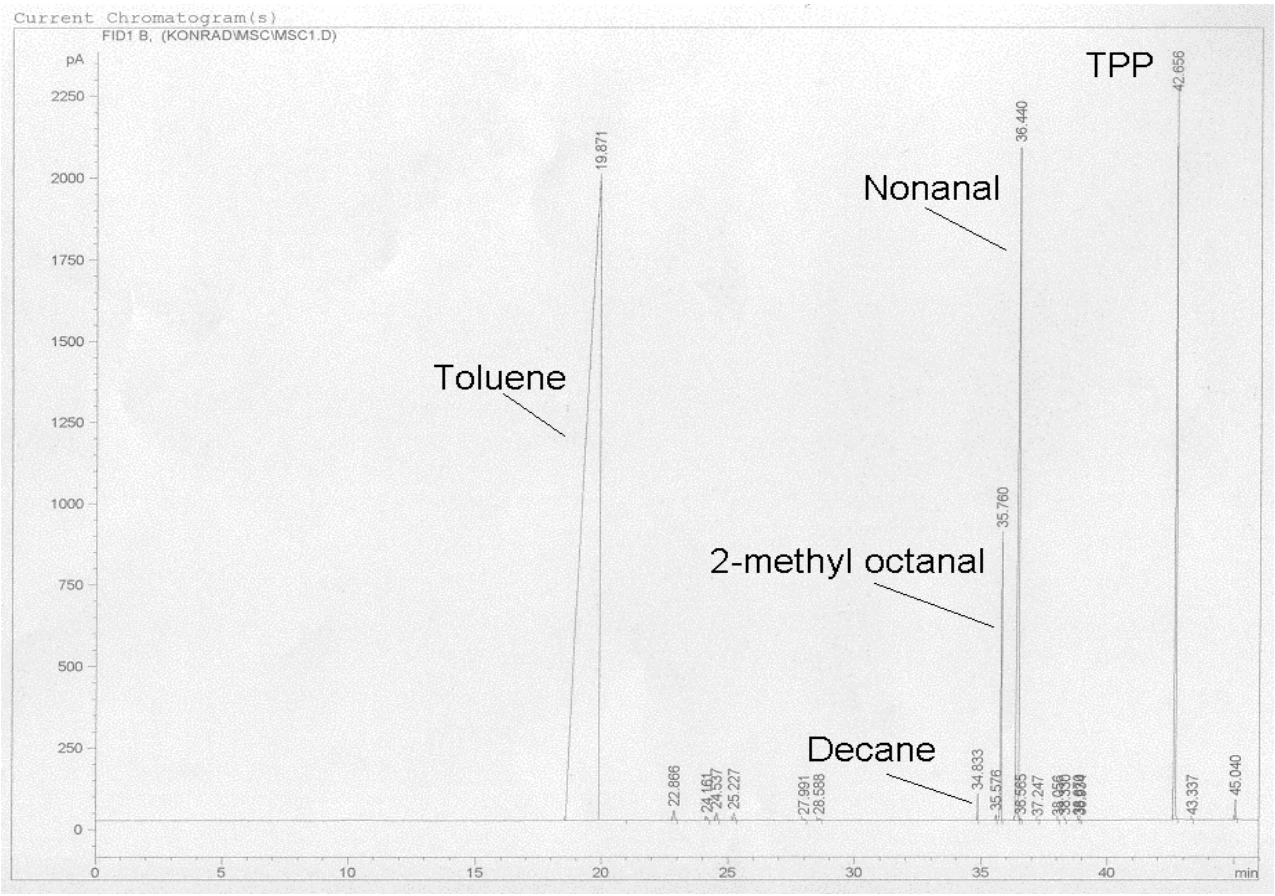

Figure 5.4. A GC chromatogram displaying product distribution after a 240 minutes 1-octene hydroformylation reaction with $[RhH(CO)_2(PPh_3)_2]$ run at 90 °C and 20 bar syngas. X-axis represent retention time in minutes and y-axis the intensity of the peaks.

The small unlabelled peaks between the toluene and decane are due to the residual octene isomers. All these peaks added together constitute less than 1 % of the product distribution. A clearer picture of the products formed is illustrated by Figure 5.5, which expands into the aldehyde region, indicating the normal and branched aldehyde products.

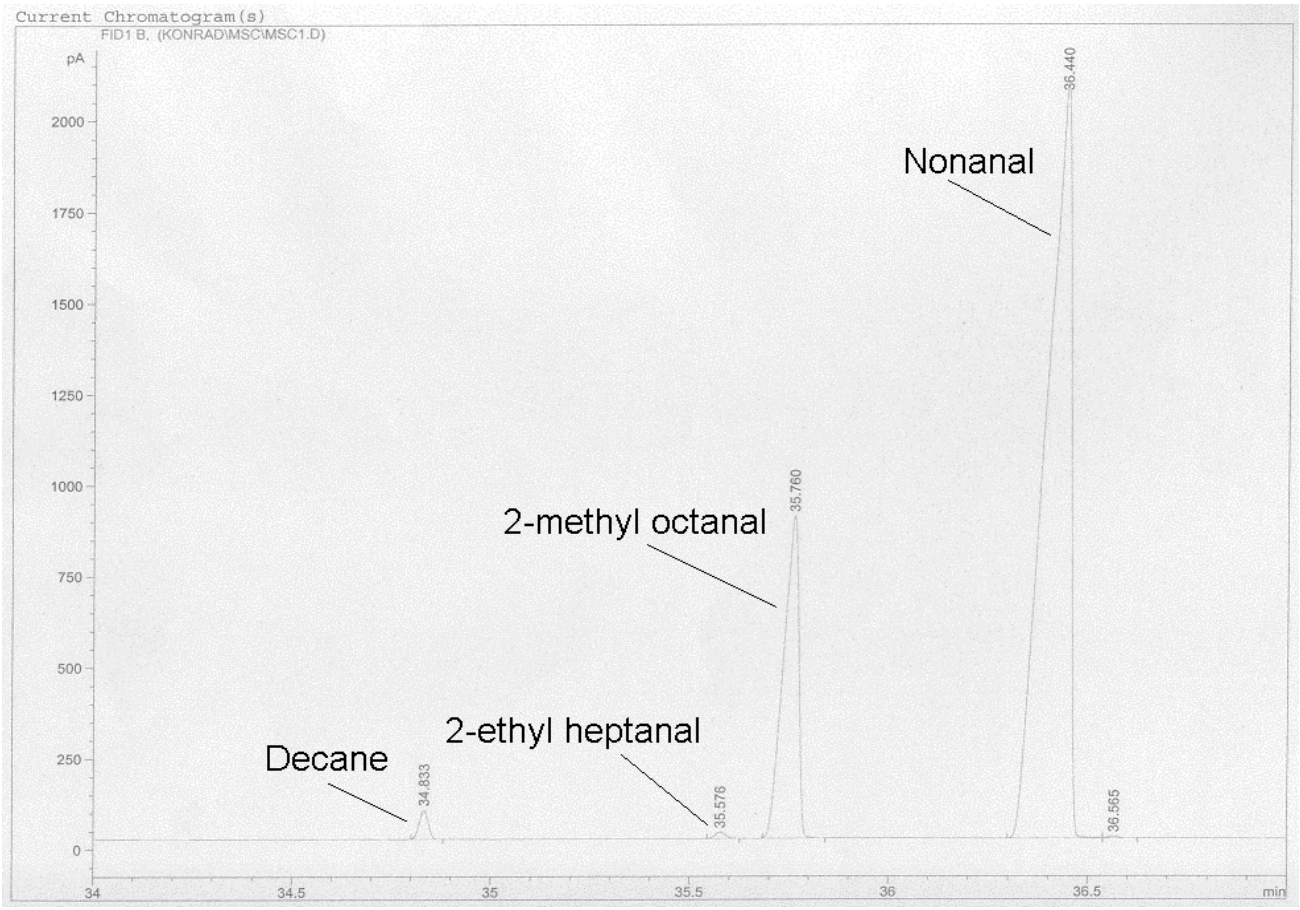

Figure 5.5. GC chromatogram of the expanded **Figure 5.4** aldehyde region displaying *n*- and *iso*-aldehyde formed after a 240 minutes 1-octene hydroformylation reaction with $[RhH(CO)_2(PPh_3)_2]$ at 90 °C and 20 bar syngas. X-axis represent retention time in minutes and y-axis the intensity of the peaks.

The above data clearly show that under the conditions employed, the traditional $[RhH(CO)_2(PPh_3)_2]$ system gives relative low n:iso values (maximum of 4:1) and less than 80 % linearity. In comparison, the $[RhH(CO)_2$(xantphos)] system displayed remarkable n:iso ratios in excess of 40:1 and very high linearities of more than 90 %. The GC chromatogram in Figure 5.6 below displays the product distribution obtained from the $[RhH(CO)_2$(xantphos)] system.

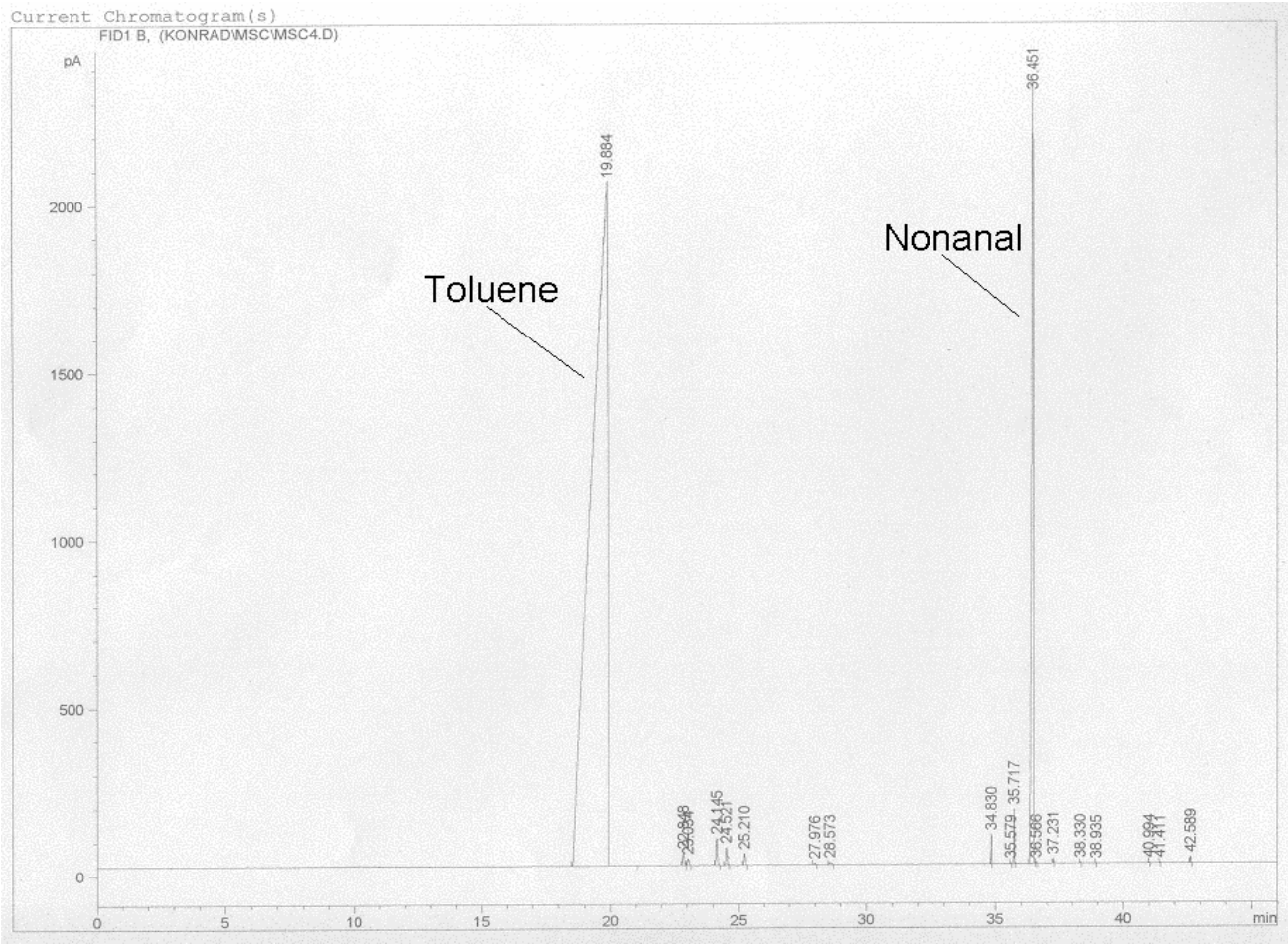

Figure 5.6. A GC chromatogram displaying product distribution after a 240 minutes 1-octene hydroformylation reaction with [$RhH(CO)_2$(xantphos)] at 90 °C and 20 bar syngas. X-axis represent retention time in minutes and y-axis the intensity of the peaks.

Slightly higher olefin isomers and paraffins were produced by the pure [$RhH(CO)_2$(xantphos)] suggesting that this catalyst is also a better isomerisation and hydrogenation catalyst. More results and discussions are given below.

The GC chromatogram shown in Fig. 5.7 highlights the aldehyde region indicating the remarkable n:iso ratios obtained with the [$RhH(CO)_2$(xantphos)] system.

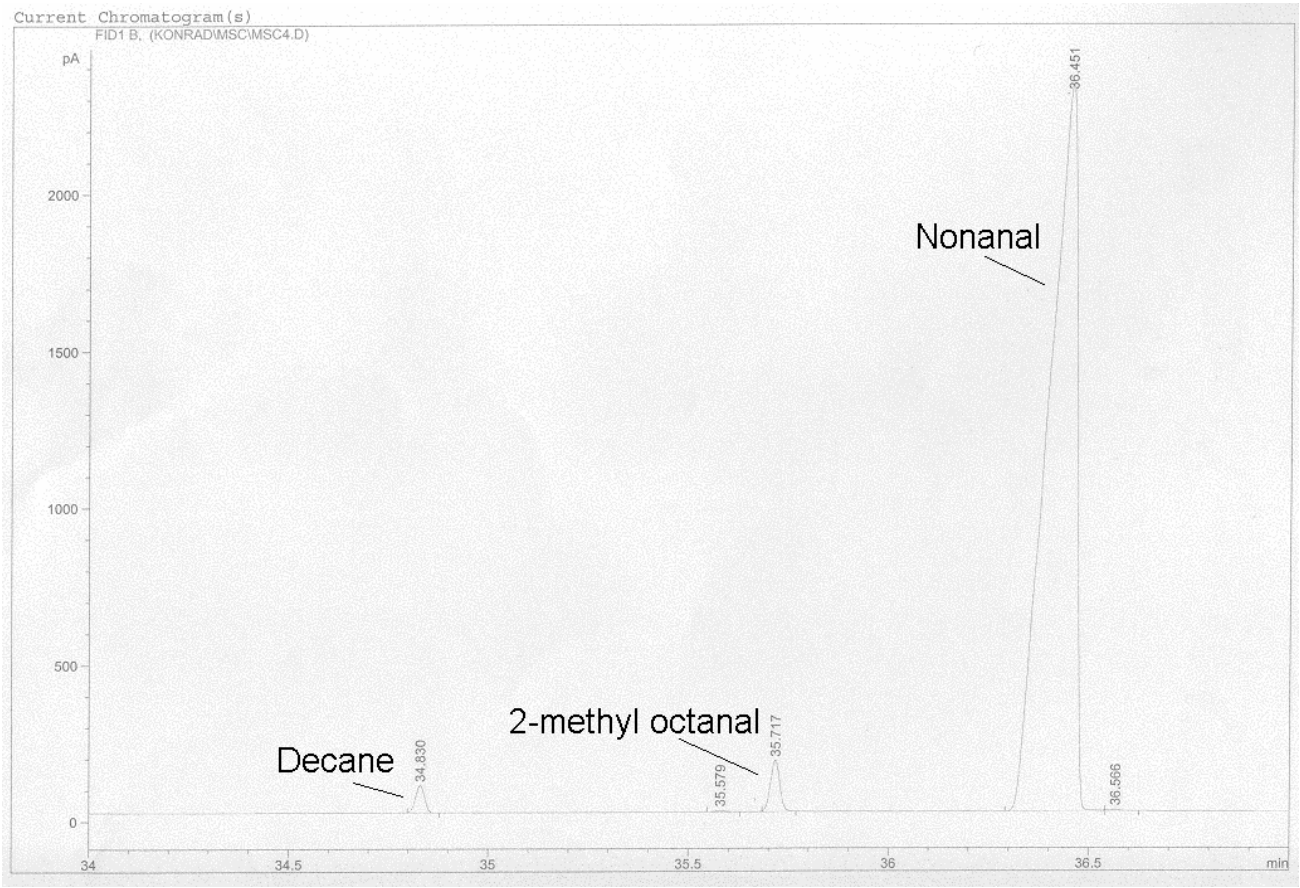

Figure 5.7. GC chromatogram of the expanded **Figure 5.6** aldehyde region displaying *n*- and *iso*-aldehyde formed after a 240 minutes 1-octene hydroformylation reaction with [$RhH(CO)_2$(xantpos)] at 90 °C and 20 bar syngas. X-axis represent retention time in minutes and y-axis the intensity of the peaks.

Based on this validation, the methods used for analyses were judged to be sufficient for the planned experimental program.

5.3 Results and Discussion: Autoclave studies

5.3.1 Dual catalyst system: $[RhH(CO)_2(PPh_3)_2]$ and $[RhH(CO)_2(xantphos)]$ studies

5.3.1.1 Variation of $Rh:PPh_3:Xp$ ratio, temperature and pressure

A number of high pressure autoclave reactions were carried out to obtain an understanding of how the different catalyst systems work. In these reactions, the effect of ligand concentration was evaluated so that the influence of the monodentate PPh_3 and bidentate PP- ligands could be better understood, as well as the dynamics between them in a dual catalyst system. In these studies, not only the rate at which these catalysts hydroformylated 1-octene were recorded, but just as importantly, the selectivities of the reactions. To allow for consistent analyses, all reactions were allowed to run for 7 hours. This duration made provision for the slowest reactions to go to completion (e.g. Rxn 4; Table 5.2). The effect of temperature on the kinetics and selectivity was also investigated.

Table 5.2. A summary of the dual catalyst autoclave experiments of hydroformylation of 1-octene.[a]

Reaction ID	T/ ℃	P / bar	PPh_3:M[b]	Xp:M[b]	n:iso[c]	L / %[d]	I / %[e]	H / %[f]	k_{obs} (min^{-1})[g]
Rxn 1	90	20	170	0	3.9	78.0	1.0	0.7	0.0467(3)
Rxn 2	90	20	170	5	13.2	92.9	3.2	2.0	0.01090(2)
Rxn 3	90	20	100	5	17.1	94.4	3.1	2.4	0.01067(3)
Rxn 4	90	20	0	5	43.9	97.7	3.5	2.7	0.0096(4)
Rxn 5	90	20	170	3	9.5	90.4	2.6	1.8	0.0139(5)
Rxn 15	90	20	170	1	4.9	82.8	1.6	0.7	0.0254(6)
Rxn 6	100	20	170	5	12.4	92.3	2.7	2.1	0.0307(2)
Rxn 7	100	20	170	0	3.7	77.7	0.6	0.2	0.1202(9)
Rxn 8	100	20	0	5	40.2	97.4	3.3	2.8	0.02556(7)
Rxn 9	110	20	170	5	11.9	91.8	3.0	2.3	0.0501(2)
Rxn 10	110	20	170	0	3.6	76.8	0.2	0.2	0.274(4)
Rxn 11	110	20	0	5	37.4	97.0	3.6	3.0	0.04961(1)
Rxn 12	100	10	170	5	16.2	94.2	3.4	2.6	0.02620(7)
Rxn 13	100	10	170	0	4.4	80.5	0.7	0.7	0.115(1)
Rxn 14	100	10	0	5	44.4	97.6	5.0	2.2	0.0370(2)

[a] Reaction conditions given in Section 5.2.1.
[b] The molar ratio of ligand to rhodium.
[c] n:iso = normal:iso aldehyde product ratio.
[d] Amount of linear aldehyde produced during the reaction expressed as a percentage relative to the total aldehyde produced.
[e] Amount of isomerised octene produced during the reaction expressed as a percentage relative to the amount of 1-octene consumed.
[f] Amount of octene hydrogenated during the reaction expressed as a percentage relative to the amount of octene consumed.
[g] Observed first-order rate constant from Eq. 5.8.

The following stepwise observations were made from the data collected in Table 5.2:

- Activities as high as 0.0467(3) min^{-1} were recorded with the pure $[RhH(CO)_2(PPh_3)_2]$ system (Rxn 1) with less than 1 % hydrogenation and as little as 1 % isomerisation. These results were accompanied by low n:iso ratios of less than 4:1 and linearities of less than 80 %.

- Studying Rxn 2 reveals a significant change upon addition of the bidentate ligand, xantphos. With a bidentate ligand such as xantphos, one only requires one ligand per Rh atom since the stability is very high. However, due to phosphine oxidation it is necessary to increase the bidentate concentration slightly hence the PPh_3:Xp ratio of 170:5 was used as a baseline for xantphos studies. Reaction rates decreased by 75 % (from 0.0467(3) min^{-1} to 0.01090(2) min^{-1}) whilst the n:iso ratio more than tripled. The presence of the xantphos ligand in the reaction solution therefore results in lower rates and higher selectivities. The amount of isomerisation and hydrogenation also increased.

- To investigate the effect of Rh:PPh_3:Xp ratio on the rate and selectivity, the PPh_3:Xp was decreased from 170:5 to 100:5 (Rxn 3). The n:iso ratios, and hence linearities, increased further, suggesting that xantphos co-ordinated species was present under these conditions. A further increase in isomerisation and hydrogenation was recorded. The results thus far suggest that there exists an equilibrium between $[RhH(CO)_2(PPh_3)_2]$ and $[RhH(CO)_2(xantphos)]$ catalysts where a PPh_3 drop from 170:5 to 100:5 is enough to allow the $[RhH(CO)_2(xantphos)]$ to become a dominant species.

- To complete the first part of the study, where the effect of decreasing PPh_3 concentration (while keeping the xantphos concentration constant) was investigated, a PPh_3:Xp ratio of 0:5 was employed (Rxn 4). Here, the n:iso ratio increased to 40:1 with linearities of more than 97 %. The isomerisation and hydrogenation increased by less than a percent and no significant change in reaction rates was observed. $[RhH(CO)_2(PPh_3)_2]$ increases the rate of catalysis, but the bidentate ligand, for entropic reasons and chelate effect, preferentially

co-ordinates shifting the equilibrium away from the PPh_3 co-ordinated species resulting in slower catalysis. Despite this, the small amount of the PPh_3 species is still able to have a significant effect on the selectivities of the reaction. This is most clearly seen by comparing the n:iso ratios of Rxn 3 and Rxn 4. Without PPh_3 present, the n:iso is 44:1, however, when 100 equivalents of PPh_3 are added there is a dramatic decrease to 17:1 despite the appearance that the xantphos co-ordinated catalyst is the dominant species. Thus, despite only being present in low concentrations, $[RhH(CO)_2(PPh_3)_2]$ catalyst hydroformylates octene faster than the $[RhH(CO)_2(xantpos)]$ catalyst, in effect lowering the overall n:iso ratios.

- In the above experiments, the equilibrium was shifted towards the $[RhH(CO)_2(PPh_3)_2]$ species by increasing the PPh_3 concentration. The effect of shifting the equilibrium to the $[RhH(CO)_2(xantphos)]$ was also studied. This was done by keeping the PPh_3 concentration constant at a Rh:PPh_3 ratio of 1:170. The PPh_3:Xp ratio of 170:5 was taken as the baseline reaction. At 170:3 (Rxn 5), a shift towards the $[RhH(CO)_2(PPh_3)_2]$ species was witnessed by decreased n:iso and linearities while the rates increased. The n:iso ratios and linearities obtained, 9.5:1 and 90.4 respectively, were higher than those obtained with the pure $[RhH(CO)_2(PPh_3)_2]$ system and yet lower than those obtained with the PPh_3:Xp ratio of 170:5 confirming the increased concentration of $[RhH(CO)_2(PPh_3)_2]$ species with the $[RhH(CO)_2(xantphos)]$ species still present. In agreement with this observation, the rates obtained were higher than the pure $[RhH(CO)_2(xantphos)]$ system, but lower than the pure $[RhH(CO)_2(PPh_3)_2]$ system (0.0139(5) min^{-1} vs. 0.0467(3) min^{-1}).

- To obtain a better understanding of this equilibrium, an even lower xantphos concentration was employed. A PPh_3:Xp ratio of 170:1 (Rxn 15) was chosen as it would be low enough to allow for the Rh-PPh_3 to be a dominant species and still ensure a bidentate bis-substituted species. Similar trends were observed where the rates (0.0254(6) min^{-1}) were higher than the pure $[RhH(CO)_2(xantphos)]$ and yet lower than the pure $[RhH(CO)_2(PPh_3)_2]$ system. The selectivities obtained were also in support of the previous observations where the n:iso as well as the linearities were 4.9:1 and 82.8 % respectively.

A graphic representation of these observations is given below in Figure 5.8.

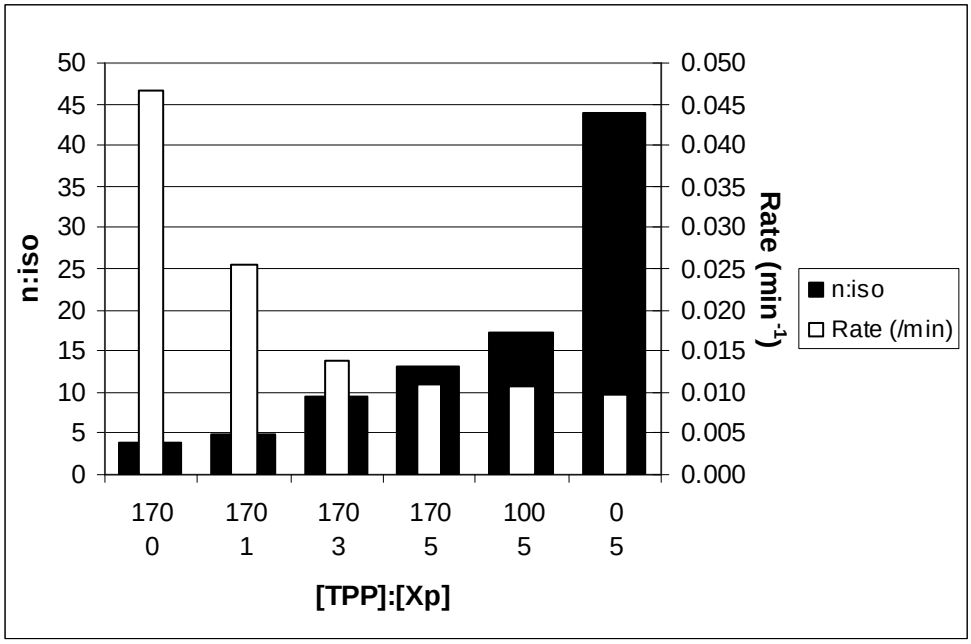

Figure 5.8. The effect of different Rh:PPh_3:Xp ratios on the rate (min^{-1}) and selectivity (n:iso ratio) of 1-octene hydroformylation at 90 °C and 20 bar syngas .

In conclusion, higher [$RhH(CO)_2$(xantphos)] species concentrations result in higher selectivities (both the n:iso ratios and linearities) where the maximum selectivities were obtained with the pure Rh-Xp system. These beneficial properties, however, were negated by a drop in reaction rates. An increase in isomerisation and hydrogenation products was also observed with an increase in the [$RhH(CO)_2$(xantphos)] species concentrations. Presumably, once in the bisequatorial position of the $18e^-$ trigonal bipyramidal intermediate, with a hydride in the apical position (similar to an intermediate in Wilkinson's hydrogenation catalyst), the catalyst is rendered a better hydrogenation catalyst after it enters the catalytic cycle. On employing both ligands in the same reactor (Rxn 2) it is seen that the chelate-effect and the increase in entropy realised by displacing two mono-dentate ligands with a bidentate one, did not completely dominate due to the large amount of PPh_3 present in the reaction solution. This can be seen by comparing the selectivities (n:iso ratios will be used for comparisons purposes) of the pure and the mixed systems, 3.9:1 *vs*. 13.2:1 vs. 43.9:1. The pure Rh-Xp system (Rxn 4) gave a

marked improvement in the product linearity compared to the pure Rh-PPh_3 system (Rxn 1), but a quarter of that was achieved when employing the mixed system (Rxn 2).

- Increasing the temperature leads to an increase in the rate of the reaction for all systems investigated. This can be clearly seen from a comparison of the pure $[RhH(CO)_2(PPh_3)_2]$ system. A rate of 0.0467(2) min^{-1} obtained at 90 ℃ was increased to 0.1202(9) min^{-1} after a temperature increase of 10 ℃ and a further increase of rate to 0.274(4) min^{-1} was realised at 110 ℃. A decrease in isomerisation and hydrogenation was observed although this increase may arguably be within experimental error (less than a percentage point). Below in Figure 5.9 is a graphical representation of the temperature effect on the $[RhH(CO)_2(PPh_3)_2]$ and the $[RhH(CO)_2(xantphos)]$ systems.

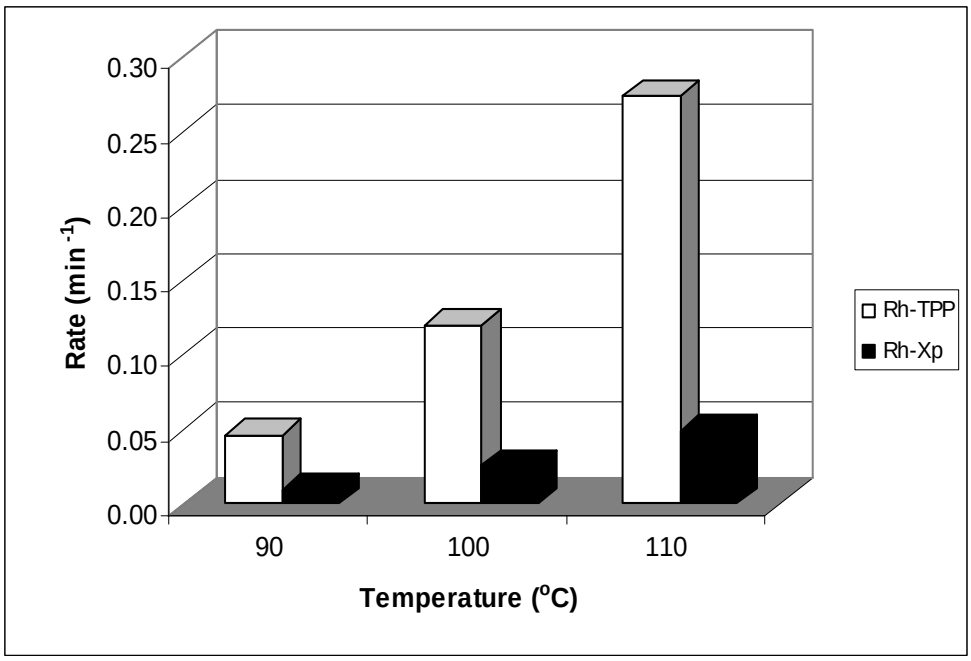

Figure 5.9. The effect of temperature on Rh-PPh_3 and Rh-Xp reaction rates of 1-octene hydroformylation at 20 bar syngas .

Although there was a slight decrease in the rate upon decreasing the pressure, the selectivity increased for both the mixed and individual pure systems. In comparison to the corresponding data collected at 20 bar syngas, the n:iso ratios showed an increased tendency from 3.9:1 to 4.4:1, 13.2:1 to 16.2:1 and 43.9:1 to 44.4:1 for the

pure $[RhH(CO)_2(PPh_3)_2]$, mixed $[RhH(CO)(PPh_3)(xantphos)]$ and the pure $[RhH(CO)_2(xantphos)]$ respectively. Figure 5.10 below illustrates this observation.

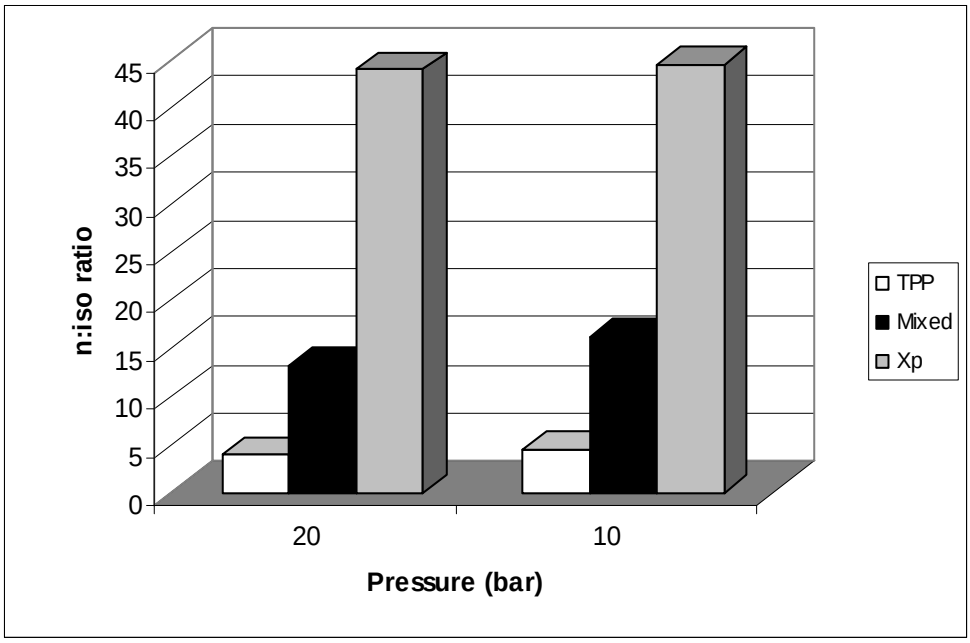

Figure 5.10. Pressure effect on the n:iso ratios of 1-octene hydroformylation with $[RhH(CO)_2(PPh_3)_2]$, $[RhH(CO)(PPh_3)(xantphos)]$ and $[RhH(CO)_2(xantphos)]$ systems as obtained in Table 5.2.

The reason for this observation can be formulated with the aid of Scheme 5.1 below:

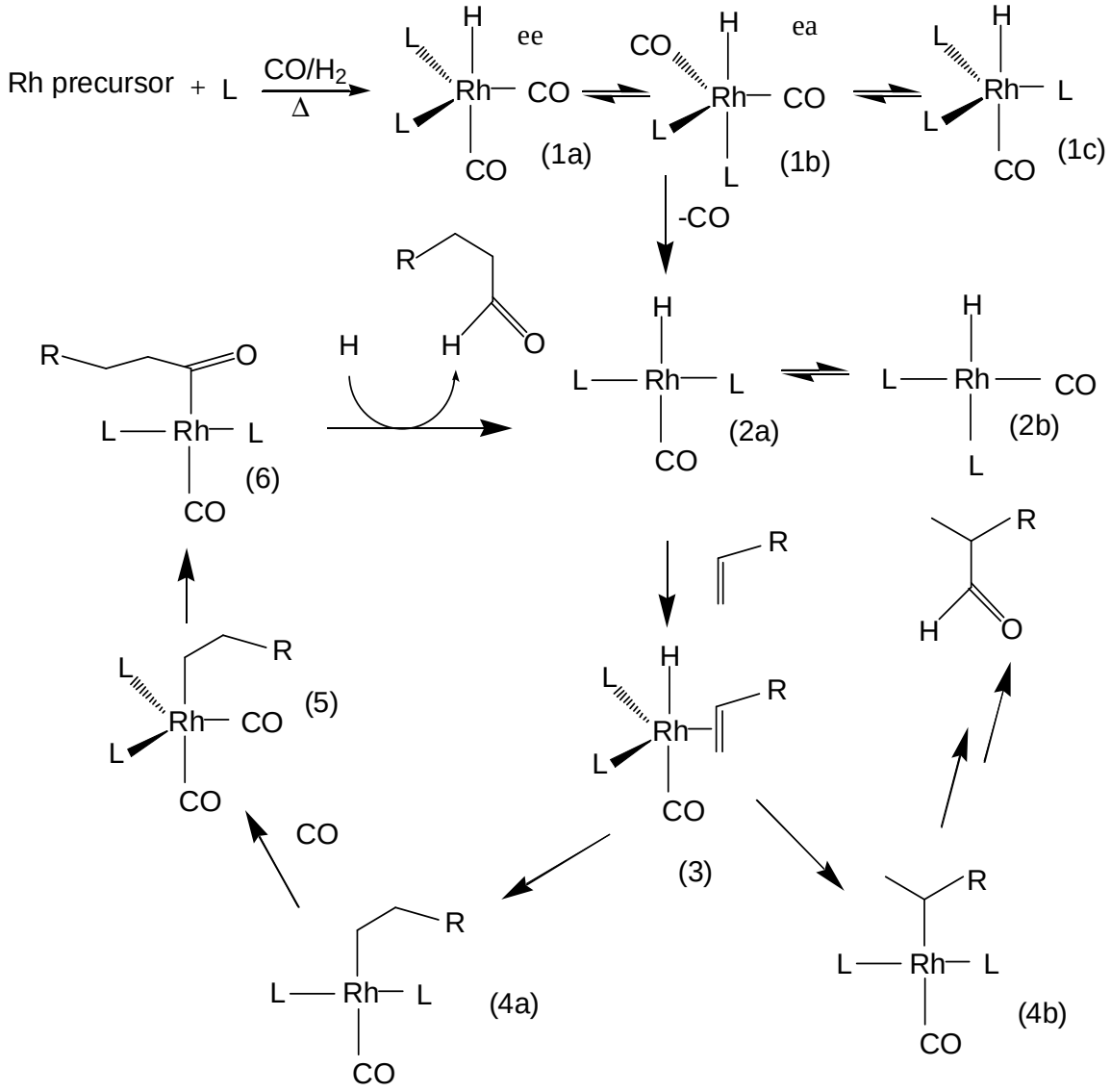

Scheme 5.1. Simplified rhodium hydroformylation mechanism.

When considering the hydroformylation catalytic circle, β-hydride elimination may occur at step **4** to give the Rh-H and alkene (**3**). This reverse reaction usually leads to a preference of the formation of the thermodynamically more stable internal-olefin. There are also two additional important points to remember, *viz*. (i) the straight chain alkyl species (**4a**) preferentially undergoes CO insertion to give an aldehyde, and (ii) the branched alkyl species (**4b**) preferentially undergoes β-hydride elimination to give an alkene. Therefore, under conditions where the forward reaction (steps **4** and **5**) to yield the aldehyde are slightly disfavoured and the reverse reaction rate increased, more n-product will form, but with a

concomitant loss of feed to isomerised product. Lower pressures (less CO present in solution and hence greater probability for β-hydride elimination) promotes such conditions.[5] This is yet confirmed by consistently higher isomerised product with 10 bar experiments compared to 20 bar experiments (Table 5.2) for both pure and mixed ligand systems.

5.3.1.2 Conclusions

The following conclusions can therefore be drawn based on the results obtained as discussed above and summarized in Table 5.2:

- Decreasing PPh_3 concentration while keeping the Xp concentration constant leads to an increase in n:iso ratios and linearities, as evident from Rxn 2 to Rxn 4. This, however, resulted in a decrease in the reaction rates due to the increase in the Rh-Xp species.
- Conversely, decreasing Xp concentration while keeping the PPh_3 concentration constant leads to a decrease in n:iso ratios and linearities. This was accompanied by an increase in reaction rates as seen from Rxn 1, Rxn 2, Rxn 5 and Rxn 15.
- An increase in temperature leads to an increase in reaction rate, consistent with all catalysts *i.e.* $[RhH(CO)_2(PPh_3)_2]$, $[RhH(CO)_2(xantphos)]$ and $[RhH(CO)(PPh_3)(xantphos)]$. This can be seen by comparing the following set of experiments: Rxn 1 vs. Rxn 7 *vs.* Rxn 10, Rxn 2 vs. Rxn 6 *vs*. Rxn 9 and Rxn 4 *vs*. Rxn 8 *vs*. Rxn 11.
- Although the effect of pressure on the reaction rate may be argued negligible, there was an unambiguous increase in n:iso ratios and linearities when syngas pressure was decreased from 20 bar to 10 bar at 100 ℃.

5.3.2 Inhibition studies on the dual catalyst system

5.3.2.1 Variation of Rh:PPh_3:Xp ratio in the presence of an inhibitor

As mentioned in the introduction to this chapter, studies already undertaken revealed that xantphos type ligands confer some inhibitor resistance to the rhodium catalyst. It was therefore decided to test the dual ligand catalyst system in the

presence of methyl vinyl ketone (MVK), a known hydroformylation inhibitor, to see to what extent this resistance is retained.

The effect of PPh_3:Xp ratio on inhibition was investigated where the inhibition time was recorded for different ratios employed. Additionally, product distribution was also investigated for comparison purposes. All experiments were carried out at 90 ℃ and 20 bar syngas. Constant rhodium metal concentration of 1.6 mM and MVK concentration of 0.32 M (Rh:MVK molar ratio of 1:200) were employed. Similar procedures were followed (See Section 5.2.1) At the reaction temperature, 1-octene (10 mL) spiked with MVK (200 molar equivalences relative to rhodium) was injected through over-pressure as described previously. The reactor was then switched to a ballast vessel where the rate of the synthesis gas uptake was monitored by means of a pressure transducer, recording the fall in the gas reservoir's pressure.

Inhibition time was witnessed by a slow gas uptake curve in the initial stage of the reaction before a faster gas uptake curve became evident. Gas uptake curves of different inhibition runs with various PPh_3 concentrations were collected to illustrate the effect of different PPh_3 concentrations on inhibition. Due to the inhibition period, these reactions were allowed to run for 16 hours.

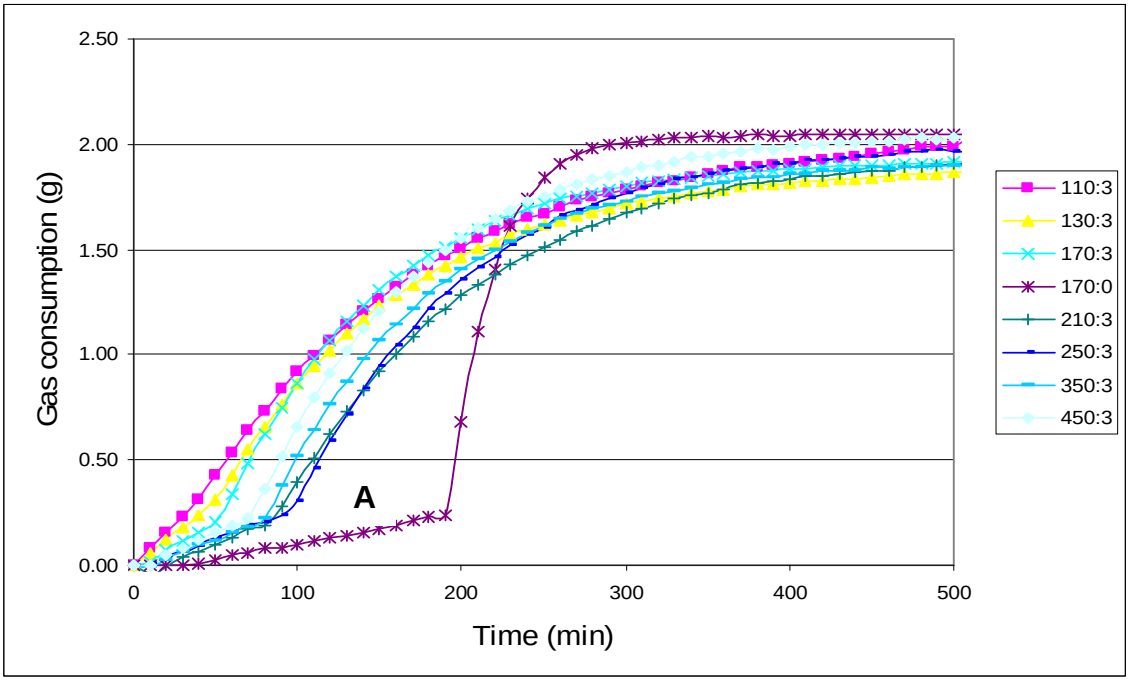

Figure 5.11. Gas uptake curve vs. time showing the effect of Rh:PPh_3:Xp ratio on inhibition during 1-octene hydroformylation at 90 °C and 20 bar syngas.

It is clear from Figure 5.11 that these reactions gave gas uptake profiles consistent with two distinct processes. The first, slow curve is attributed to the inhibition period during which the inhibiting MVK is reacted away to free the catalyst to perform the hydroformylation reaction. The second faster curve indicates the gas consumption due to the hydroformylation of 1-octene. Due to this initial inhibition period, it was difficult to accurately calculate the rate of the reactions in these studies. Although the initial gas consumption is mainly due to inhibition, it is likely that small quantities of the olefin may be reacted away during this period. The interesting observation of the sudden 'switch' (**A** in Fig. 5.11) in reactivity of the catalyst when all the MVK is seemingly reacted away, is unexplained at this point, but could indicate a significant stability of the unreactive metal complex formed due to the MVK interaction.

Table 5.3. Effect of PPh_3:Xp ratio on MVK inhibition of $[RhH(CO)_2(PPh_3)_2]$, $[RhH(CO)_2(xantphos)]$ and $[RhH(CO)(PPh_3)(xantphos)]$ catalysts (Rh = 1) at 90 ℃ and 20 bar syngas .[a]

Reaction ID	[PPh_3]	[Xp]	n:iso	L / %	I / %	H / %	Inhib. Time [b]
Rxn 16	90	3	11.4	90.4	1.7	1.0	0 min
Rxn 17	110	3	10.9	90.3	1.7	1.0	36 min
Rxn 18	130	3	9.6	89.0	1.5	0.9	45 min
Rxn 19	170	3	8.8	89.1	2.1	1.6	57 min
Rxn 20	170	0	3.3	75.6	0.6	0.4	190 min
Rxn 21	170	5	11.9	91.0	1.6	1.0	0 min
Rxn 22	210	3	7.5	87.0	1.3	0.8	86 min
Rxn 23	250	3	6.1	84.4	1.2	0.7	97 min
Rxn 24	350	3	6.4	85.1	1.3	0.9	82 min
Rxn 25	450	3	6.2	84.7	0.9	0.6	75 min

[a] See Section 5.2.1 for detailed reaction procedures and quantities.
[b] Inhibition time before hydroformylation of 1-octene could commence; A in Fig. 5.11.

The following stepwise conclusions can be drawn from Table 5.3:

- At low PPh_3 concentrations (Rxn 16) no inhibition was observed, nor was it observed in the run where higher Xp ratios were employed. This observation suggests that under these conditions, the equilibrium is shifted towards the $[RhH(CO)_2(xantphos)]$ species that is inhibitor resistant. Higher PPh_3 concentrations shift the equilibrium more to the $[RhH(CO)_2(PPh_3)_2]$ species that is inhibited as witnessed by an increase in inhibition time.

- Although higher PPh_3 concentrations result in an increase in inhibition time, the curve appears to level off at very high PPh_3 concentrations (at a Rh:Xp ratio of 1:3). This observation suggests that high PPh_3 concentrations may act as a shield towards the metal center rendering it inhibitor resistant. Thus PPh_3 may be used as an inhibitor resistant catalyst under these conditions as illustrated in Figure 5.12 below. This figure represents the effect of PPh_3 concentration where the xantphos was kept constant (Rh:Xp = 1:3).

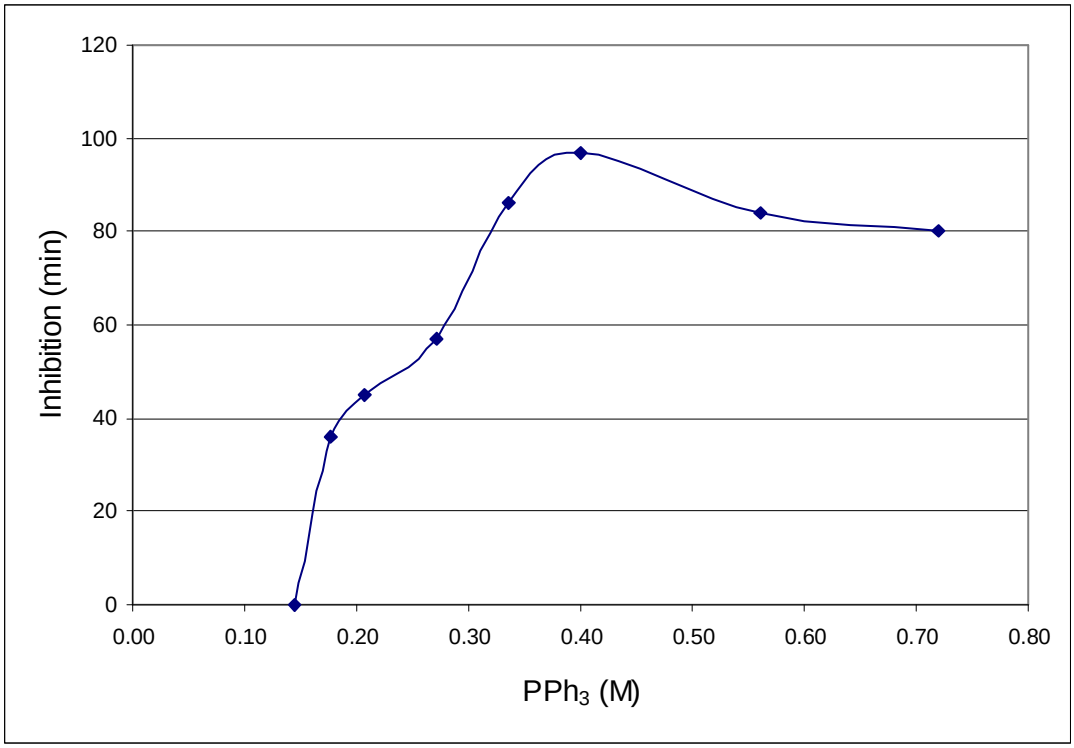

Figure 5.12. A graph displaying the relationship between $[PPh_3]$ and inhibition time as extracted from Table 5.3. This data was collected at 90 ℃ and 20 bar syngas with MVK as an inhibitor (Rh:MVK = 1:200 molar equivalents).

Results in Table 5.3 indicated that there is no inhibition when more Xp is employed making the $[RhH(CO)_2(xantphos)]$ species the dominant species (Rxn 21). These results suggest that in the mixed ligand systems, both the $[RhH(CO)_2(PPh_3)_2]$ and $[RhH(CO)_2(xantphos)]$ catalytic species are present in the reaction solution. Due to the chelate effect, most of the catalyst will be present in the xantphos modified form at the beginning of the reaction. However, there is always a small equilibrium resulting in the PPh_3 modified catalyst. Unlike in Rxn 21 where it is not possible for the MVK to coordinate (due to the sterically demanding Xp) in an inhibiting fashion, the aforementioned equilibrium will result in the catalyst, which is converted to the PPh_3 form, becoming inhibited hence the inhibition times observed in the mixed ligand systems (Scheme 5.2). This suggests that the more dominant the $[RhH(CO)_2(PPh_3)_2]$ catalyst becomes, the more the equilibrium below will be shifted towards the inhibited species.

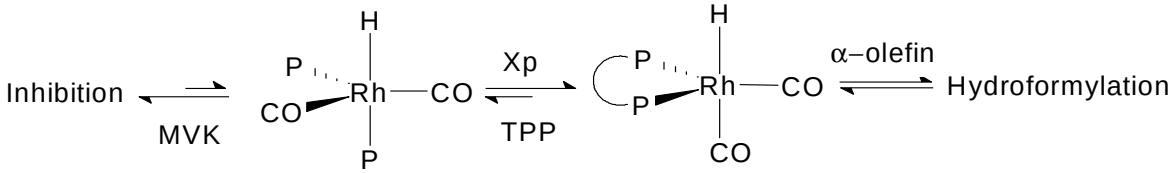

Scheme 5.2. Postulated equilibria and species formation in the Hydroformylation of 1-octene by $[RhH(CO)(PPh_3)(xantphos)]$ in the presence of MVK.

- Selectivity analyses performed on these runs displayed similar trends to those observed with reactions carried out without an inhibitor added as discussed in paragraph 5.3.1. A decrease in n:iso ratios and linearities was observed with an increase in PPh_3 concentration were the $[RhH(CO)_2(PPh_3)_2]$ species was being populated. However, n:iso ratios and linearities recorded were lower for these MVK inhibition reactions. For instance; n:iso ratios of 9.5:1 and linearities of 90.4 % were obtained when there was no inhibitor present (Rxn 5), but these decreased to 8.8:1 and 89.1 % respectively when MVK was added (Rxn 19). Although one may argue that these differences are not statistically significant, a repeat of selected experiments gave the same results. This observation suggests that even though the catalyst may be liberated from the inhibitor to

perform hydroformylation, there is still part of the affected species present throughout the reaction that is responsible for the drop in selectivity.

- Highest selectivities were obtained with runs where the equilibrium was shifted more towards the [$RhH(CO)_2$(xantphos)] catalyst and away from the [$RhH(CO)_2(PPh_3)_2$] catalyst (See Scheme 5.2). This observation was witnessed in Rxn 16 and Rxn 21 with Xp:PPh_3:M ratio of 3:90:1 and 5:170:1 respectively. What is worth noting when comparing these two runs is that with Rxn 16, a minimum amount of PPh_3 (relative to other runs) was employed with the same amount of xantphos thereby shifting the equilibrium more towards the [$RhH(CO)_2$(xantphos)] species. Similarly, a maximum amount of xantphos was employed with Rxn 21 shifting the equilibrium more towards the [$RhH(CO)_2$(xantphos)] species. Conversely, the lowest n:iso ratios and linearities were obtained when the [$RhH(CO)_2(PPh_3)_2$] was the dominant species as observed with Rxn 20. Higher PPh_3 concentrations were seen to yield higher n:iso ratios and linearities as observed with Rxn 25. It is also worth noting that under these conditions, [$RhH(CO)_2(PPh_3)_2$] would most likely be the dominant species.

5.3.2.2 Conclusions

Based on the data presented in Table 5.3, the following conclusions concerning inhibition on the mixed system may be drawn:

- Increasing PPh_3 concentration leads to the population of the [$RhH(CO)_2(PPh_3)_2$] species that is more susceptible to inhibition thus giving longer inhibition periods. In support of this, selectivities drop and rates increase with an increase of PPh_3 concentration.

- The reverse is also true where decreasing the PPh_3 concentration leads to the population of the [$RhH(CO)_2$(xantphos)] species that is more stable towards inhibition resulting in shorter inhibition periods. Selectivities increased and rates dropped with a decrease in PPh_3 concentration.

- Excess PPh_3 acts as a shield towards the metal center thereby preventing further inhibition of the catalyst as witnessed by a decrease in the inhibition time with an increase in the PPh_3 concentration.

5.3.3 Effect of PP bidentate ligand bite angle on inhibition

In the previous section it was mentioned that xantphos, which has a large bite-angle (111 °), [1] confers inhibitor resistance to a hydroformylation catalyst. It was therefore decided to study the effect of bite-angle on inhibitor resistance. For this study a set of ligands was chosen where the bite angle was changed, but with minimal changes in the ligands electronic properties. Bis(diphenylphosphine)methane (DPPM), bis(diphenylphosphine)ethane (DPPE), bis(diphenylphosphine)propane (DPPP) and bis(diphenylphosphine)butane (DPPB) were chosen for this study. The procedure followed involved preforming the catalyst with the desired bidentate ligand and then injecting 1-octene spiked with MVK (100 molar equivalences to Rh). All reactions were carried out at 90 °C and 20 bar syngas.

Table 5.4. The effect of various P-P bidentate ligand systems on MVK inhibition: rates and selectivities.[a]

Reaction ID	[PPh_3]	[P-P]	Inhib. Time[b]	n:iso	L / %[b]	I / %[b]	H / %[b]
Rxn 26	170	3 (DPPM)	50 min	3.8	58.6	2.2	0.1
Rxn 27	0	3 (DPPM)	No rxn	–	–	–	–
Rxn28	0	3 (DPPE)	0 min[c]	1.0	50.1	0	0
Rxn29	0	3 (DPPP)	4 min	2.4	69.4	2.4	0.1
Rxn30	0	3 (DPPB)	15 min	3.1	75.4	0.2	0.4

a. See **Table 5.2** for legends.
b. See **Table 5.3**.
c. A very slow reaction; see text for explanation.

The following stepwise conclusions can be drawn from Table 5.4:

- In the first experiment, DPPM was run with PPh_3 at a Rh:PPh_3:DPPM ratio of 1:170:3. An inhibition period of 15 minutes was observed after which a very slow gas uptake was evident for 35 minutes (reaction of MVK) followed by the hydroformylation of 1-octene. This profile suggests that the catalyst is initially inhibited and only once the inhibitor has been reacted away can normal hydroformylation proceed.

- The second experiment was carried out under the same conditions, but PPh_3 was omitted (Rxn 27). No reaction was observed as illustrated by a constant ballast vessel pressure. A slight drop in pressure after 150 minutes could be distinguished from the normal fluctuations in ballast vessel pressure attributable to variations in the laboratory temperature. In support of this, an olefin conversion of only 50 % was recorded by GC after two days as opposed to the normally observed > 90 % attained usually within 3 hours. This was assumed to be due to possible "Rh-cages" likely to be formed with the DPPM thereby taking the Rh out of the hydroformylation cycle as illustrated in Figure 5.13.[6, 7] Thus when PPh_3 is present it is possible that a Rh-PPh_3 catalyst, in equilibrium with the Rh-DPPM cage species, is responsible for hydroformylating the olefin.

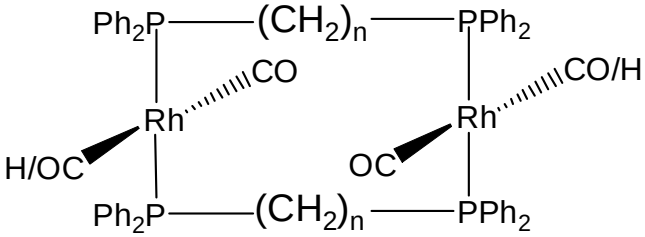

Figure 5.13. Proposed rhodium 'cage complexes' with bidentate ligands; e.g. n=1 with DPPM.

- A normal, but very slow gas uptake curve was observed with DPPE with no apparent inhibition. This was surprising as inhibition was evident with DPPP (an initial slow gas uptake curve followed by a normal faster curve). To investigate this, DPPE was run without the inhibitor and the reaction rates compared (Figure 5.14.).

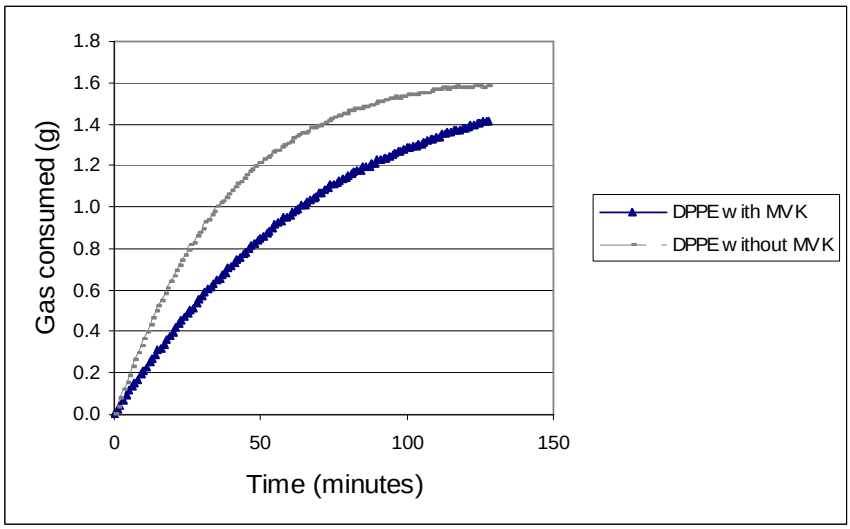

Figure 5.14. DPPE (M:L = 1:3) comparisons of gas consumption over time, with and without MVK at 90 ℃ and 20 bar syngas.

A slow reaction with MVK shows that the catalyst is inhibited, but unlike other ligands tested where the catalyst is eventually freed, the inhibited catalyst appears to be in equilibrium with the active one. Thus part of the catalyst is inhibited through the entire reaction.

- A reaction profile similar to DPPP was observed with DPPB where a slow gas uptake was observed in the initial stage of the reaction followed by a faster gas uptake curve thereby giving a curve with two slopes. Clearly the above results point to a very interesting relationship between the bite-angle of the ligand and resistance to inhibitors. Observed results suggest that the bigger the bite angle, the more resistant the catalyst becomes towards inhibition. A low rate observed with DPPB may also be attributed to dimeric rhodium species where the ligand bridges two rhodium centres.[4]

- The n:iso for the DPPM:PPh_3 is consistent with a $[RhH(CO)_2(PPh_3)_2]$ run, i.e. no DPPM used. Although the linearities and n:iso ratios were low, they were fairly consistent with all ligands tested in the series apart from DPPE. This also held for the yields, isomerisation and hydrogenation. A customary trend is seen where the n:iso ratios as well as the linearities increase with an increase in bite angle size, consistent with the trends observed in the literature.[8]

5.3.4 Effect of PPh_3 concentration on selectivity and inhibition for the hydroformylation of 1-octene

It is known that higher linearities are achieved at higher PPh_3 concentrations. Scheme 5.2 is proposed to aid in explaining this observation.

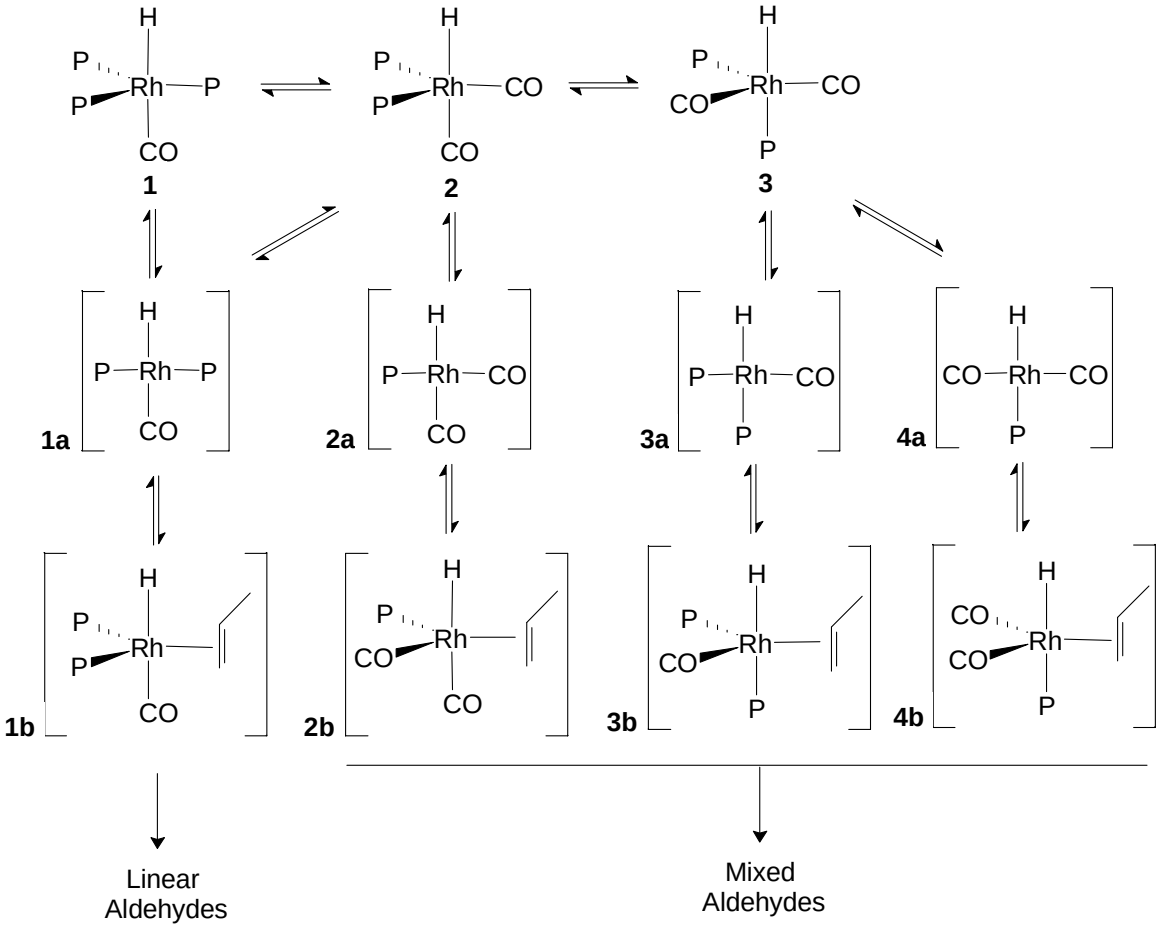

Scheme 5.3. Different catalyst isomers *vs*. selectivity.

Under hydroformylation conditions, **2** and **3** are dominant species, however, as the PPh_3 concentration increases, more **1** is formed. These species lose a CO or P-ligand to give the species **1a** – **4a**. Thus, more of the trans-phosphine substituted square planar (**1a**) and equatorial-equatorial (*ee*) trigonal bipyramidal (**1b**) species are present at high PPh_3 concentrations. This *ee*-bonding of the ligands is preferred by members of the xantphos family of ligands, which also result in the high linearities observed. However, it now appears that this mode of bonding may also prevent the inhibitor from chelating or reacting with the rhodium metal centre to form an inhibited species. If a bidentate ligand with a smaller bite angle is employed, the preferential bonding mode will be equatorial-axial (*ea*) and *ee*, or *ea*, which will in turn allow the inhibitor to access the bonding sites that will lead to a dormant species being formed.

With DPPE a more equal distribution of the ee and ea diastereomers exists resulting in only the ea portion being kept in an incubated, inactive state. The shortest dormant state is formed for the DPPP modified catalyst with its bite angle preferring coordination sites where inactive states are minimised. In conclusion, at high PPh_3 concentrations and when bidentate ligands bonding in an *ee*-fashion are used the **1a** and **1b** intermediates are favoured. However, at low PPh_3 concentrations **2a**, **2b**, **4a** and **4b** are formed. Also, *ea*-coordinating bidentates form the species **3a** and **3b**. All of the latter are species which will form inhibited intermediates in the presence of compounds such as MVK.

The effect of the PPh_3 concentration on rhodium catalyst inhibition was evaluated where the reaction rates and selectivities were recorded. Similar procedures as above (Section 5.3.2.) were employed where 1-octene was injected into the reactor together with the inhibitor being tested. The results from the studies are collected in Table 5.5.

Table 5.5.. Effect of [PPh_3] on inhibitor resistance during hydroformylation of 1-octene.[a]

Reaction. ID	PPh_3	Inhibitor	Inhib. Time (min)	k / h^{-1}	n:iso	I / %	H / %
Rxn 31	90:1	None	None	3.5	3.0	1.0	0.1
Rxn 32	170:1	None	None	2.2	3.2	0.9	0.1
Rxn 33	90:1	MVK	200	3.5	2.9	0.2	0.09
Rxn 34	170:1	MVK	150	2.1	3.1	0.9	0.1
Rxn 35	90:1	Isoprene	None	1.3	2.9	0.9	0.09
Rxn 36	170:1	Isoprene	None	1.4	3.1	0.6	0.1

[a] See **Table 5.2** for legends

The following conclusions can be drawn based on the data in Table 5.5:

- With no inhibitor present, it is seen that the there is a 37 % drop in catalyst activity by increasing the L:M ratio from 90:1 to 170:1. MVK and isoprene have very different effects on the catalyst with the former resulting in complete inhibition of the catalyst, whilst only a slower reaction rate is observed upon the addition of the diene. It is also seen that the catalyst regains its original activity once the MVK has been reacted away. What is worth noting is that the

inhibition time is reduced by a full hour at a higher L:M ratio. Clearly, the catalyst that is formed at these ratios is better able to deal with the inhibitor.

- The use of a higher L:M ratio in the case of isoprene also gives a very interesting result. Here the reaction rates at the two L:M ratios, despite being lower than when no inhibitor is present, are almost the same. Thus, at 90:1 there is a 62 % drop in activity, but only a 36 % decrease in activity when the ligand ratio is increased to 170:1. Although the percentage drop in activity for the bidentate ligated ligand was less (when compared to the hydroformylation of 1-octene), both reacted at the *same rate* with the diene.

- These results lend further credence to the proposals put forth earlier with bidentate ligands that the equatorial-equatorial trigonal bipyramidal and the trans ligated intermediates (*i.e.* those populated by ligands with a larger bite-angle) provide more inhibitor resistance. The same theory can be applied to mono-dentate phosphine ligands where increasing the L:M ratio, more of the species **1** is formed together with **2** and **3** (Scheme 5.2). If this is true then there is statistically a better chance of forming **1a** and **1b**, the species which our experiments suggest lessen the extent of chelate formation by an inhibitor.

- In addition to this, in the case of MVK we see that these intermediates are better able to react with it and hence remove it from the reaction solution. This is not too surprising as it has been evident in previous studies that increasing the L:M ratio or by employing a bidentate ligand, such as xantphos, there is an increase in the amount of isomerised and hydrogenated feed as illustrated in Section 5.3.1.1. These traits are presumably also advantageous in dealing with inhibitors.

5.4 Kinetics of the formation of [RhH(CO)(PPh_3)(xantphos)] from [RhH(CO)(PPh_3)$_3$] and subsequent catalytic hydroformylation of 1-octene

5.4.1 Introduction to kinetics studies

Autoclave studies reported above (Section 5.3.1 and 5.3.2) displayed an equilibrium between the $[RhH(CO)_2(PPh_3)_2]$ and the $[RhH(CO)_2(xantphos)]$ catalysts when both PPh_3 and Xp are present in the reaction mixture. In the aim of gaining more understanding on this equilibrium, it was decided that the kinetics of the formation of the $[RhH(CO)(PPh_3)(xantphos)]$ species be studied in more detail. Kinetic studies on the formation of this mixed species were seen as a complimentary study towards the characterisation studies performed during spectroscopic investigations (Section 4.2.3.2). The effect of temperature on the substitution reaction was investigated to subsequently obtain activation parameters. The effect of excess PPh_3 concentration on catalyst stability was also investigated, complementary to spectroscopic studies in Section 4.1.3.1. Results from autoclave experiments were collected for the calculation of rate constants as well as the equilibrium constant. This section will also highlight derivation of rate equations and conclusions drawn from the experiments carried out.

5.4.2 Stability studies of $[RhH(CO)(PPh_3)_3]$ in the presence of PPh_3

Significant scattering (See Section 5.4.3 below), as a result of catalyst instability, was observed during the evaluation of the kinetics of the substitution reactions performed at higher temperatures (45 ℃). This scattering worsened at higher ligand concentrations (9.75 mM). The reasons for these instabilities were assumed to be due to dimer formation and/or other equilibria involved other than the reaction studied, e.g. an equilibrium between the trigonal bipyrimidal species ($[RhH(CO)(PPh_3)_3]$) and the square planar species ($[RhH(CO)(PPh_3)_2]$). In order to obtain a better understanding on these observations, stability experiments were conducted on a Cary100 instrument. The effect of additional PPh_3 was also studied over time.

A known concentration of $[RhH(CO)(PPh_3)_3]$ (0.15 mM) was dissolved in toluene and its absorbance spectrum recorded over time at room temperature. Below (Figure 5.15) is the graph of absorbance change over time against wavelength. The cycle time was set at 5 minutes and 24 cycles were recorded, thus the experiment duration was 120 minutes. This duration was judged to be sufficient to display any changes/instabilities should there be any.

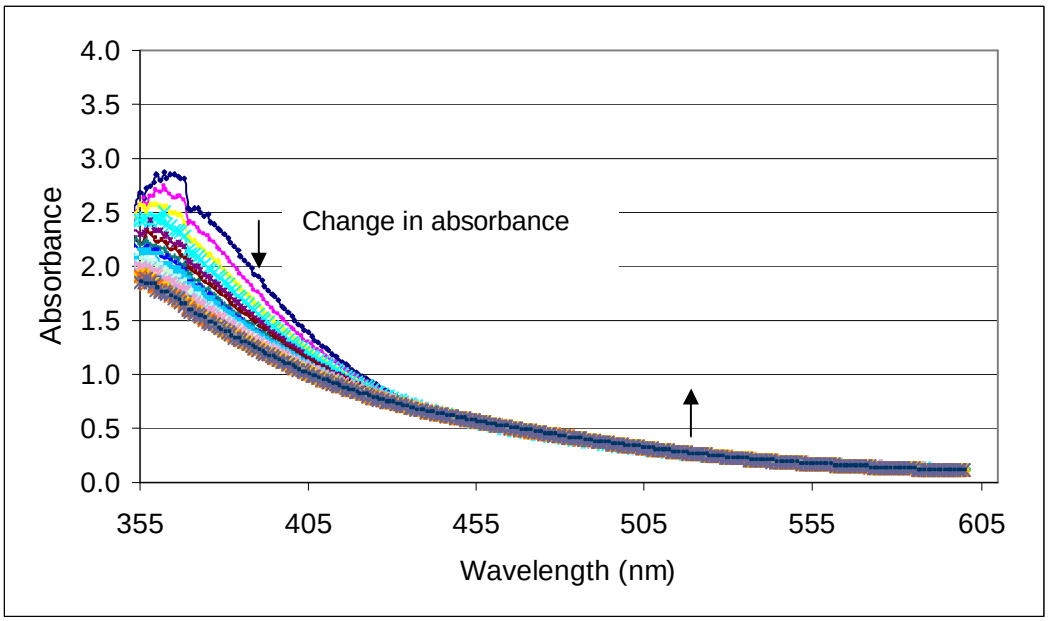

Figure 5.15. Change in Absorbance over time vs. Wavelength of $[Rh(CO)(PPh_3)_3]$ at room temperature. Data was collected at 12 seconds per scan, shown in Figure 5.15 is a cycle completed in 5 min with [Rh] = 0.015 mM in toluene.

It is clear from Fig. 5.15 above that a significant change in absorbance was observed over 120 minutes suggesting changes in the species studied under the selected conditions. The effect of additional PPh_3 was evaluated where 20 molar equivalents of PPh_3 were added to a freshly prepared $[RhH(CO)(PPh_3)_3]$ solution. For valid comparisons, a freshly prepared solution had to be used to prevent uncertainties on the effect of the PPh_3. Similar procedures as above were followed and spectra recorded over time as illustrated in the figure below.

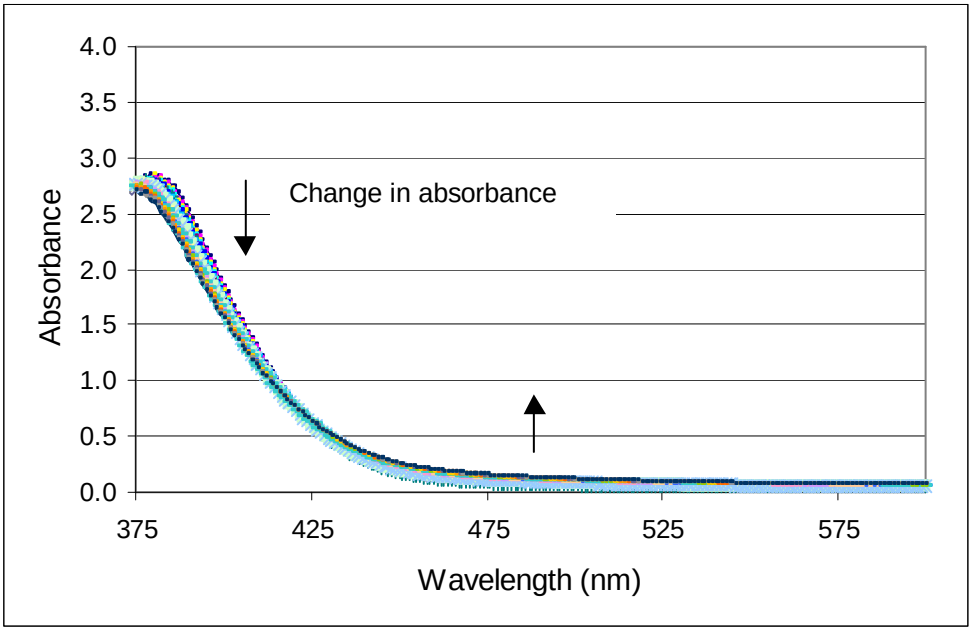

Figure 5.16. The effect of extra PPh_3 on the stability of $[Rh(CO)(PPh_3)_3]$: Change in Absorbance over time vs. Wavelength. Data was collected at 12 seconds per scan, shown in Figure 5.16 is a circle completed in 5 min with the same change in absorbance as in Figure 5.15 and [Rh] = 0.015 mM and M:L molar ratio = 1:20.

A significant stabilising effect upon adding additional PPh_3 to the $[RhH(CO)(PPh_3)_3]$ solution was observed. These observations are in agreement with stability studies conducted with NMR spectroscopy as illustrated in Section 4.1.3.1.

5.4.3 Kinetics of the substitution reaction between $[RhH(CO)(PPh_3)_3]$ and xantphos studied by Stopped-flow spectrophotometry

Substitution reactions with Wilkinson's hydride derivative $[RhH(CO)(PPh_3)_3]$ and xantphos (See NMR studies, Scheme 4.1) were studied on a diode array stopped-flow instrument. The aim of these studies was to evaluate the rate of substitution of PPh_3 by a bidentate ligand in forming a bidentate derivative complex (Also see NMR studies, Section 4.2.3.2). Temperature variations were also performed to study the effect thereof on the substitution reaction. The actual catalyst precursor, $[Rh(acac)(CO)_2]$, could not be employed as it requires syngas pressure to preform the active hydride. Although Wilkinson's hydride derivative only gave the highly

phosphine modified species, it was the only catalyst precursor that could be employed to represent the catalytic species formed under hydroformylation reaction without the need for syngas pressure and elevated temperature.

A solution of $[RhH(CO)(PPh_3)_3]$ (0.15 mM) in toluene (25 mL) was prepared in a volumetric flask after degassing the solvent. Subsequently, a series of xantphos solutions were prepared for the study of the substitution reaction at different ligand concentrations. Data points at a wavelength of 400 nm were found to be optimal for these experiments and were therefore selected as given below.

Table 5.6. Observed pseudo first order rate constants of the substitution reaction between $[RhH(CO)(PPh_3)_3]$ and xantphos in toluene at different temperatures with various ligand concentrations.

[Xp] (mM)	Final [Xp] (mM)	k_{obs} (s^{-1}) at different temperatures (℃) [a]				
		5	**15**	**25**	**35**	**45**
1.5	0.75	0.2357(4)	0.4680(3)	0.3900(2)	1.0848(4)	2.5578(3)
3.0	1.50	–	–	0.503(4)	1.488(2)	4.0282(5)
4.5	2.25	–	–	0.691(3)	1.8173(2)	4.2604(5)
6.0	3.00	–	–	0.935(2)	1.9870(3)	4.9283(8)
7.5	3.75	0.2632(3)	0.5927(2)	1.0886(4)	2.274(2)	5.0129(6)
15.0	7.50	0.3276(5)	0.7775(4)	2.1237(3)	–	–
18.0	9.00	–	–	2.3764(4)	–	–
19.5	9.75	–	–	2.6627(4)	–	–
30.0	15.00	0.3883(3)	1.3100(5)	3.8294(6)	–	–

[a] Obtained from fitting Abs. vs. time data to Eq. 5.8, assuming Abs = P

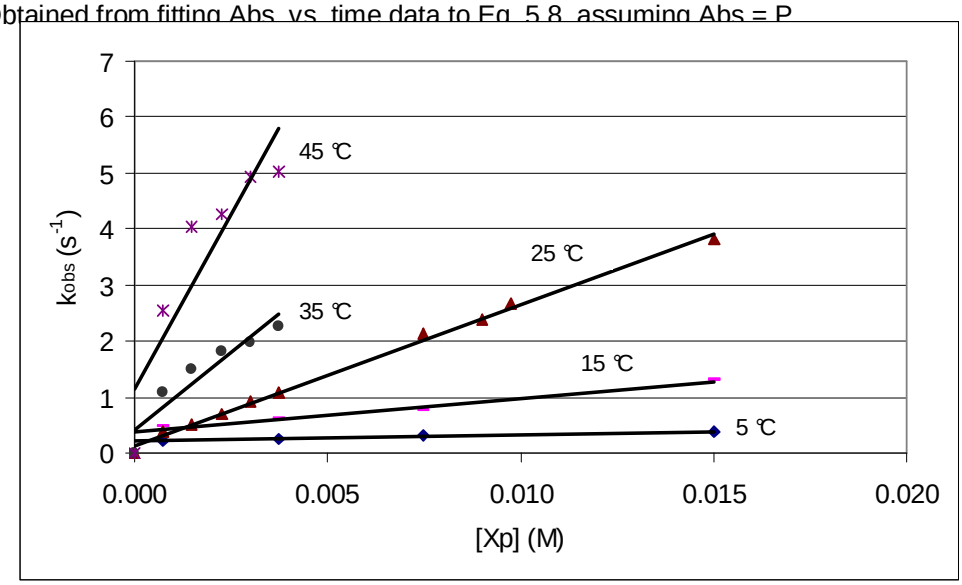

Figure 5.17. A graphic representation of k_{obs} vs. ligand concentration ([Xp]) at different temperatures in toluene. Reactions were performed under pseudo 1st order conditions where [Xp] >>[M] at a constant metal concentration of 0.075 mM.

There were some deviations observed with the points at higher temperatures and higher ligand concentrations which were assumed to have been due to dimer formation. Under these conditions (higher temperatures), it was also speculated that the ee and ea exchange of the chelating phosphines could also be the cause of the deviations.

The substitution reaction, however, showed a linear dependence of k_{obs} vs. [Xp] and was therefore interpreted as a typical reversible substitutions reaction for which the following equation holds:

$$[RhH(CO)(PPh_3)_3] + Xantphos \underset{k_{-1}}{\overset{k_1}{\rightleftharpoons}} [RhH(CO)(PPh_3)(xantphos)] + 2PPh_3 \qquad 5.1$$

where k_1 is the forward rate, k_{-1} the reverse rate, and K_1 the equilibrium constants, respectively.

The simple rate expression in Eq. 5.2 describes the reaction in equation 5.1.

$$\text{Rate} = k_1[RhH(CO)(PPh_3)_3][xantphos] - k_{-1}[RhH(CO)(PPh_3)(xantphos)][PPh_3]^2 + k_s[RhH(CO)(PPh_3)_3] \qquad 5.2$$

Under the conditions where [Xp] >>[Rh], following integration with respect to [Rh], Eq. 5.3 is obtained, which describes the pseudo first-order rate constant for the formation of [RhH(CO)(PPh_3)(xantphos)].

$$k_{obs} = k_1[Xp] + k_{-1}[PPh_3]^2 + k_s \qquad 5.3$$

The relationship between the reaction rate and the free energy of activation, $\Delta G^{\neq}$, defined in terms of the enthalpy ($\Delta H^{\neq}$) and entropy ($\Delta S^{\neq}$) of activation, defines the Eyring relationship, given by Eq. 5.4 (exponential) and Eq. 5.5 (natural logarithmic form).

$$k_1 = (k_B T/h)\exp(-\Delta H^{\neq}/RT)\exp(\Delta S^{\neq}/R) \qquad 5.4$$

$$\ln(k_1/T) = -\Delta H^{\neq}/RT + (\ln k_B/h + (\Delta S^{\neq}/R) \quad 5.5$$

where k_B = Boltzmann constant, h = Planck constant, R = universal gas constant and T = absolute temperature.

Figure 5.19 below gives the Eyring plot ($\ln(k_1/T)$ vs. $1/T$, *from Eq. 5.5*) from the Scientist[4] program, yielding the typical linear relationship, for the reaction given in Eq. 5.1.

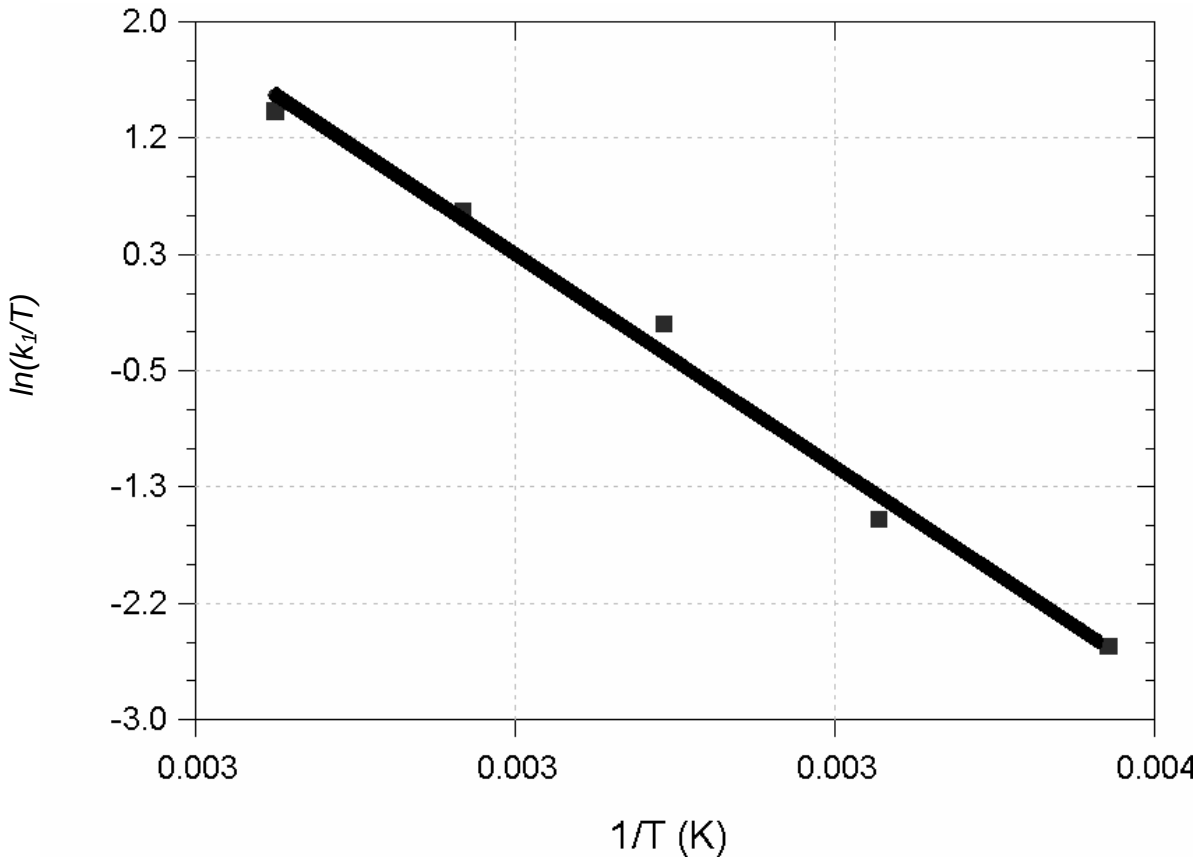

Figure 5.18. A graphic representation of ln(k/T) vs. 1/T obtained from the substitution reaction of $[RhH(CO)(PPh_3)_3]$ and xantphos under pseudo 1st order conditions where [Xp] >>[M] at a constant metal concentration of 0.15 mM. . Square points: Experimental values, Line: Predicted/calculated values.

Activation enthalpy, $\Delta H^{\#}$ = 72.85(8) kJ.mol^{-1} as obtained from the slope was calculated where activation entropy, $\Delta S^{\#}$ = 43.65(6) J.mol^{-1}.K^{-1} was obtained from the y-intercepts. The equation $\Delta G^{\#} = \Delta H^{\#} - T\Delta S^{\#}$ was used to obtain the free energy of activation, $\Delta G^{\#}$ = 59.84(7) kJ.mol^{-1}.

5.4.4 Kinetics of catalytic hydroformylation of 1-octene with the Rh-PPh_3-Xp system

Data collected in Section 5.3.1 from autoclave runs was used to calculate rate constants for individual [$RhH(CO)_2$(xantphos)] and [$RhH(CO)_2(PPh_3)_2$] catalysts. The ballast vessel pressure drop was recorded from individual runs to calculate different k_{obs} for different [Xp] and [P] using the equation $P_{obs} = P_{inf} – (P_{inf} – P_0)\exp(-k_{obs}.t)$ (Eq. 5.10). Also see Figure 5.2 for illustration of fits obtained.

Very accurate first-order fits from the experimental data points to Eq. 5.10 were obtained with all reactions investigated as illustrated in Figure 5.2. These reactions clearly showed a decrease in reaction rate upon addition of Xp to the system. To explain this, an equilibrium was postulated. After obtaining different k_{obs} for different runs, data was collected to calculate the equilibrium constant, K_e. To enable this, a complete rate law was derived (see Par. 5.4.4.2 below) which yielded the relationship in Eqs. 5.25 and 5.26. The data correlation to this relationship is further illustrated below.

The qualitative illustration of the experimental data is first described, followed by the accurate determination of the different kinetic and thermodynamic constants, after which a detailed derivation of relevant model equations is presented.

5.4.4.1 Results and Discussion

The observed kinetic data for the hydroformylation of 1-octene by the Rh-PPh_3-Xp system showed behaviour dependent on both the [Xp] and [PPh_3].

Table 5.7 displays the experimental and calculated k_{obs} values as obtained from "Scientist"[4] using Eq. 5.25 and 5.26 while Fig. 5.19 illustrates the graphical dependence of the observed catalysis rate constant as a function of both [PPh_3] and [Xp].

Table 5.7. Correlation between observed and calculated rate constants: k_{obs} (experimental; obtained using Eq. 5.10) and k_{calc} (predicted by Eq. 5.25, iteratively using Eq. 5.26 to determine K_e) at different [Xp] and [PPh_3] runs of hydroformylation of 1-octene at 90 ℃ and 20 bar syngas with [Rh] = 1.65 mM.

[Xp] (M)	[PPh_3]	k_{obs} exp (min^{-1})	k_{obs} calc (min^{-1})
0	0.28	0.0467(3)	0.0468(2)
0.00165	0.28	0.0254(6)	0.0250(4)
0.00495	0.28	0.0139(5)	0.0140(3)
0.00825	0.28	0.0109(2)	0.0119(3)
0.00825	0.17	0.0107(3)	0.0102(4)
0.00825	0.00	0.0096(4)	0.0093(5)

A graphical representation of values obtained using Eqs. 5.25 and 5.26 (See Section 5.4.4.2) is given in Figure 5.19.

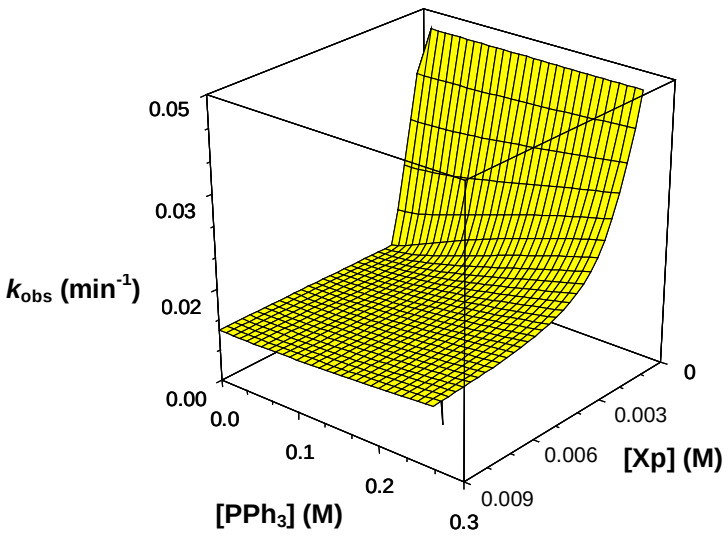

Figure 5.19. Three-dimensional representation (k_{obs} *vs*. [PPh_3] *vs*. [Xp]) data used for the calculation of K_e using the complete rate law and equilibrium model described by Eqs. 5.25 and 5.26 (see Par 5.4.4.2 below).

An increase in k_{obs} is observed with an increase in [PPh_3] and a decrease in [Xp]. Conversely, higher [Xp] and lower [PPh_3] result in slower rates. The rate constants associated with the [$RhH(CO)_2(PPh_3)_2$] and [$RhH(CO)_2$(xantphos)] species, k_P and k_{Xp}, were calculated to be 0.0468(7) min^{-1} and 0.0093(5) min^{-1} respectively, which

agree well with the rates obtained. The equilibrium constant, K_e, was found to be 158(21) M.

5.4.4.2 Derivation Rate law and reaction mechanism

In order to obtain rate and equilibrium constants for the reactions described above, complete rate equations had to be derived. This exercise included the derivation of the forward reaction rate as well as the equilibrium constant equation based on results obtained from autoclave experiments. The aim of the derivation was to obtain equilibrium constants for both the $[RhH(CO)_2(PPh_3)_2]$ and $[RhH(CO)_2(xantphos)]$ systems. Moreover, the equilibrium constant for the mixed $[RhH(CO)(PPh_3)(xantphos)]$ system was also obtained.

The following strategy was followed:

Initially, one may consider the simple forward reaction were reactants A and B react to form C as given below:

$$aA + bB \xrightarrow{k} cC \qquad 5.6$$

In this instance, the rate can be expressed as

$$rate = -\frac{dA}{dt} = k[A]^a[B]^b \qquad 5.7$$

Assuming pseudo 1st order conditions where [B] >>> [A] and a = b = 1, the above equation may be rearranged and written in the form:

$$\frac{dA}{[A]} = -k_{obs}dt \qquad 5.8$$

Where k_{obs} is the observed first order rate constant for the formation of C. Integrating the above equation gives

$$\ln \frac{[A]_t}{[A]_0} = -k_{obs}.t \qquad 5.9$$

Consider a typical hydroformylation reaction where the rate is calculated from the pressure drop recorded from a ballast vessel. $[A]_0$ and $[A]_t$ can be expressed in terms of P_0, P_t and P_{inf} where

P_0 = pressure at time 0

P_t = pressure at a given time t during the reaction

P_{inf} = Pressure at time infinity, at the end of the reaction

Then:

$[A]_0 \equiv P_0 - P_{inf}$ and $[A]_{obs} \equiv P_{obs} - P_{inf}$ where $A_{obs} \equiv A_t$ and $P_{obs} \equiv P_t$

$$\therefore P_{obs} = P_{inf} - (P_{inf} - P_0)\exp(-k_{obs}.t) \qquad 5.10$$

The above substitution is graphically illustrated in Figure 5.20 below taking the actual ballast vessel pressure drop. Equation 5.10 was used to fit the experimental data to obtain the pseudo first order rate constants, k_{obs}.

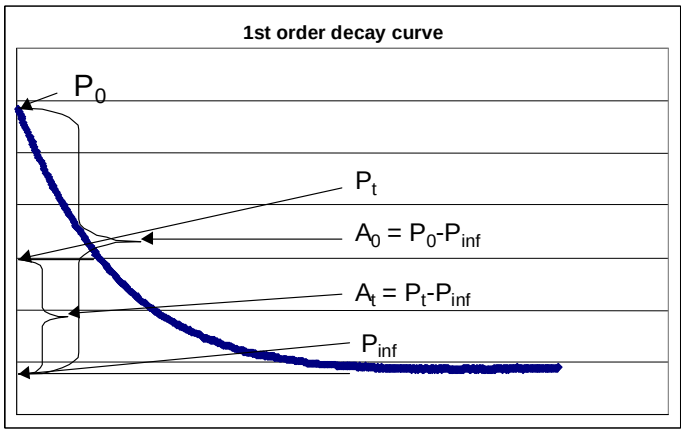

Figure 5.20. First order curve decay as taken from the ballast vessel pressure drop at baseline conditions run (example 90 °C and 20 bar syngas, Rh:PPh_3 1:170, see Section 5.3.1.1).

In this study, the mixed system where Rh-PPh_3 and Rh-Xp catalysts are present in the reaction solution is considered. Two separate reaction routes are then possible that can be expressed as in the following scheme:

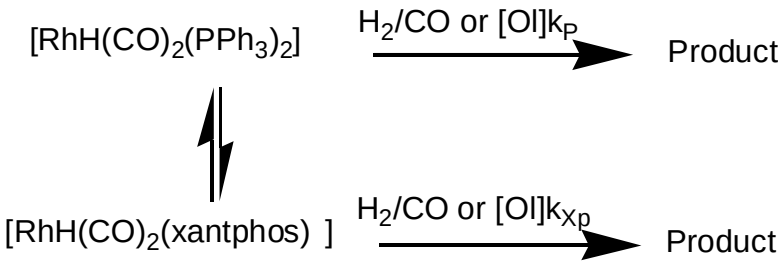

Scheme 5.4. A schematic representation of two possible separate reaction routes where both PPh_3 and xantphos are employed in the mixed ligand catalyst system during hydroformylation of olefin.

Where:

$[H_2/CO]$ = syngas fed on demand

[Ol] = olefin concentration

k_p and k_{Xp} forward rate constants of $[RhH(CO)_2(PPh_3)_2]$ and $[RhH(CO)_2(Xp)]$ species, respectively

Prod = products

(a) Rate Law

From the above scheme, the total rate of product formation due to the Xp modified and Xp-unmodified species, can be expressed as:

$$rate = k_p[RhP][Ol] + k_{Xp}[RhXp][Ol]$$
$$\therefore rate = [Ol](k_p[RhP] + k_{Xp}[RhXp]) \qquad 5.11$$

Assuming Rh-PPh_3 as the initial catalyst from which Rh-Xp is formed ($[RhH(CO)_2(PPh_3)_2]$ and $[RhH(CO)_2(Xp)]$ species) upon reacting with Xp, then the following equation holds:

$$[RhH(CO)_2(PPh_3)_2] + \text{Xantphos} \underset{}{\overset{K_{Xp}}{\rightleftharpoons}} [RhH(CO)_2(\text{xantphos})] + 2P \qquad 5.12$$

Thus,

$$K_{Xp} = \frac{[RhXp][P]^2}{[RhP][Xp]}$$

$$[RhXp] = \frac{K_{Xp}[RhP][Xp]}{[P]^2} \qquad 5.13$$

The total [Rh] can be expressed as the sum of Xp and non-Xp species.

$$[Rh]_{tot} = [RhP] + [RhXp]$$

$$[Rh]_{tot} = [RhP] + \frac{K_{Xp}[RhP][Xp]}{[P]^2} \qquad 5.14$$

Rearranging the above equation to express it in terms of Rh-PPh_3 gives

$$[RhP] = \frac{[Rh]_{tot}}{1 + \frac{K_{Xp}[Xp]}{[P]^2}} \qquad 5.15$$

Expressing [RhP] further in terms of [RhXp] from Eq. 5.13 gives

$$[RhP] = \frac{[RhXp][P]^2}{K_{Xp}[Xp]} \qquad 5.16$$

$$\therefore [Rh]_{tot} = [RhXp] + \frac{[RhXp][P]^2}{K_{Xp}[Xp]} \qquad 5.17$$

Rearranging the above equation then gives:

$$[RhXp] = \frac{[Rh]tot}{1 + \frac{[P]^2}{K_{Xp}[Xp]}} \qquad 5.18$$

Thus,

$$[RhXp] = \frac{[Rh]_{tot}\dfrac{K_{Xp}[Xp]}{[P]^2}}{1+\dfrac{K_{Xp}[Xp]}{[P]^2}} \qquad 5.19$$

Since the concentration of the olefin remaining [Olefin] is directly proportional to the observed pressure drop, denoted by "P_{obs}", the rate equation (5.10) can be rewritten as:

$$Rate = P_{obs}\left(k_p\frac{[Rh]_{tot}}{1+\dfrac{K_{Xp}[Xp]}{[P]^2}} + k_{Xp}\frac{[Rh]_{tot}\dfrac{K_{Xp}[Xp]}{[P]^2}}{1+\dfrac{K_{Xp}[Xp]}{[P]^2}}\right) \qquad 5.20$$

$$Rate = [Rh]_{tot}P_{obs}\left(\frac{k_P}{1+\dfrac{K_{Xp}[Xp]}{[P]^2}} + \frac{k_{Xp}\dfrac{K_{Xp}[Xp]}{[P]^2}}{1+\dfrac{K_{Xp}[Xp]}{[P]^2}}\right) \qquad 5.21$$

Upon integration with respect to $[Rh]_{tot}$, the observed first-order rate constant for the forward process becomes:

$$k_{obs} = P_{obs}\left(\frac{k_P + k_{Xp}\dfrac{K_{Xp}[Xp]}{[P]^2}}{1+\dfrac{K_{Xp}[Xp]}{[P]^2}}\right) \qquad 5.22$$

From Eq. 5.22, assuming $k_{obs} = P_{obs}.k_f$, where k_f = total forward rate constant, the following expression is obtained:

$$k_f = \left(\frac{k_P + k_{Xp} \dfrac{K_{Xp}[Xp]}{[P]^2}}{1 + \dfrac{K_{Xp}[Xp]}{[P]^2}} \right) \qquad 5.23$$

Multiplying the above equation by $[P]^2/[P]^2$ gives the expression for the observed forward rate constant, as obtained by monitoring the pressure drop, involving contributions by the Xp modified and unmodified catalytic species, $[RhH(CO)_2(xantphos)]$ and $[RhH(CO)_2(PPh_3)_2]$, respectively.

$$k_f = \frac{[P]^2 k_P + k_{Xp} K_{Xp}[Xp]}{[P]^2 + K_{Xp}[Xp]} \qquad 5.24$$

Next, the expression describing the equilibrium constant, is considered.

(b) Equilibrium Constant

Consider Eq. 5.10, which denotes the first horizontal process in Scheme 5.4

From simple mass-balance considerations, the following conditions will hold (C_R, C_P an C_{Xp} are the starting [Rh], $[PPh_3]$ and [Xp], respectively):

C_R	C_{Xp}:	0	C_P	At the start
$(C_R - X)$	$(C_{Xp} - X)$:	X	$C_P + 2X$	At equilibrium:

The equilibrium constant, K_e or K_{Xp}, using Eq. 5.11, can then be expressed as follows:

$$K_e = \frac{[X][C_P + 2X]^2}{[C_R - X][C_{Xp} - X]} \qquad 5.25$$

If $Y = C_{Xp} - X$, then $X = C_{Xp} - Y$.

$$\therefore K_e = \frac{[C_{Xp} - Y][C_P + 2(C_{Xp} - Y)]^2}{[C_R - C_{Xp} + Y][Y]} \qquad 5.26$$

The above expressions describes the observed experimental behaviour of the Rh-PPh_3-Xp systems quite well, and was therefore used to evaluate the experimental data and determine the relevant rate and equilibrium constants as described in Par. 5.4.4.1

5.4.5 Concluding remarks

The following conclusions may be drawn from this chapter:

- The effect of different Rh:PPh_3:Xp ratio was better understood where the higher the PPh_3 concentration, the higher the rates became but with a consequence of lower n:iso ratios and linearities (See Section 5.3.1). Conversely, higher Xp concentrations lead to slower rates and better selectivities in terms of n:iso ratio and linearities.

- Lower pressures (10 bar vs. 20 bar) lead to better selectivities and a small drop in rates (Section 5.3.1). There was, however, an increase in feed loss resulting from hydrogenation and isomerisation.

- During inhibition studies (Section 5.3.2), xantphos displayed its ability to confer some inhibitor resistance towards the Rh catalyst where no inhibition was observed at higher xantphos concentrations. A Rh:Xp ratio of 1:5 was sufficient to display this effect.

- Although longer inhibition periods were observed with an increase in PPh_3 concentration (a shift towards the $[RhH(CO)_2(PPh_3)_2]$ species), there was a drop in inhibition period at much higher Rh:PPh_3 ratios (1:200) as observed in Section 5.3.2. This observation suggests that PPh_3 acts an inhibitor resistant ligand at these conditions, possibly due to the more shielded metal centre resulting in a sterically hindered complex thereby preventing co-ordination of the inhibitor.

- A correlation between bite angle size and inhibition was established in Section 5.3.3 where wider bite angles lead to more inhibitor resistant catalysts. This observation was accompanied by improved selectivities in terms of n:iso ratios and linearities.

- Autoclave studies assisted in obtaining crucial information on the equilibrium between the two catalytic species investigated, $[RhH(CO)_2(PPh_3)_2]$ and $[RhH(CO)_2(xantphos)]$. Results obtained from autoclave experiments were successfully employed to derive rate equations and subsequently calculate rate constants as well as the equilibrium constant. The $[RhH(CO)_2(xantphos)]$ species is quite stable, even in the presence of free PPh_3 [K_e = 158(21) M]. The chelate effect of xantphos was therefore displayed, the $[RhH(CO)_2(xantphos)]$ being the predominant species, even at as high Rh:PPh_3 ratios as 1:170 and Rh:Xp ratios of 1:5, as evident from the rates obtained (see Figure 5.19). This observation was consistent with selectivities obtained with the mixed system, where the dominating effect of xantphos was displayed by high n:iso ratios and linearities (Table 5.2). Rate constants calculated from the derived equations were in good agreement with rates obtained from autoclave experiments.

References

1. Walczuk, E. B.; Kamer, P. C. J.; Van Leeuwen, P. W. N. M. *Angew. Chem. Int. Ed.* **2003**, *42*, 4665.

2. van Leeuwen, P. W. N. M. private communication.

3. Information obtained from several patents e.g. US 4,593,127 and 4,277,627

4. Scientist for Windows, ver. 4.10.1998, MicroMath, Utah, USA, 1990.

5. Van Leeuwen, P. W. N. M.; Claver, C. *Rhodium Catalysed Hydroformylation*, Kluwer Academic Publishers, Dordrecht: The Netherlands, **2000**.

6. Pryde, A. J.; Shaw L. B.; Weeks, B. *Chem. Commun*. **1973**, 947.

7. Sanger, A. R.; *Chem. Commun*. **1975**, 893.

8. van der Veen, L. A.; Keeven, P. H.; Schoemaker, G. C.; Reek, J. N. H.; Kamer, P. C. J.; van Leeuwen, P. W. N. M.; Lutz, M.; Spek, A. L. *Organometallics* **2000**, *19*, 872.